!

Very Short-Lived Halogenated Species: Modelling their Tropospheric Distribution, Contribution to Stratospheric Bromine and Impact on Ozone.

Ryan Hossaini

Submitted in accordance with the requirements for the degree of
Doctor of Philosophy

University of Leeds
School of Earth and Environment
October 2012

Declaration of Authorship

The candidate confirms that the work submitted is his own, except where work which has formed part of jointly-authored publications has been included. The contribution of the candidate and the other authors to this work has been explicitly indicated below. The candidate confirms that appropriate credit has been given within the thesis where reference has been made to the work of others.

Chapters 3 and 4 are based on Hossaini et al. (2010), which was jointly authored with Professor M. P. Chipperfield, Dr B. M. Monge-Sanz, Dr N. A. D. Richards, Professor E. L. Atlas and Professor D. R. Blake. The candidate devised and performed all experiments with Professor Chipperfield providing scientific comments. Dr Monge-Sanz performed the trajectory analysis based on data provided from the candidate. Dr Richards provided computational support. Professors Atlas and Blake provided aircraft data. The publication text was written by the candidate.

Chapter 5 is based on Hossaini et al. (2012b), which was jointly authored with Professor M. P. Chipperfield, Dr W. Feng, Dr T. J. Breider, Professor E. L. Atlas, Dr S. A. Montzka, Dr B. R. Miller, Dr F. Moore, and Dr J. Elkins. The candidate devised and performed all experiments with Professor Chipperfield providing scientific comments. Modelling support was provided by Dr Feng. Dr Breider provided model data and the remaining coauthors provided aircraft data. The publication text was written by the candidate.

Chapter 7 is based on Hossaini et al. (2012a), which was jointly authored with Professor M. P. Chipperfield, Dr S. Dhomse, Dr C. Ordóñez , Dr A. Saiz-Lopez, Dr L. Abraham, Dr A. Archibald, Dr P. Braesicke, Dr P. Telford, Professor J. Pyle, Dr N. Warwick and Dr X. Yang. The candidate devised and performed all experiments with Professor Chipperfield providing scientific comments. Modelling support was provided by Dr Abraham. The remaining coauthors provided scientific comments on the work. The publication text was written by the candidate.

Acknowledgements

First, a huge thank you to my supervisor Martyn Chipperfield, who has provided tremendous support and guidance over the last 5 or so years. I am extremely grateful.

Secondly, I would like to thank all my friends and colleagues in the Leeds atmospheric modelling group, with whom I've had many scientific discussions. In particular, Nigel Richards, Sandip Dhomse and Wuhu Feng, who have all provided support in one way or another.

Thirdly, I wish to acknowledge the modelling support of Luke Abraham and Mohit Dalvi. In addition, thank you to the many people who have provided data during this project; Beatriz Monge-Sanz, Tom Breider, Carlos Ordóñez, Alfonso Saiz-Lopez, Qing Liang, Marcel Dorf and the whole SHIVA community. A particularly big thanks to Steven Montzka, Elliot Atlas and Franziska Wittke, who provided unpublished data on multiple occasions.

For funding my PhD, I thank the Natural Environment Research Council (NERC).

Beyond these, I am grateful to everyone that made my PhD years enjoyable. In particular, my friends within the School, of whom there are too many to list. Although, for endless laughter over the last few years, David Tupman and Mike Hollaway deserve a mention.

A special thanks is reserved for Amber, who has supported me through stressful times and kept insanity at bay. A final thank you goes to my loving family who have also provided much support over the years.

Abstract

A three-dimensional (3-D) chemical transport model (CTM) has been used to study the tropospheric chemistry and troposphere-stratosphere transport of biogenic very short-lived species (VSLS). Calculations have been performed in order to quantify their contribution to stratospheric bromine loading and also the relative importance of the source gas injection (SGI) and product gas injection (PGI) pathways. Simulations with a chemistry-climate model (CCM) have also been performed to assess the impact of VSLS on stratospheric ozone (O_3) and how their transport to the stratosphere may respond to climate change.

Five brominated VSLS were considered in this work; bromoform ($CHBr_3$), dibromomethane (CH_2Br_2), dibromochloromethane ($CHBr_2Cl$), bromodichloromethane ($CHBrCl_2$) and bromochloromethane (CH_2BrCl). The CTM shows these gases contribute ∼5 parts per trillion (pptv) of inorganic bromine (Br_y^{VSLS}) to the stratosphere, representing ∼25% of total stratospheric bromine in 2009. SGI accounts for between ∼69-75% of this supply, with the remainder from PGI. The longest lived organic product gas (PG) from $CHBr_3$ and CH_2Br_2 degradation is carbonyl dibromide (CBr_2O). Its tropospheric lifetime with respect to photolysis is ∼7 days. It is unlikely that organic PGs make a significant contribution to the total PGI from VSLS. The CTM performs reasonably well in reproducing tropospheric VSLS observations from a number of aircraft campaigns. In the tropical tropopause layer (TTL), CH_2Br_2 is overestimated when vertical transport is diagnosed from the meteorological analyses. An improved agreement is obtained when vertical transport is calculated using diabatic heating rates, resulting in slower transport through the TTL.

CCM runs show during periods of background aerosol loading, the impact of Br_y^{VSLS} on mid-latitude O_3 is small. The impact is larger in polar regions, where Br_y^{VSLS} enhances the BrO-ClO loss cycle, resulting in a reduction of up to ∼15 Dobson units (DU) of the total O_3 column over Antarctica. The CCM has also been used to diagnose the potential response of SGI to climate change. For 2000, the modelled SGI is ∼1.7 pptv, lower than the CTM estimate but still in good agreement with observations. For 2100, the CCM estimate increases to ∼1.9 and ∼2.7 pptv when the model is forced with Intergovernmental Panel on Climate Change (IPCC) representative concentration pathways (RCPs) 4.5 and 8.5, respectively. The increase is due to enhanced tropical deep convection, reducing transport time-scales in the upper troposphere, particularly over the tropical Western Pacific region.

Contents

List of Figures

List of Tables

Abbreviations

AGAGE	**A**dvanced **G**lobal **A**tmospheric **G**ases **E**xperiment
BAS	**B**ritish **A**ntarctic **S**urvey
CCM	**C**hemistry **C**limate **M**odel
CCMVal	**C**hemistry-**C**limate **M**odel **V**alidation **A**ctivity
CFC	**C**hloro**F**luoro**C**arbon
CPT	**C**old **P**oint **T**ropopause
CR-AVE	**C**osta **R**ica **A**ura **V**alidation **E**xperiment
CTM	**C**hemical **T**ransport **M**odel
DOAS	**D**ifferential **O**ptical **A**bsorption **S**pectroscopy
ECMWF	**E**uropean **C**entre for **M**edium-Range **W**eather **F**orecasts
ESRL	**E**arth **S**ystem **R**esearch **L**aboratory
FID	**F**lame **I**onization **D**etector
GC	**G**as **C**hromatography
GHG	**G**reen**H**ouse **G**as
HADISST	**Had**ley Centre Sea **I**ce and **S**ea **S**urface **T**emperature Data Set
HALOCAT	**Haloc**arbons in the Ocean and **At**mosphere
HCFC	**H**ydro-**C**hloro-**F**luoro-**C**arbon
INTEX	**Int**ercontinental Chemical Transport **Ex**periment
IPCC	**I**ntergovernmental **P**anel on **C**limate **C**hange
JPL	**J**et **P**ropulsion **L**aboratory
LS	**L**ower **S**tratosphere
MBL	**M**arine **B**oundary **L**ayer
MCM	**M**aster **C**hemical **M**echanism
MS	**M**ass **S**pectrometry
NASA	**N**ational **A**eronautics and **S**pace **A**dministration

NOAA	**N**ational **O**ceanic and **A**tmospheric **A**dministration
NSF	**N**ational **S**cience **F**oundation
ODS	**O**zone-**D**epleting **S**ubstance
PBL	**P**lanetary **B**oundary **L**ayer
PEM	**P**acific **E**xploratory **M**ission
PG	**P**roduct **G**as
PGI	**P**roduct **G**as **I**njection
PRE-AVE	**Pre A**ura **V**alidation **E**xperiment
PSC	**P**olar **S**tratospheric **C**loud
RCP	**R**epresentative **C**oncentration **P**athway
SCIAMACHY	**Sc**anning **I**maging **A**bsorption Spectro**m**eter for **A**tmospheric **C**artograp**hy**
SG	**S**ource **G**as
SGI	**S**ource **G**as **I**njection
SHIVA	**S**tratospheric **H**alogen **I**mpacts in a **V**arying **A**tmosphere
SPARC	**S**tratospheric **P**rocesses **A**nd their **R**ole in **C**limate
SST	**S**ea **S**urface **T**emperature
TTL	**T**ropical **T**ropopause **L**ayer
UT	**U**pper **T**roposphere
UV	**U**ltra**V**iolet
VMR	**V**olume **M**ixing **R**atio
VSLS	**V**ery **S**hort-**L**ived **S**pecies
WMO	**W**orld **M**eteorological **O**rganization

Chapter 1

Introduction

1.1 General Background

Ozone (O_3) is an extremely important trace gas for the Earth's biosphere. In the stratosphere, it absorbs a large fraction of incoming solar ultraviolet (UV) radiation and thus shields the surface. The peak stratospheric O_3 abundance occurs at approximately 20-30 km in altitude. Without this so-called *ozone layer*, human life on Earth could not exist.

Depletion of stratospheric O_3 has been a major environmental concern of the late 20th and early 21st century. Reduction in the overhead O_3 column increases the amount of potentially harmful UV radiation reaching the surface. Excessive exposure to UV-B (280-315 nm) and UV-A (315-400 nm) is detrimental to both animal and plant life. In humans, this exposure can lead to cataracts on the eyes, premature ageing of the skin and also skin cancer such as melanoma (e.g., Kanavy and Gerstenblith, 2011).

Depletion of stratospheric O_3 has been observed on a global scale since the late 1970s. Extreme depletion events have been well documented in polar regions, in particular the South Pole. Here, seasonal O_3 loss leads to the formation of the Antarctic Ozone Hole, first observed by a team of scientists from the British Antarctic Survey (BAS) in 1984 (Farman et al., 1985). Since the discovery of the Ozone Hole, a wealth of scientific research has been dedicated to understanding the substances and processes that control global O_3.

The primary cause of observed global O_3 depletion has been anthropogenic emissions of ozone-depleting substances (ODS) such as chlorofluorocarbons (CFCs) and halons. CFCs

are gases that contain chlorine and fluorine atoms (e.g. CFC-12, CCl_2F_2), while halons contain bromine (e.g. Halon-1301, $CBrF_3$). These compounds are relatively inert in the Earth's troposphere and thus their atmospheric lifetimes may be long (order of decades). Therefore, they can be transported to the stratosphere where, upon degradation, they release their chlorine/bromine content. These reactive halogen radicals can then take part in efficient O_3-depleting cycles (e.g., Molina and Rowland, 1974; Wofsy et al., 1975).

Mass production of CFCs began in the mid 20th century for applications that exploited their low toxicity and flammability. CFCs have been used used as refrigerants, aerosol propellants, blowing agents and also solvents for cleaning electronic components. Similarly, production of halons increased substantially during the 1960s for use in fire suppression systems on board aircraft and ships. The Nobel Prize-winning work of Molina and Rowland (1974) and other influential studies (e.g., Stolarski and Cicerone, 1974), along with the alarming discovery of the Ozone Hole, eventually led the international community to act. In 1987 *The Montreal Protocol on Substances That Deplete the Ozone Layer* was opened for signature. This international treaty was designed to phase out production of anthropogenic ODS and has since been ratified by 197 nations. The Montreal Protocol and further amendments (e.g. London 1990, Vienna 1995) has generally been very effective in achieving these goals.

Due to the success of the Montreal Protocol, the atmospheric abundance of a number of ODS (e.g. certain CFCs, methyl bromide) peaked around the turn of the century (Montzka et al., 2003). As a result, we expect stratospheric chlorine and bromine to steadily decline over coming years. Global O_3 is thus expected to recover (to pre-1980 levels) at some point towards the mid-late 21st century (WMO, 2011). The nature and timescale of recovery will also be determined by other (uncertain) factors. An increase in the atmospheric burden of greenhouse gases (GHGs) and the resulting dynamical/chemical changes in both the troposphere and stratosphere, will likely influence the evolution of O_3 in the 21st century. In order to make educated predictions on these potentially important changes, we must now increase our understanding of a range of complex chemistry-climate interactions.

"Perhaps the single most successful international agreement to date"

- Kofi Annan on the Montreal Protocol

1.2 Motivation

The bromine (Br) budget of the stratosphere is largely governed by emissions of long-lived ODS (e.g. halons) and methyl bromide (CH_3Br). Recent attempts to quantify total stratospheric bromine have shown that there is more bromine in the stratosphere than can be explained by these long-lived gases alone (e.g. Pfeilsticker et al., 2000; Dorf et al., 2008). Figure 1.1 shows a time series of expected stratospheric inorganic bromine (Br_y) based on observed tropospheric CH_3Br and also the sum of CH_3Br plus halons. Also shown (post 1992) are measurements of total stratospheric Br_y, derived from balloon-borne and ground-based measurements of bromine monoxide (BrO) combined with three-dimensional (3-D) chemical transport model (CTM) calculations. While CH_3Br plus halons can account for most of the observed stratospheric Br_y, there remains a significant shortfall of of ∼3-8 parts per trillion (ppt). This additional Br_y is thought to arise from the breakdown of naturally-occurring *very short-lived species* (VSLS) in both the troposphere and the stratosphere (Law and Sturges, 2007; Montzka and Reimann, 2011).

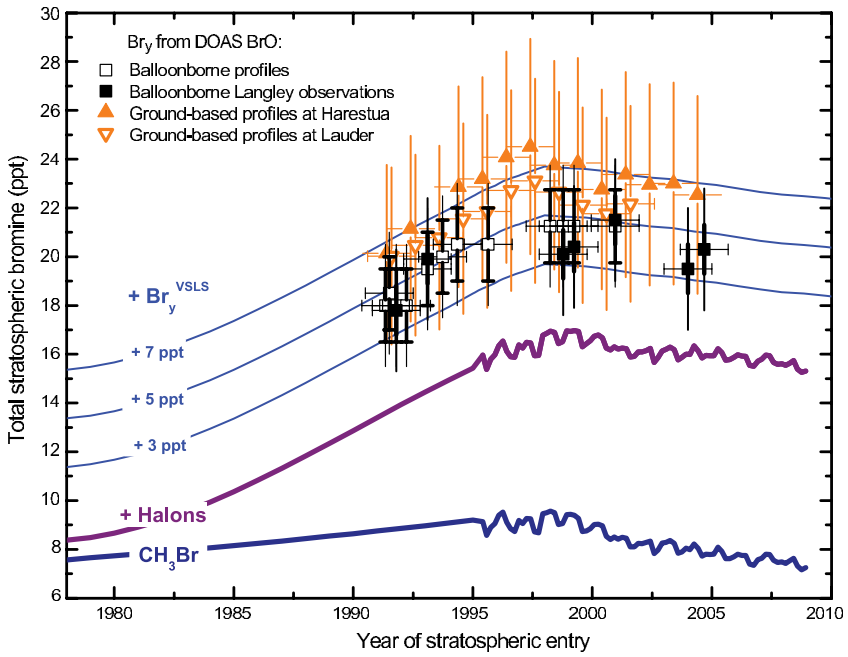

FIGURE 1.1: Stratospheric inorganic bromine (ppt) derived from balloon-borne/ground-based measurements of BrO and photochemical modelling (open and filled squares /rectangles). The expected contribution from methyl bromide (blue line), methyl bromide plus the halons (purple line) and methyl bromide plus halons plus an assumed 3, 5 and 7 ppt from very short-lived species, is shown. Figure from Montzka and Reimann (2011).

Brominated VSLS are thought to be emitted from various species of seaweed and also phytoplankton (e.g. Carpenter and Liss, 2000; Butler et al., 2007). Examples include bromoform ($CHBr_3$) and dibromomethane (CH_2Br_2), whose emissions are highly variable in both space and time (e.g., Quack and Wallace, 2003). It has been suggested that biogenic emissions of VSLS may potentially change under a future, potentially warmer climate (Law and Sturges, 2007; Montzka and Reimann, 2011). The nature of this response is poorly understood and is an area of ongoing research. However, it is reasonable to think that changes to sea surface temperatures (SST), salinity and also surface wind speeds, could perturb VSLS emissions (Law and Sturges, 2007). Based on a range of in-situ measurements, Butler et al. (2007) established a positive correlation between the sea-air flux of $CHBr_3$ and SST. Furthermore, land use change and practice, also has the potential to increase emissions of VSLS (Pyle et al., 2011). For example, the farming of seaweed in tropical regions is currently a growing industry.

Potentially enhanced emissions of VSLS could be most significant in the tropics, where troposphere-stratosphere transport is rapid (e.g., Fueglistaler et al., 2009). While it is thought that overall the tropical circulation will weaken in response to global warming (Vecchi et al., 2006), model studies have shown an increase in VSLS loading into the stratosphere under future climates (Pyle et al., 2007; Dessens et al., 2009). The dynamical processes responsible are currently poorly understood and poorly quantified. However, as they have the potential to increase the anount of bromine and chlorine that reaches the stratosphere from VSLS, they can potentially impact the timescale for global O_3 recovery. More certain is that the relative importance of VSLS for stratospheric bromine (and chlorine) loading will increase due to the phase out of controlled substances under the Montreal Protocol.

Given the significance of atmospheric O_3, an important radiative gas in both the troposphere and stratosphere, the processes which control its abundance must be understood. For the above reasons, VSLS need to be considered in global model calculations to determine their impact on O_3 and how this may change in a future atmosphere.

1.3 Thesis Aims

The overarching goal of this thesis is to improve the current understanding of the transport and chemistry of (predominantly) bromine-containing VSLS and their impact on stratospheric O_3. To achieve this, a 3-D chemical transport model (CTM) and also a chemistry-climate model (CCM) have been used. The specific aims of the thesis are:

[1.] Develop and test detailed chemical schemes describing the tropospheric degradation of major bromine-containing source gases. Further develop and implement existing schemes describing the tropospheric degradation of $CHBr_3$ and CH_2Br_2 within the TOMCAT/SLIMCAT CTM. Assess the production of organic product gases arising from $CHBr_3$ and CH_2Br_2 degradation. Assess the local lifetime of expected major products formyl bromide (CHBrO) and carbonyl dibromide (CBr_2O). Determine the importance of these organic product gases for the transport of bromine to the stratosphere.

[2.] Investigate the troposphere-stratosphere transport of bromine-containing VSLS and their impact on stratospheric bromine loading. Assess the importance of the source gas injection (SGI) and product gas injection (PGI) pathways for stratospheric delivery of bromine from VSLS. Assess the sensitivity of SGI and PGI to the treatment of model vertical transport, convection, the hydroxyl radical (OH) concentration and also Br_y lifetime. Investigate the transport/lifetimes of VSLS in the tropical tropopause layer (TTL) and evaluate the CTM in this region with high-altitude aircraft observations. Infer a modelled total contribution to the stratospheric bromine budget from VSLS (Br_y^{VSLS}).

[3.] Assess the present day impact of VSLS on stratospheric O_3 and how SGI may change under potential future climates. Use the UKCA CCM to investigate the impact of present day Br_y^{VSLS} on global stratospheric O_3. Quantify potential changes to the stratospheric SGI of bromine from VSLS under projected 2100 IPCC climates scenarios. Assess if any SGI change is primarily due to perturbed tropospheric dynamics and/or chemistry. Determine the SGI sensitivity to moderate-high climate change.

1.4 Thesis Layout

The thesis is organised as follows. Chapter 2 contains a literature review covering the key principles of O_3 production and halogen-mediated loss. A discussion of halogen-containing ODS, both anthropogenic and natural, is included. The emphasis is placed on VSLS, their oceanic emission, their troposphere-stratosphere transport and previous modelling work.

Chapter 3 and 4 focus on major VSLS $CHBr_3$ and CH_2Br_2. In Chapter 3, tropospheric degradation schemes for these source gases are described. In Chapter 4, these schemes are incorporated into a 3-D CTM and simulations are performed to study their tropospheric chemistry and transport. Their modelled distribution is evaluated using aircraft observations.

In Chapter 5, model simulations are extended to include all important brominated VSLS, both natural and anthropogenic. The total contribution of VSLS to stratospheric bromine is quantified. The impact of model convection on this estimate is assessed.

Chapter 6 describes the treatment of VSLS in a CCM, which is validated with both ground-based and aircraft observations and further used to quantify the impact of VSLS on stratospheric O_3. Chapter 7 is also a CCM study which investigates how the abundance of VSLS in the lower stratosphere may respond to climate change. Finally, Chapter 8 summarises the results of the thesis and draws overall conclusions. Recommendations for future work are also discussed here.

Chapter 2

Review of Key Literature

2.1 Introduction

This literature review provides a brief background on stratospheric ozone (O_3) and key processes controlling its abundance. O_3 is extremely important as it absorbs and greatly reduces the intensity of potentially harmful ultraviolet (UV) radiation (from the sun) transmitted to the Earth's surface. Excessive exposure to, for example, UV-B (280-315 nm) is generally detrimental to the biosphere (e.g. van der Leun et al., 2007).

This review focuses on halogenated ozone depleting substances (ODS), in particular brominated very short-lived species (VSLS) - the primary focus of the thesis. The chapter is structured as follows. Section 2.2 (and subsections therein) contain a discussion of key O_3 chemistry, including natural production and loss. Emphasis is placed on catalytic O_3 loss due to reactive chlorine (Cl) and bromine (Br) species in the mid-latitude and polar stratosphere. The special dynamical/chemical conditions occurring at the South Pole and leading to the Antarctic O_3 hole are also discussed.

Section 2.3 introduces the major long-lived ODS. The production and trends in anthropogenic compounds, such as chlorofluorocarbons (CFCs) and halons, are discussed. Section 2.4 introduces brominated-VSLS and includes discussion on their oceanic sources, atmospheric chemistry and troposphere-stratosphere transport. The impact of VSLS on stratospheric O_3, previous modelling work examining these processes and key uncertainties are also discussed.

2.2 Stratospheric Ozone

In the stratosphere, background O_3 is typically present at the parts per million (ppm) level. Globally, its abundance is controlled by numerous factors, including stratospheric photochemistry, solar variability, aerosol loading and transport/dynamics (e.g. Chipperfield and Fioletov, 2007; Harris et al., 2008). These processes contribute to the seasonal trends and variability of observed O_3. In the stratosphere, O_3 is continually produced and destroyed. However, anthropogenic emissions of ODS have led to perturbed stratospheric photochemistry and enhanced chemical O_3 loss (e.g. WMO, 2003, 2007, 2011).

Figure 2.1 shows the distribution and seasonality in the total O_3 column observed by satellite. Production of O_3 is largest in the tropical mid stratosphere, where there is an abundance of oxygen molecules and the intensity of solar radiation is relatively large (see Section 2.2.1). The large-scale Brewer-Dobson circulation (Brewer, 1949) transports air polewards, resulting in a redistribution of stratospheric O_3 and an accumulation at high latitudes.

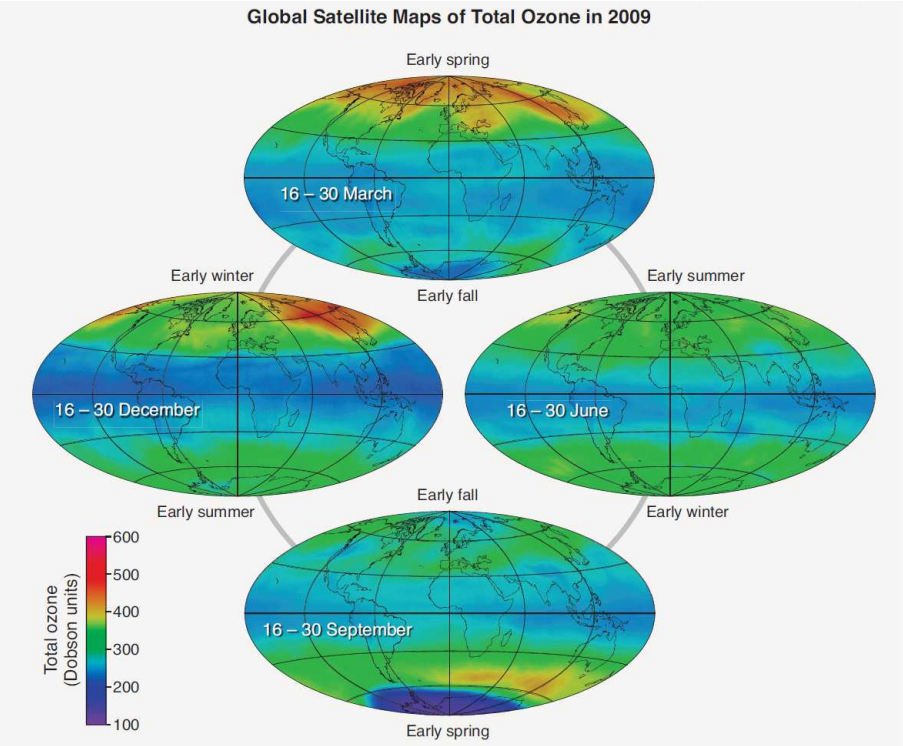

FIGURE 2.1: Total column ozone (DU) and seasonality from compiled 2009 satellite data. Figure taken from (WMO, 2011).

2.2.1 Production and Loss

The natural chemical production (and loss) of stratospheric O_3 can be partially explained by the so-called *Chapman mechanism* (Chapman, 1930). Initially, photolysis of molecular oxygen (O_2) produces two reactive oxygen atoms (O, R2.1). These atoms may combine with O_2 in a termolecular reaction (R2.2) to produce O_3.

$$O_2 + h\nu \ (\lambda{<}240nm) \rightarrow O + O \qquad \text{R2.1}$$

$$2 \times (O + O_2 + M \rightarrow O_3 + M) \qquad \text{R2.2}$$

$$3O_2 + h\nu \rightarrow 2O_3 \qquad \textbf{R2.3, NET}$$

O_3 itself may then undergo photolysis (R2.4) to yield O_2 and O. Further O_2 is formed from the subsequent reaction of O_3 and O (R2.5).

$$O_3 + h\nu \rightarrow O_2 + O \qquad \text{R2.4}$$

$$O + O_3 \rightarrow O_2 + O_2 \qquad \text{R2.5}$$

$$2O_3 + h\nu \rightarrow 3O_2 \qquad \textbf{R2.6, NET}$$

It is known that O_3 and O can inter-convert rapidly between each other via reactions R2.2 and R2.4 (Chapman, 1930). Only a small amount of the O atoms produced from O_3 photolysis will take part in reaction R2.5. Therefore, R2.5 represents a slow removal of the sum of [O] and [O_3] - much slower than the timescales (seconds) for the interconversion of O and O_3. Therefore, it is useful to consider the sum of [O] and [O_3] as a family, *odd oxygen*, produced only in reaction R2.1 (e.g. Solomon, 1999). The oxygen-only chemistry described by Chapman (1930) cannot quantitatively explain observed O_3. Calculations considering only Chapman chemistry significantly overestimate its abundance. Laboratory measurements have also confirmed R2.5 to be too slow to destroy O_3 at the rate it is produced globally (Wayne, 1991). Therefore, it follows that additional loss pathways for O_3 must exist.

In the stratosphere, odd oxygen loss cycles involving hydrogen oxide (HO_x = [H] + [HO_2] + [OH]) and also nitrogen oxide (NO_x = [NO] + [NO_2]) families, are also important. HO_x and NO_x are present naturally in the stratosphere and these species take part in efficient catalytic cycles, whereby the initial reactant is conserved. A general form of a catalytic cycle is given below (R2.7-2.9). Here, X may be H, OH and NO or even a halogen atom, such as Cl or Br, which also (to some degree) occur naturally in the stratosphere (see Section 2.4).

General Cycle

$X + O_3$	$\rightarrow XO + O_2$	R2.7
$XO + O$	$\rightarrow X + O_2$	R2.8
$O + O_3$	$\rightarrow O_2 + O_2$	**NET, R2.9**

Reactions R2.10-2.12 and R2.13-2.15 below show the HO_x catalytic cycles involving H and OH, respectively. Catalytic cycles involving HO_x were first proposed by Bates and Nicolet (1950). Changes in the abundance of water vapour (H_2O) and methane (CH_4), due to anthropogenic activity, may perturb (natural) background levels of atmospheric HO_x. For example, oxidation of CH_4, whose emissions have increased significantly since pre-industrial times (e.g., Forster et al., 2007), is an in-situ source of hydroxyl radicals (OH) in the stratosphere (e.g. Lary and Toumi, 1997).

HOx Cycle 1

$H + O_3$	$\rightarrow OH + O_2$	R2.10
$OH + O$	$\rightarrow H + O_2$	R2.11
$O + O_3$	$\rightarrow O_2 + O_2$	**NET, R2.12**

HOx Cycle 2

$OH + O_3$	$\rightarrow HO_2 + O_2$	R2.13
$HO_2 + O$	$\rightarrow OH + O_2$	R2.14
$O + O_3$	$\rightarrow O_2 + O_2$	**NET, R2.15**

Catalytic cycles involving NO_x (reactions R2.16-2.18) have also been identified as playing an important role in odd oxygen chemistry (Crutzen, 1970; Johnston, 1971). The primary source of stratospheric NO_x is naturally-occurring surface emissions of the source gas, nitrous oxide (N_2O). Anthropogenic industrial, agricultural and other activities, has led to an increase in atmospheric N_2O of ∼50% since pre-industrial levels (Forster et al., 2007). 2-D model calculations indicate that N_2O (weighted by ozone-depleting potential) is the most important anthropogenic ODS of the 21st century (Ravishankara et al., 2009). Future emissions of N_2O, and other greenhouse gases (GHG), will influence the evolution of stratospheric O_3 in coming years (e.g. Chipperfield, 2009).

NOx Cycle

$NO + O_3$	$\rightarrow NO_2 + O_2$	R2.16
$NO_2 + O$	$\rightarrow NO + O_2$	R2.17
$O + O_3$	$\rightarrow O_2 + O_2$	**NET, R2.18**

2.2.2 Halogen-mediated Loss

Reactive chlorine (Cl_x = [Cl] + [ClO]) species are also known to take part in catalytic O_3-depleting cycles (R2.19-2.21) (Stolarski and Cicerone, 1974). Anthropogenic emissions of CFCs (and other chlorine-containing ODS) have significantly increased the abundance of chlorine in the stratosphere (Molina and Rowland, 1974). As a result, global O_3 loss has been enhanced over the past few decades (WMO, 2003, 2007, 2011).

Cl Cycle 1

$$\mathrm{Cl} + \mathrm{O_3} \rightarrow \mathrm{ClO} + \mathrm{O_2} \qquad \text{R2.19}$$

$$\mathrm{ClO} + \mathrm{O} \rightarrow \mathrm{Cl} + \mathrm{O_2} \qquad \text{R2.20}$$

$$\mathrm{O} + \mathrm{O_3} \rightarrow 2\mathrm{O_2} \qquad \textbf{NET, R2.21}$$

The conversion of Cl_x to more stable *reservoir* species, such as hydrogen chloride (HCl), can terminate the above cycle. R2.22 shows the production of HCl from the reaction of Cl with CH_4. The formation of chlorine nitrate ($ClONO_2$) (R2.23), also an important reservoir, couples the Cl_x and NO_x families (e.g Solomon, 1999). Finally, ClO may also react with hydroperoxyl radicals (HO_2) to produce HOCl (R2.24). This partitioning of inorganic chlorine (Cl_y) between reactive and reservoir form determines the amount of Cl_x available for stratospheric O_3 destruction. In the troposphere, soluble Cl_y, such as HCl and $ClONO_2$, can be effectively *washed out* of the atmosphere in precipitation (e.g., Deiber et al., 2004).

$$\mathrm{Cl} + \mathrm{CH_4} \rightarrow \mathrm{CH_3} + \mathrm{HCl} \qquad \text{R2.22}$$

$$\mathrm{ClO} + \mathrm{NO_2} + \mathrm{M} \rightarrow \mathrm{ClONO_2} + \mathrm{M} \qquad \text{R2.23}$$

$$\mathrm{ClO} + \mathrm{HO_2} \rightarrow \mathrm{HOCl} + \mathrm{O_2} \qquad \text{R2.24}$$

Similarly, reactive bromine (Br_x = [Br] + [BrO]) may catalyze O_3 destruction (R2.25-2.27) (e.g. Wofsy et al., 1975; Salawitch, 2006). Its reservoirs, hydrogen bromide (HBr) and bromine nitrate ($BrONO_2$), are relatively unstable, meaning Br_x dominates the total stratospheric inorganic bromine budget (Br_y).

Br Cycle 1

$Br + O_3$	$\rightarrow BrO + O_2$	R2.25
$BrO + O$	$\rightarrow Br + O_2$	R2.26
$O + O_3$	$\rightarrow 2O_2$	**NET, R2.27**

Although present in the atmosphere, fluorine and iodine-containing species are thought to be insignificant for stratospheric O_3. For fluorine, its reservoir (hydrogen fluoride - HF) is extremely stable and thus it is tied up and non-reactive towards O_3. Iodine-containing compounds, such as methyl iodide (CH_3I) which is emitted from the ocean, generally have short atmospheric lifetimes. As a result, only a very small amount (∼0.1 ppt) of iodine reaches the stratosphere (Butz et al., 2009; Montzka and Reimann, 2011). Figure 2.2 shows the formation of key halogen reservoirs. It also shows O_3 loss by a coupled Cl_x and Br_x cycle which is responsible for a significant portion of seasonal Antarctic O_3 loss (e.g. McElroy et al., 1986) (see Section 2.2.3).

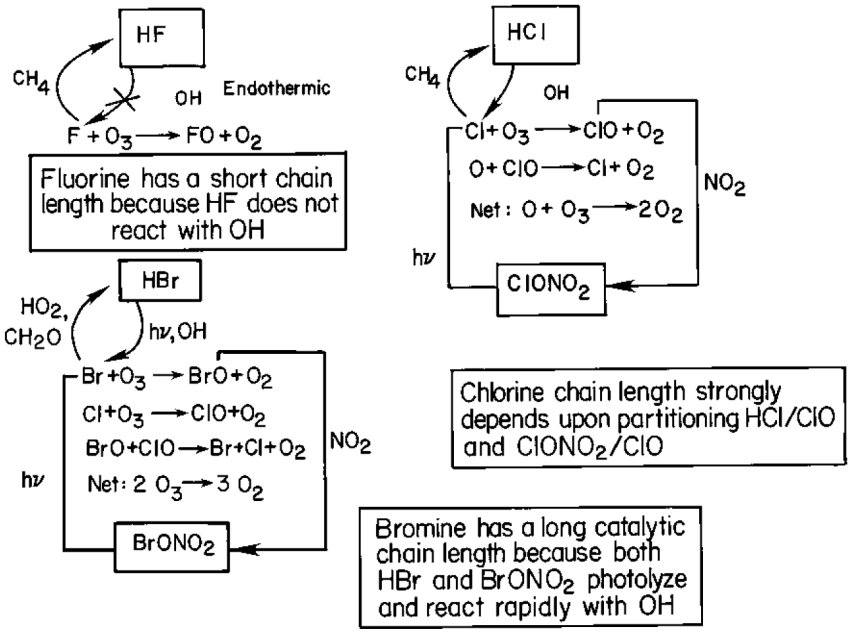

FIGURE 2.2: Formation of key halogenated reservoir species and O_3 loss via a coupled Cl_x and Br_x catalytic cycle. Figure taken from Solomon (1999).

2.2.3 The Antarctic Ozone Hole

Since its discovery, the Antarctic Ozone Hole (Farman et al., 1985) has been the subject of a wealth of theoretical, laboratory-based, observational and modelling research. A full review of this work, which spans nearly three decades, is beyond the scope of this literature review. Here some key principles concerning the anomalous chemical/dynamical conditions that lead to the seasonal depletion of Antarctic O_3 are discussed.

Polar meteorology plays a key role in the onset of the Ozone Hole. As discussed, Cl_x may destroy O_3 through Cl Cycle 1 (R2.19-R2.21), when oxygen atoms are available. Alternatively, cold temperatures during the Antarctic winter favour the self reaction of ClO (R2.28) and hence the formation of chlorine peroxide (Cl_2O_2). Photolysis of this *dimer* leads to the release of chlorine atoms (R2.29) and is responsible for the majority of O_3 loss in the Antarctic stratosphere (Molina and Molina, 1987).

Cl Cycle 2

$ClO + ClO + M$	$\leftrightarrow Cl_2O_2 + M$	R2.28
$Cl_2O_2 + h\nu$	$\rightarrow ClOO + Cl$	R2.29
$ClOO + M$	$\rightarrow Cl + O_2 + M$	R2.30
$2 \times (Cl + O_3$	$\rightarrow ClO + O_2)$	R2.31
$2O_3$	$\rightarrow 3O_2$	**NET, R2.32**

Furthermore, during winter a strong westerly circulation leads to the formation of a vortex over Antarctica, minimising mixing with air from lower latitudes (e.g., WMO, 2003, 2007). Extremely cold temperatures within this vortex (T<$\sim$195 K) favour the the formation of so-called polar stratospheric clouds (PSCs) (e.g., McCormick et al., 1982). PSCs, which may be made up of ice (and/or other) particles (e.g., Toon and Tolbert, 1995), provide a surface for relatively fast heterogeneous reactions to occur. Such reactions can release active chlorine (or bromine) from reservoirs and significantly alter the local ClO/Cl_y (BrO/Br_y) ratio. For example, the reaction of $ClONO_2$ and HCl (R2.33) takes place on ice particles and results in the release of gaseous Cl_2 (e.g., Solomon et al., 1986; Molina et al., 1987). When sunlight returns in spring, photolysis of Cl_2 releases Cl_x (R2.34).

$$\mathrm{ClONO_2(g) + HCl(s)} \rightarrow \mathrm{Cl_2(g) + HNO_3(s)} \qquad \text{R2.33}$$

$$\mathrm{Cl_2 + h\nu} \rightarrow \mathrm{Cl + Cl} \qquad \text{R2.34}$$

An important feature of R2.33 is that nitric acid (HNO_3) remains on the PSC surface. It may then be removed from the stratosphere as particles sediment under gravity (e.g., Toon et al., 1986). Ultimately for O_3, this *denitrification* exacerbates depletion as, available nitrogen which could reform the $ClONO_2$ reservoir, is reduced. Other known heterogeneous reactions include R2.35 and R2.36 (e.g., Solomon, 1999), whose products HOCl and $ClNO_2$ also release Cl_x upon photolysis.

Figure 2.3 shows enhanced ClO and evidence for denitrification and dehydration (associated with PSCs), as observed from the ER-2 high-altitude aircraft over Antarctica.

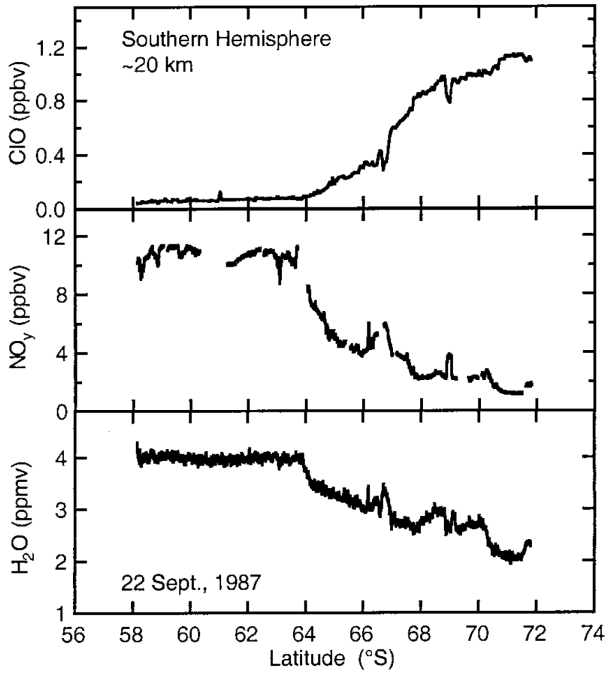

FIGURE 2.3: Observations and latitudinal dependence of ClO, NO_y and H_2O from ER-2 aircraft flight over Antarctica during September 1987. Figure taken from Solomon (1999).

$$\mathrm{ClONO_2(g) + H_2O(s) \rightarrow HOCl(g) + HNO_3(s)} \qquad \text{R2.35}$$

$$\mathrm{N_2O_5(g) + HCl(s) \rightarrow ClNO_2(g) + HNO_3(s)} \qquad \text{R2.36}$$

Similar heterogeneous reactions involving brominated species are also known (e.g. R2.37-R2.39) (e.g., Lary et al., 1996; Erle et al., 1998).

$$\mathrm{BrONO_2(g) + H_2O(s) \rightarrow HOBr(g) + HNO_3(s)} \qquad \text{R2.37}$$

$$\mathrm{BrONO_2(g) + HCl(s) \rightarrow BrCl(g) + HNO_3(s)} \qquad \text{R2.38}$$

$$\mathrm{HOBr(g) + HCl(s) \rightarrow BrCl(g) + H_2O(s)} \qquad \text{R2.39}$$

As brominated reservoirs are short-lived with respect to analogous chlorinated species, heterogeneous chemistry has a smaller impact on Br_y partitioning between reactive and reservoir form. However, these reactions do significantly alter the partitioning of Cl_y. For example, the hydrolysis of $\mathrm{BrONO_2}$ (R2.37) leads to increased OH, which in turn reduces the HCl lifetime and reduces the HCl/ClO ratio (Figure 2.4) (Lary et al., 1996).

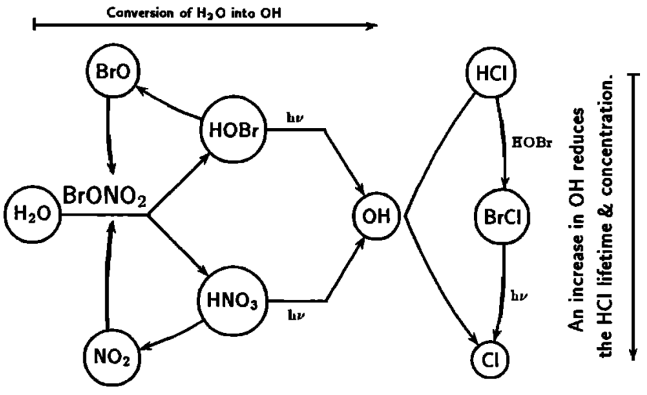

FIGURE 2.4: Schematic of heterogeneous $\mathrm{BrONO_2}$ hydrolysis and formation of OH. Figure taken from Lary et al. (1996).

These reactions, which ultimately lead to enhanced ClO, are also important in the mid-latitude lower stratosphere, where they can occur on sulphate aerosols (e.g., Erle et al., 1998). The loading of which is generally greatly enhanced in the stratosphere following large volcanic eruptions (e.g. Mount Pinatubo, 1991). The gas-phase and heterogeneous processes discussed above have all contributed to observed stratospheric O_3 depletion and the seasonal formation of the Antarctic Ozone Hole.

Figure 2.5 shows the long-term trend in total column O_3 over Antarctica in October. The Ozone Hole, which can be defined as the region where the total column is less than 220 DU, first appeared in the 1980s. Prior to this, significant depletion events were not observed as the stratospheric concentration of reactive halogens was likely too low. In the early 2000s, it covered an area of around 25 million km^2 (WMO, 2011). The onset of the Antarctic Ozone Hole begins in winter, as isolated polar air is chemically preconditioned by the gas-phase and heterogeneous processes discussed previously. In spring, as sunlight returns and photolysis reactions release Cl_x, extensive O_3 depletion begins. However, as temperatures gradually rise, PSC formation ends and heterogeneous chemistry is limited. The polar vortex also weakens allowing for an influx of O_3-rich air from lower latitudes. The Ozone Hole is thus displaced by around December (WMO, 2007, 2011).

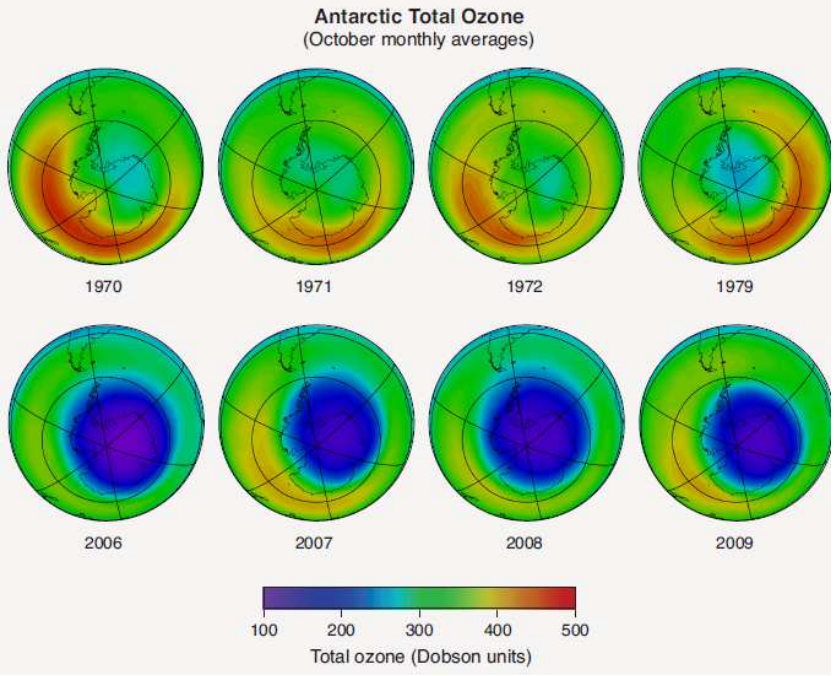

FIGURE 2.5: Long-term changes in the mean October total ozone column (DU) over Antarctica from satellite observations. Figure taken from WMO (2011).

2.2.4 Recent Trends and Recovery

Since the early 1980s, observations have shown a decrease in total global O_3, relative to a baseline period of 1964-1980 (Figure 2.6). This decrease, which peaked at ∼5% below the baseline in the early 1990s, has been due to anthropogenic emissions of ODS (WMO, 2011). O_3 loss was exacerbated following the 1991 eruption of Mount Pinatubo as stratospheric aerosol loading increased and heterogeneous halogen activation was enhanced (e.g., Hofmann and Solomon, 1989).

As the abundance of halogenated ODS declines under the terms of the Montreal Protocol (and amendments), global O_3 is expected to recover in coming decades. The evolution of 21st century O_3 will also depend on other, less certain factors. For example, stratospheric cooling, associated with rising carbon dioxide (CO_2) levels (e.g., Forster et al., 2007), will likely impact O_3 photochemistry and may impact PSC formation. Changes to stratospheric dynamics (e.g. Deushi and Shibata, 2011), such as a strengthening of the Brewer-Dobson circulation (e.g., Young et al., 2012), will likely impact the global distribution of O_3. Proposed *geoengineering* projects, such as injection of sulphate aerosol in to the stratosphere, are also likely to impact stratospheric composition, including O_3. Examining these complex feedbacks is an area of active research involving chemistry-climate models forced with projected future greenhouse gas loading (CCMVal, 2010).

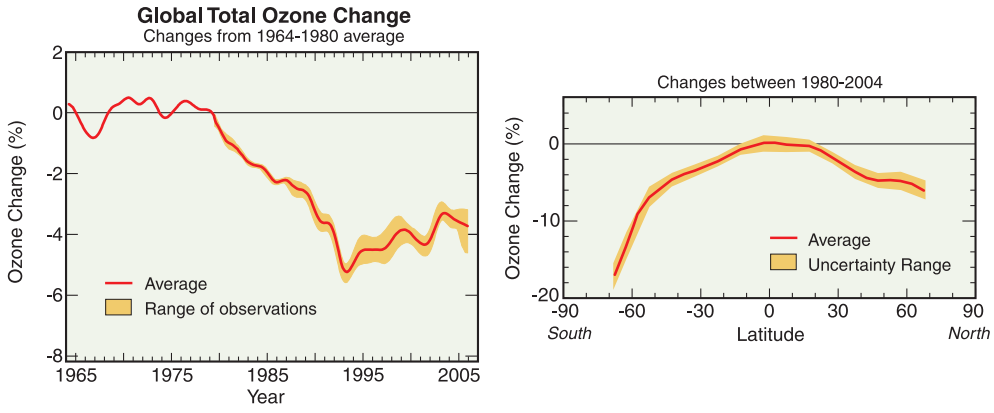

FIGURE 2.6: Global total ozone trends from compiled satellite observations. The left panel shows the mean annual change (%) with respect to the average of the period 1964-1980. The impact of seasonality and solar variability has been removed from observations. The right panel shows how observed ozone change varies with latitude for the period 2005-2009. Figure adapted from WMO (2011).

2.3 Long-lived Halogenated Source Gases

There are a variety of halogen-containing source gases (SGs) that are emitted at Earth's surface. Some of these have been briefly mentioned in earlier sections. Here, the discussion is concerned with long-lived gases only. These gases are generally inert in the troposphere and thus a large fraction of the gas emitted at the surface may reach the stratosphere. For the discussion here, "long-lived" refers to a gas with a surface lifetime of greater than approximately 6 months. However, many of the gases discussed have atmospheric lifetimes of many decades. As the primary focus of this thesis is stratospheric bromine, the discussion is weighted towards brominated SGs and their trends, although, a brief discussion on CFCs and other chlorinated gases is also included.

2.3.1 Chlorinated Species

CFCs, first synthesised in the early 20th century, have an exclusively anthropogenic source. They contain chlorine and fluorine atoms (e.g. CFC-13, CCl_2F_2 and CFC-12, CF_2Cl_2) and have become synonymous with O_3 depletion. Due to their long atmospheric lifetime (decades) (Lovelock and Maggs, 1973), CFCs may reach the stratosphere where, upon photolysis, Cl_y is released in-situ (R2.40). As previously discussed, both gas-phase and heterogeneous chemistry can then partition Cl_y among reservoir and reactive forms (Cl_x).

$$CF_2Cl_2 + h\nu \rightarrow CF_2Cl + Cl \qquad \text{R2.40}$$

The production of CFCs has been phased out under the terms of the Montreal Protocol and its amendments (WMO, 2003, 2007, 2011). As a result, the atmospheric burden of these gases is now in decline. However, the growth rate of hydrochlorofluorocarbons (HCFCs), CFC replacement compounds, is presently increasing. For $CHClF_2$ (HCFC-22), its growth in the period 2007-2008 was ∼7.6-10 ppt yr^{-1} (Montzka and Reimann, 2011). For comparison, CCl_2F_2 (CFC-12) decreased at a rate of -0.3-2.9 ppt yr^{-1} for the same period. CFCs and HCFCs, along with carbon tetrachloride (CCl_4) and methyl chloroform

(CH_3CCl_3), together exert a positive radiative forcing of climate of ∼0.3 W m^{-2} (WMO, 2011). Therefore, their phaseout under the Montreal Protocol will be beneficial for both global O_3 recovery and also global warming.

Figure 2.7 shows the derived total organic chlorine in the troposphere from source gas observations during the 1990-2010 period. Clearly, the near present day abundance is significantly lower than the peak observed around 1995. However, the decline has slowed in recent years due to the accelerated growth of HCFCs. At present, these compounds only account for ∼7.5% of the total organic chlorine (Montzka and Reimann, 2011) and their production is due to be phased out under the Montreal Protocol.

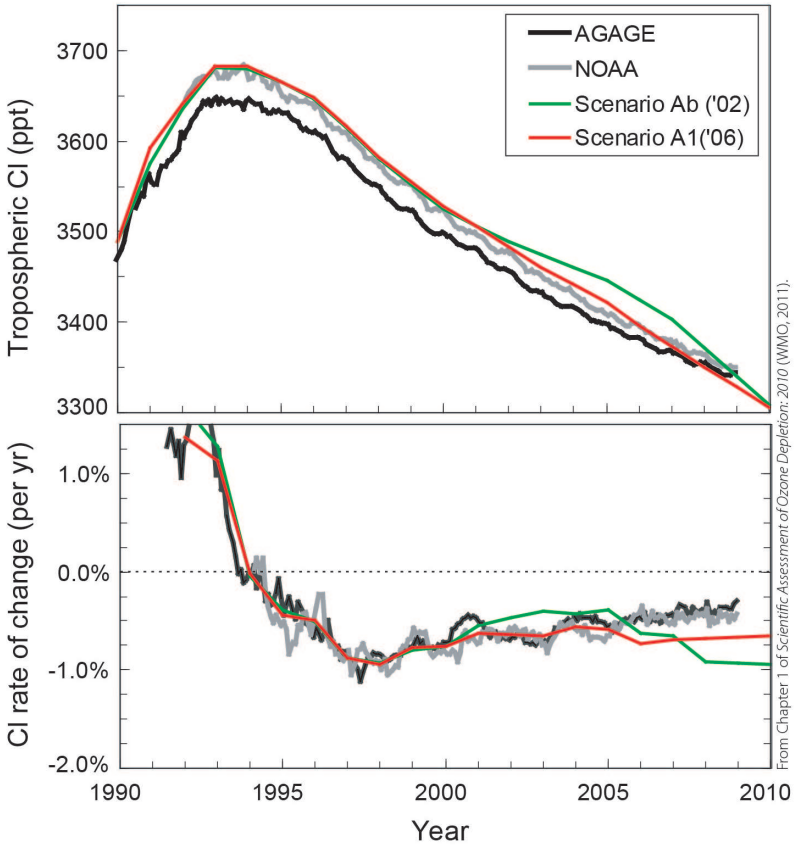

FIGURE 2.7: Time series of tropospheric organic chlorine (ppt) from source gas measurements from NOAA (red) and AGAGE (black) global measurement networks. Source gas measurements include CFCs, HCFCs, CH_3CCl_3, CCl_4 and $CBrClF_2$ (Halon 1211). An assumed contribution of 550 ppt from methyl chloride (CH_3Cl) and 80 ppt from chlorinated very short-lived substances (e.g. chloroform, $CHCl_3$) is added. Figure taken from Montzka and Reimann (2011).

2.3.2 Brominated Species

Major brominated SGs include the anthropogenic halons (e.g. Halon 1211, $CBrClF_2$), which were used in fire extinguishers, and methyl bromide (CH_3Br), the most abundant brominated SG. These long-lived species are a significant source of stratospheric Br_y and are summarised with their atmospheric lifetime in Table 2.1.

TABLE 2.1: Long-lived brominated source gases and their lifetime (years). Data from Table 1.3 of Montzka and Reimann (2011).

Source Gas	Formula	Source [1]	Lifetime (years)
Methyl bromide	CH_3Br	N(A)	0.8
Halon-1301	$CBrF_3$	A	65
Halon-1211	$CBrClF_2$	A	16
Halon-1202	CBr_2F_2	A	2.9
Halon-2402	$C_2Br_2F_4$	A	20

[1] Source either purely natural (N), anthropogenic (A) or with a minor anthropogenic component N(A).

Major natural sources of CH_3Br include emissions from the ocean, freshwater wetlands and coastal salt marshes (Law and Sturges, 2007). Anthropogenic industrial emissions, which accounted for ∼25-35% of the total annual CH_3Br source, are now controlled under the Montreal Protocol. Due to the phase out of emissions, the observed global mean CH_3Br surface mixing ratio was ∼7.3-7.5 ppt in 2008, down from ∼9.2 ppt for the 1996-1998 period (Yvon-Lewis et al., 2009; Montzka and Reimann, 2011). These declines have been attributed to decreasing industrial production. However, significant uncertainties remain in atmospheric CH_3Br budget calculations (e.g., Reeves, 2003). Based on the present understanding of sources and sinks, the latter seems larger by ∼35 Gg yr^{-1} (∼20% of total emissions), indicating a significant missing source (Yvon-Lewis et al., 2009). Uncertainties in the temporal variability of natural CH_3Br sources, along with uncertainties in anthropogenic stockpiles, make a detailed budget calculation challenging.

Figure 2.8 shows a time series of the contribution of four major halons (see Table 2.1) to tropospheric bromine. This contribution, which increased sharply throughout the latter part of the 20th century, is no longer increasing despite, the tropospheric abundance of some halons (e.g., halon-1301) continuing to rise (see Section 2.3.3 also).

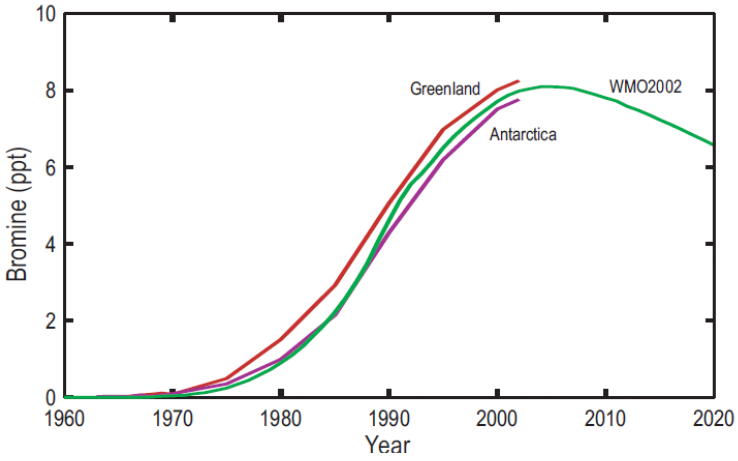

FIGURE 2.8: Time series of tropospheric bromine (ppt) from 4 halons (1301, 1211, 1202 and 2402) calculated using model-derived emissions that best fit recorded firn air data from Greenland and Antarctica (Reeves et al., 2005). Those estimates are compared with model-dervied estimates (green) for the Sothern Hemisphere using the Ab halon emission scenario of WMO (2003). Figure from Clerbaux and Cunnold (2007).

Figure 2.9 shows a time series of total tropospheric organic bromine based on global mean observations of CH_3Br and the halons. It shows a steady decline from a peak abundance of ∼16.7 ppt of bromine observed in 1998. By 2008, the total had reduced to ∼15.7 (±0.2) ppt - a reduction of ∼1.0 ppt (Montzka and Reimann, 2011).

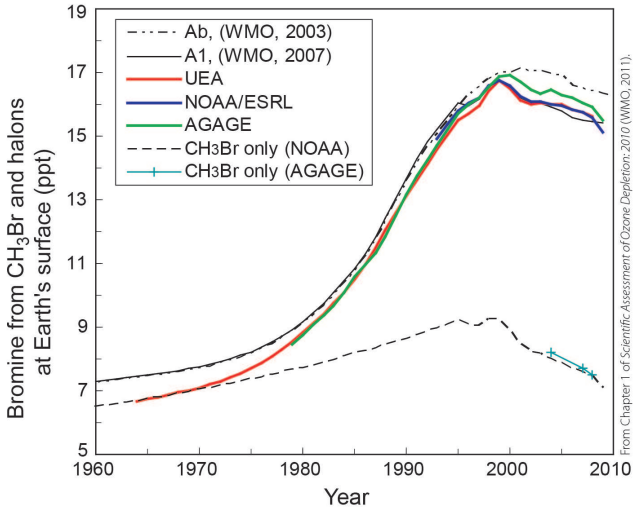

FIGURE 2.9: Time series of total tropospheric organic bromine (ppt) calculated from observations of the the long-lived gases CH_3Br and the halons. Figure taken from Montzka and Reimann (2011).

2.3.3 Trends

The temporal evolution of total chlorine and total bromine in the troposphere was shown in Figures 2.7 and 2.9. The long-term trends in the mean surface mixing ratio of individual halogen SGs is shown in Figure 2.10. The observed data here is from the National Ocean and Atmospheric Administration (NOAA) and also the Advanced Global Atmospheric Gases Experiment (AGAGE). The consistency between reported surface values is generally good. For example, the observed 2008 CFC-12 surface mixing ratio by both groups agree to within 5.0 ppt. Similarly, for CFC-11 they agree to within 1.4 ppt (Montzka and Reimann, 2011).

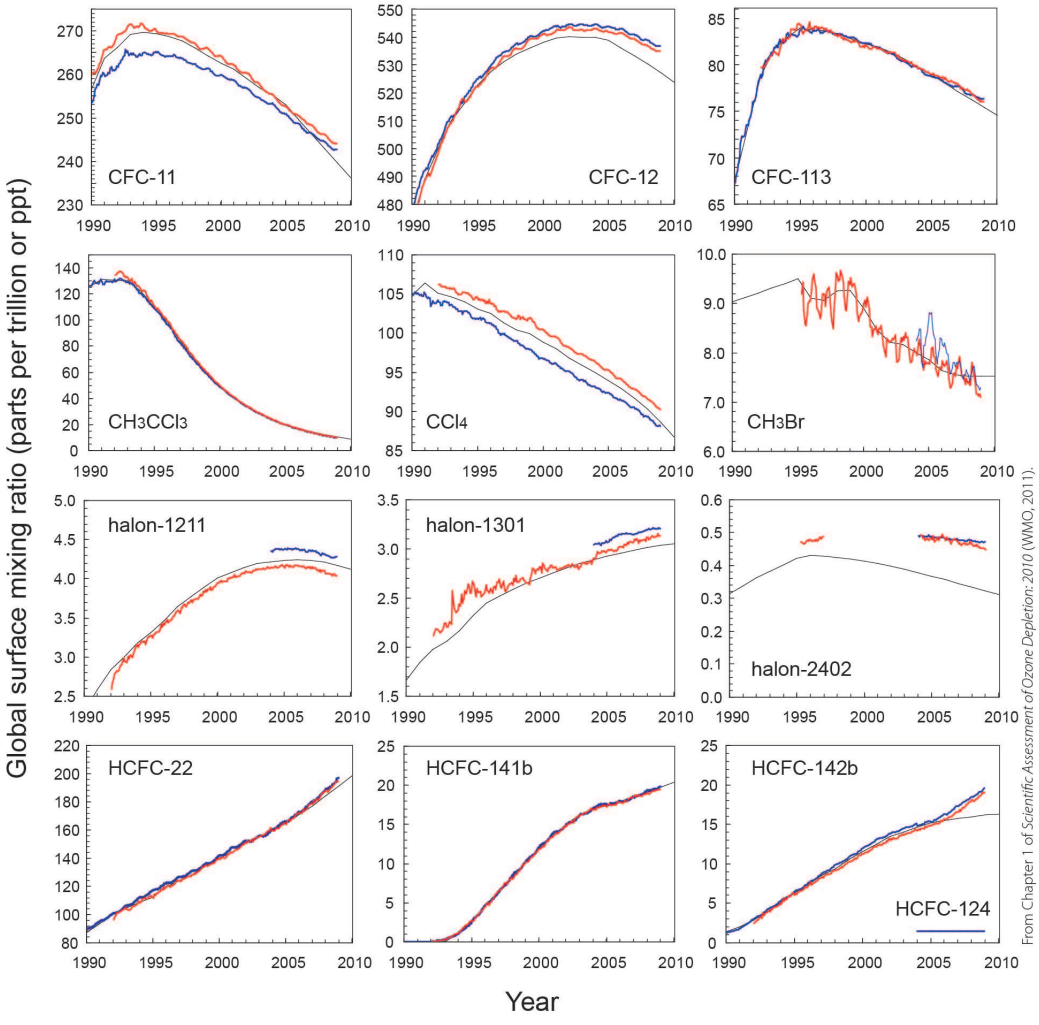

FIGURE 2.10: Mean observed global surface mixing ratio (ppt) of long-lived halogenated source gases. Red and blue lines denote observations from the NOAA and the AGAGE ground-based networks, respectively. Figure taken from Montzka and Reimann (2011).

2.4 Very Short-lived Species

Very short-lived species (VSLS) are loosely defined as gases whose atmospheric lifetime is less than approximately 6 months (Law and Sturges, 2007). Here, the general term *VSLS* refers to both very short-lived (VSL) source gases (SGs) and also their degradation product gases (PGs). In addition to long-lived SGs (Section 2.3), halogen-containing VSLS are thought to be a significant source of stratospheric Cl_y and Br_y.

VSL SGs (e.g. $CHBr_2Cl$) are known to deliver their halogen content to the stratosphere in two ways. Firstly, assuming the SG escapes tropospheric oxidation, it may enter the stratosphere, whereby on degradation Cl_y and/or Br_y is released in situ - *source gas injection* (SGI). This process is effectively the same for the long-lived gases discussed in Section 2.3. Secondly, some VSL SGs exhibit significant tropospheric gradients. Following tropospheric degradation, a variety of both organic and inorganic PGs (i.e. Br_y) may be formed. These halogen-containing PGs may also potentially reach the stratosphere - *product gas injection* (PGI) (e.g, Ko and Poulet, 2003; Law and Sturges, 2007). The relative importance of the SGI and PGI pathways differs between SGs. The efficiency of each pathway depends also on background chemical/dynamical conditions. These processes are discussed further in Sections 2.4.2 and 2.4.3.

The local lifetime of a VSL SG (τ_{local}) may be expressed using equation 2.1 (E2.1). Here, τ_{OH} and $\tau_{h\nu}$ are the lifetimes with respect to oxidation with OH and to photolysis.

$$\tau_{\mathrm{local}}^{-1} = \tau_{\mathrm{OH}}^{-1} + \tau_{\mathrm{h}\nu}^{-1} \qquad \text{(E2.1)}$$

Table 2.2 shows known mixed Br/Cl-containing VSL SGs and their local lifetimes at the surface. Note, some VSL SGs also contain iodine; e.g. methyl iodide (CH_3I) and di-iodomethane (CH_2I_2). These species are typically shorter-lived than most Br and Cl-containing SGs and likely supply only a small (sub ppt) amount of inorganic iodine (I_y) to the lower stratosphere (e.g. Butz et al., 2009). O_3 loss involving reactive I_y species (e.g. IO) is important in the troposphere (e.g., Ordóñez et al., 2012) but only of minor importance for the stratosphere (Solomon, 1999).

TABLE 2.2: Very short-lived halogen-containing source gases and their local lifetime (days). Adapted from Table 2.1 of Law and Sturges (2007).

Source Gas	Formula	Source [1]	Lifetime (days) [2]
Bromoform	$CHBr_3$	N(A)	26
Dibromomethane	CH_2Br_2	N	120
Dibromochloromethane	$CHBr_2Cl$	N(A)	69
Bromodichloromethane	$CHBrCl_2$	N(A)	78
Bromochloromethane	CH_2BrCl	N	150
Ethyl bromide	C_2H_5Br	A	34
Ethylene dibromide (EDB)	CH_2BrCH_2Br	A	55
n-propyl bromide (nPB)	n-C_3H_7Br	A	13

[1] Source either purely natural (N), anthropogenic (A) or with a minor anthropogenic component N(A).

[2] Local lifetime calculated using equation 2.1, assuming [OH] = 1×10^6 molecule cm^{-3}, T=275 K and a globally/seasonally averaged solar flux for 5 km altitude.

For the remainder of this chapter, emphasis is placed on primary Br-containing VSLS, bromoform ($CHBr_3$) and dibromomethane (CH_2Br_2).

2.4.1 Emissions

Emissions of Br-containing VSL SGs are predominately of natural origin. Observations have shown elevated mixing ratios in the marine boundary layer (MBL) suggesting a significant oceanic source (e.g., Quack and Wallace, 2003) that is thought to represent ∼90-95% of the total global flux (Law and Sturges, 2007). Primary producers of VSLS include marine phytoplankton, macro-algae (e.g. seaweed, Figure 2.11) and certain terrestrial vegetation (e.g. CH_3I is emitted from rice). At present, both the qualitative and quantitative understanding of VSLS sources is limited.

FIGURE 2.11: Producers of biogenic halocarbons - phytoplankton (left) & seaweed (right).

The most abundant Br-containing VSLS are $CHBr_3$ and CH_2Br_2. Ocean surface waters have been observed to be saturated with these gases (Butler et al., 2007). Large sea-air fluxes may be associated with regions of upwelling, such as above the the equator and at ocean fronts (Quack et al., 2004; Butler et al., 2007). However, the importance of these regions is unclear at present (Quack et al., 2007). Observations have also highlighted the importance of the Pacific Ocean (e.g., Palmer and Reason, 2009). Butler et al. (2007) estimate the Pacific accounts for ∼64% and ∼40% of total $CHBr_3$ and CH_2Br_2 emissions, respectively. Numerous studies have also identified coastal waters to be a particularly important source region (e.g., Carpenter and Liss, 2000; Quack and Wallace, 2003). The relative contribution from open ocean and coastal emissions is uncertain, as is the total global flux for most VSL SGs. However, a compiled range of 430-1400 Gg Br yr^{-1} and 570-280 Gg Br yr^{-1} is reported by Montzka and Reimann (2011) for $CHBr_3$ and CH_2Br_2 (summarised in Table 2.3).

Anthropogenic emissions of $CHBr_3$ and CH_2Br_2 are expected to be small on a global scale. However, water chlorination treatment may represent a significant regional source of $CHBr_3$ (Law and Sturges, 2007). Some VSLS do have a predominately anthropogenic source; e.g. *n*-propyl bromide (*n*-C_3H_7Br, nPB), *i*-propyl bromide (*i*-C_3H_7Br, iPB), ethyl bromide (C_2H_5Br) and ethylene dibromide (CH_2BrCH_2Br, EDB). These gases are used for a variety of industrial applications (metal degreasing, electronic part cleaning, flame retardants) and observations are sparse (e.g., Pratt et al., 2000; Low et al., 2003).

TABLE 2.3: Compiled estimates of $CHBr_3$ and CH_2Br_2 emissions (Gg Br yr^{-1}) for open ocean, coastal and global regions based on observations and modelling. Adapted from Table 1.8 of Montzka and Reimann (2011).

	$CHBr_3$ (Gg Br yr^{-1})			**$CHBr_3$ (Gg Br yr^{-1})**		
Reference	Global	Ocean	Coastal	Global	Ocean	Coastal
Butler et al. (2007)	800	150	650	280	50	230
Carpenter et al. (2009)	-	-	200	-	-	-
Liang et al. (2010)	430	260	170	57	34	23
O'Brien et al. (2009)	820 [1] (1400 [2])	-	-	-	-	
Palmer & Reason (2009)	-	120 [3]	-	-	-	-
Yokouchi et al. (2005)	820	-	-	-	-	-
Warwick et al. (2006)	560	280	280	100	-	-

[1] Scaled to CH_2Br_2 emissions from Ko and Poulet (2003)

[2] Scaled to CH_2Br_2 emissions from Warwick et al. (2006)

[3] Tropical ocean only

2.4.2 Troposphere-Stratosphere Transport

As discussed, VSLS contribute to stratospheric halogen loading via both SGI and PGI. The efficiency of these pathways depends upon the photochemical loss rate of SGs (via reaction with OH or photolysis), the rate of removal of PGs (via wet deposition) versus the timescale for troposphere-stratosphere transport. Figure 2.12 shows the key troposphere-stratosphere transport pathways for VSLS via the tropical tropopause layer (TTL). The TTL, which is a transition layer between the troposphere and stratosphere (e.g., Fueglistaler et al., 2009), is defined here as between the level of main convective outflow (∼12 km) and the cold-point tropopause (CPT, ∼17 km, θ ∼380 K). The *upper TTL* is defined as the layer beyond the level of zero radiative heating (z_0, θ ∼360 K), where the net large-scale motion is dominated by radiative ascent (Law and Sturges, 2007).

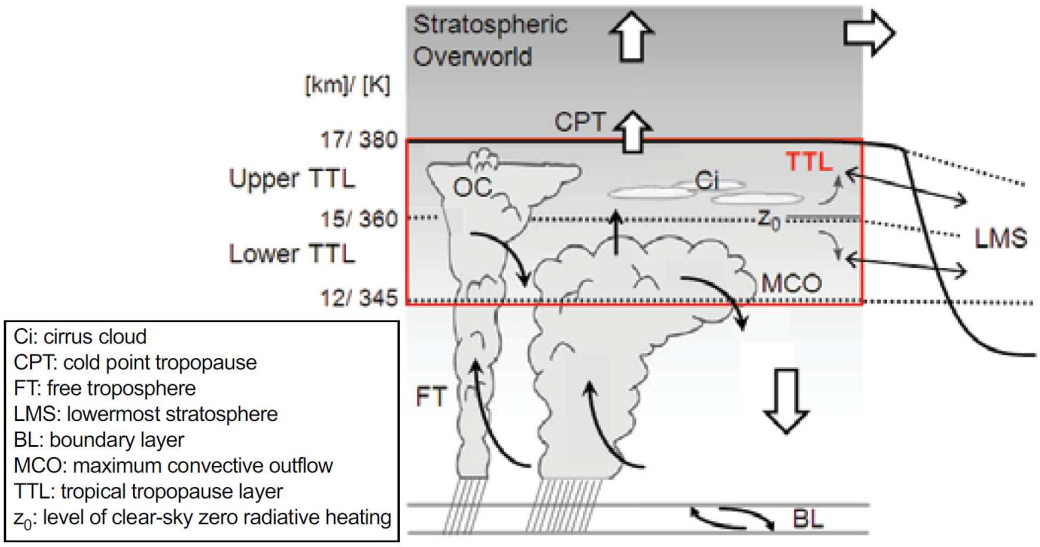

FIGURE 2.12: Key troposphere-stratosphere transport pathways for short-lived source and product gases. The tropopause is indicated by the bold black line and lies at ∼17 km or at the θ=380 K surface. Figure taken from Montzka and Reimann (2011).

Strong convective uplift allows even particularly short-lived VSLS (e.g. CH_3I) to reach the TTL, where transport to the stratosphere is then possible. The stratospheric SGI of VSLS is thus expected to be largest if their emissions coincide with regions of deep convection and upwelling. The Western Pacific, which is a strong convective source region, has been identified as important for the transport of VSLS to the TTL. Figure 2.13 shows the

calculated relative contribution of various geographical regions to the amount of a $CHBr_3$-like idealised tracer (fixed 20 day lifetime) in the tropical upper troposphere and lower stratosphere (Aschmann et al., 2009).

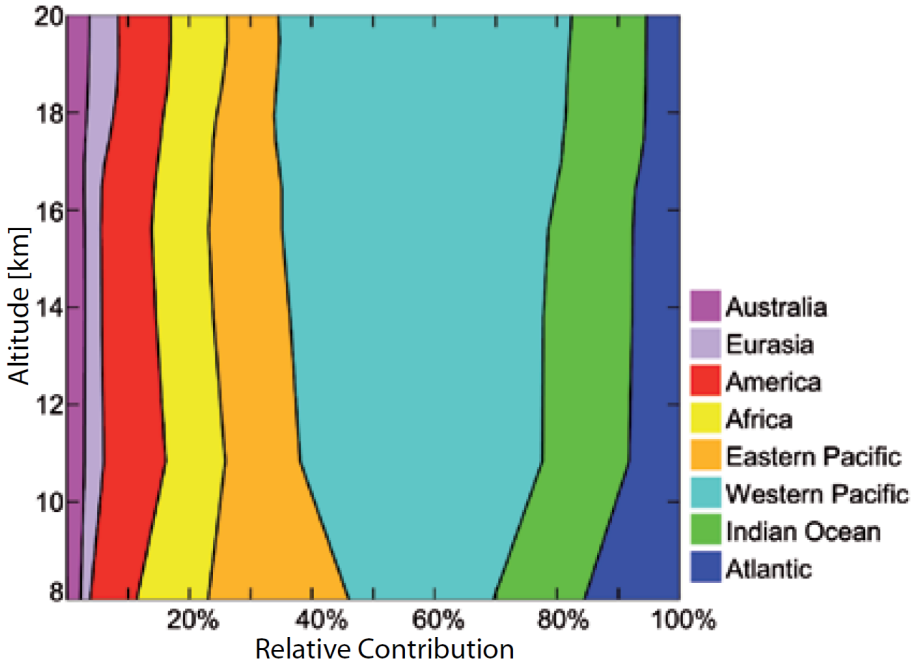

FIGURE 2.13: Relative contribution (%) of different geographical regions to the amount of a $CHBr_3$-like idealised tracer with a 20-day lifetime in the tropical atmosphere. From the 3-D chemical transport model study of Aschmann et al. (2009). Figure taken from (Montzka and Reimann, 2011).

Once in the TTL, the efficiency of the stratospheric SGI of VSLS varies with season (e.g., Aschmann et al., 2009; Gettelman et al., 2009) and is most rapid during northern hemisphere (NH) winter (Fueglistaler et al., 2009; Krueger et al., 2009). Residence times in the TTL vary with altitude with a range of 25-45 days estimated for the upper layer from Lagrangian trajectory calculations (Montzka and Reimann, 2011). While rapid transport in moist convection acts to enhance the stratospheric SGI of VSLS, the associated precipitation may remove soluble PGs (e.g. HBr, HOBr) from the atmosphere (e.g., Crutzen and Lawrence, 2000). Furthermore, the interaction of PGs with ice and other aerosols in the TTL is curently poorly understood (Aschmann et al., 2011). These processes are poorly represented in global models. In addition, observations of brominated PGs in the TTL are limited to BrO (Dorf et al., 2008). It is currently uncertain if organic PGs such as CBr_2O and CHBrO, formed following the degradation of $CHBr_3$ and CH_2Br_2, make a significant contribution to the total PGI from VSLS (WMO, 2003, 2007).

2.4.3 Bromine Loading

In recent years, quantifying the VSLS contribution to stratospheric inorganic bromine (Br_y^{VSLS}) has been the subject of numerous observational and modelling studies. Observation-based estimates generally use measurements of stratospheric BrO from either ground-based (e.g., Theys et al., 2007; Hendrick et al., 2008), baloon-borne (e.g., Dorf et al., 2006) or satellite (e.g., Sinnhuber et al., 2005; Sioris et al., 2006) platforms, in order to infer Br_y^{VSLS}. Figure 2.14 shows a range of previously published estimates. In general, satellite estimates show the largest range with significant uncertainty due to error on retrieved BrO profiles (e.g. McLinden et al., 2010). Overall, Montzka and Reimann (2011) report a best estimate based on observation-based studies of 6 (3-8) ppt. Explicit treatment of VSLS in global models can also be used to quantify Br_y^{VSLS} (e.g., Warwick et al., 2006; Liang et al., 2010) and allow for a detailed assessment of the SGI and PGI contributions.

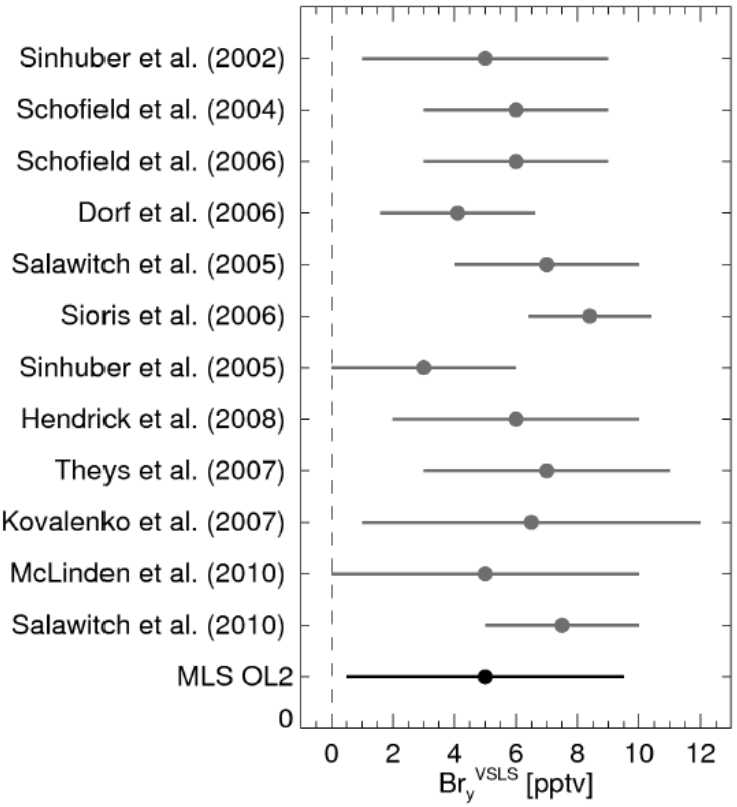

FIGURE 2.14: Range of previous published estimates of stratospheric Br_y^{VSLS} from studies which have used observations of BrO. MLS OL2 refers to the study of Millán et al. (2012), from which this figure was taken.

2.4.4 Impact on Ozone

Numerous model studies have attempted to quantify stratospheric bromine loading due to VSLS. However, their impact on global O_3 has been quantified by relatively few studies. Using the 2-D AER chemical transport model (CTM), Salawitch et al. (2005) found addition of Br_y^{VSLS} significantly enhanced O_3 loss through the BrO-HO_2 coupled loss cycle (R2.41-2.45) (Lary et al., 1996). The impact was found to be largest in the lower stratosphere (below ∼14 km) where the BrO-HO_2 cycle competes with O_3 loss from pure HO_x chemistry (HO_2 + O_3) (Salawitch et al., 2005).

BrO-HO_2 Cycle

$BrO + HO_2$	$\rightarrow HOBr + O_2$	R2.41
$HOBr + h\nu$	$\rightarrow OH + Br$	R2.42
$Br + O_3$	$\rightarrow BrO + O_2$	R2.43
$OH + O_3$	$\rightarrow HO_2 + O_2$	R2.44
$2O_3$	$\rightarrow 3O_2$	**NET, R2.45**

In addition, stratospheric Br_y^{VSLS} is known to enhance the BrO-ClO O_3 loss cycle (previously discussed). Global model studies have shown this impact to be largest during periods of elevated aerosol loading (Salawitch et al., 2005; Feng et al., 2007; Sinnhuber et al., 2009), when significant heterogeneous halogen activation can occur. Therefore, bromine-containing VSLS may enhance O_3 loss from the inorganic chlorine released from CFCs and other chlorine-containing source gases.

Using the SLIMCAT 3-D CTM, Feng et al. (2007) report a 10 DU decrease in the mid-latitude O_3 column due to a modelled 5.0 ppt of Br_y^{VSLS} in the lower stratosphere. The modelled decrease was found to be largest following the 1991 eruption of Mount Pinatubo. During periods of background aerosol loading, the impact of Br_y^{VSLS} on stratospheric O_3 has been reported by these modelling studies to be small. However the inclusion of Br_y^{VSLS} in these models improves the agreement between modelled and observed O_3 trends.

Chapter 3

A Scheme for the Tropospheric Degradation of $CHBr_3$ & CH_2Br_2

3.1 Introduction

In previous modelling work, the production of inorganic bromine (Br_y) following the degradation of a very short-lived (VSL) source gas (SG), for example bromoform ($CHBr_3$), has been assumed to be instantaneous (e.g., Sinnhuber and Folkins, 2006; Warwick et al., 2006). In reality, this degradation proceeds via various bromine-containing organic intermediates. For $CHBr_3$, the major organic products are thought to be carbonyl dibromide (CBr_2O) and formyl bromide (CHBrO), when loss is initiated by OH and photolysis, respectively (Ko and Poulet, 2003). Kinetic data on these product gases (PGs) is limited and there are no atmospheric observations. If organic PGs such as CBr_2O and CHBrO are long-lived enough, or longer lived than Br_y with respect to wet deposition, their neglect in global models could underestimate the stratospheric product gas injection (PGI) pathway. This may ultimately lead to a low bias in estimates of the total contribution of very short-lived species (VSLS) to stratospheric Br_y. This has been outlined as a major uncertainty in previous World Meteorological Organization (WMO) ozone assessments (Ko and Poulet, 2003; Law and Sturges, 2007).

The remainder of this chapter outlines a chemical scheme to describe the tropospheric degradation of $CHBr_3$ and also dibromomethane (CH_2Br_2); the two most abundant brominated VSLS (Ko and Poulet, 2003; Law and Sturges, 2007). Reasonable mechanistic and kinetic assumptions have been made and are discussed. Kinetic data are either taken from (Sander et al., 2006) (hereafter JPL06) or the Leeds Master Chemical Mechanism (hereafter MCM, see http://mcm.leeds.ac.uk/MCM/). Section 3.2 contains a detailed description of the $CHBr_3$ scheme. Similarly, the CH_2Br_2 scheme is discussed in Section 3.3. A summary of this work is in Section 3.4.

The degradation scheme for $CHBr_3$ was initially developed during the candidate's masters research. A preliminary scheme for CH_2Br_2 scheme was also developed but not implemented during that project. For completeness, and as both schemes are an integral part of this research project, both are discussed here. The work contained in this chapter has been published in the journal Atmospheric Chemistry and Physics (ACP) (Hossaini et al., 2010).

3.2 Degradation of Bromoform

The degradation of $CHBr_3$ has been examined in previous theoretical studies (McGivern et al., 2002, 2004). The local lifetime of $CHBr_3$ at the surface is ∼26 days with photolysis being the dominant sink (Ko and Poulet, 2003). The degradation scheme developed in this work considers 7 organic species; $CHBr_3$, CBr_3O_2, $CHBr_2O_2$, CBr_3OOH, $CHBr_2OOH$, CBr_2O and CHBrO. The kinetic data used are listed in Table 3.1 and the scheme is depicted in Figure 3.1.

3.2.1 Removal of Source Gas

The scheme assumes removal of $CHBr_3$ occurs via reaction with OH/Cl radicals and also, more rapidly, by photolysis (reactions R3.1-R3.3). The rates of reaction with OH and Cl ($k_3.1$, $k_3.2$) are calculated using the JPL06 recommended temperature-dependent expressions. Note, oxidation by Cl is only of minor importance but is included for completeness (Ko and Poulet, 2003). The rate of photolysis ($j_3.3$) is calculated using JPL06 absorption

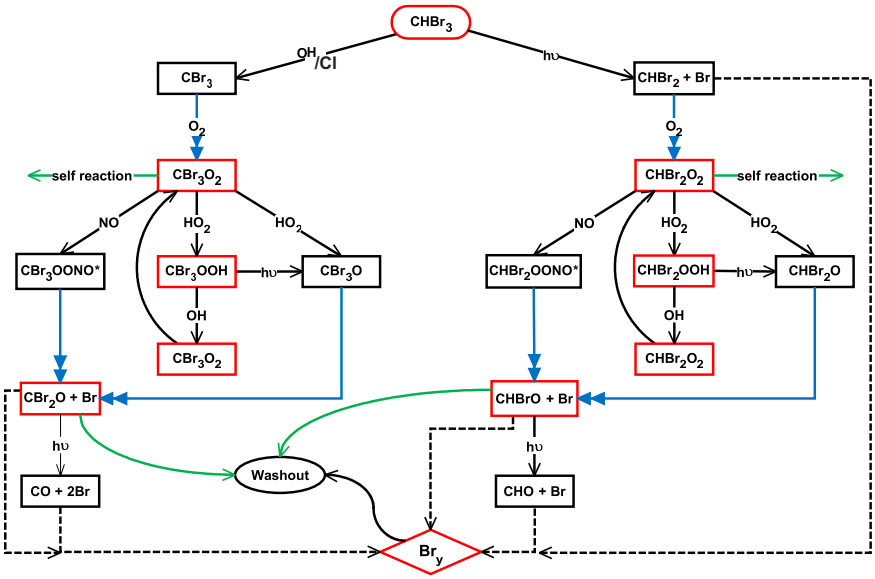

FIGURE 3.1: Scheme for the tropospheric degradation of $CHBr_3$. Red boxes denote the 7 organic species (1 SG + 6 PGs) considered directly in the scheme, i.e. species whose production and loss are both calculated explicitly (see text). Black boxes denote species which are sufficiently short-lived for exclusion from the scheme. Blue lines denote rapid reactions, dashed lines indicate the production of Br_y and green denotes reactions not considered in the present scheme. See Table 3.1 for a description of kinetic assumptions.

cross section data along with a parameterisation for their temperature dependence (Moortgat et al., 1993). The quantum yield for bromine (Br) atoms following R3.3 is assumed to be unity. It is also assumed that the immediate products of reactions R3.1-R3.3 (CBr_3 and $CHBr_2$) will be rapidly oxidised under tropospheric conditions.

$$CHBr_3 + OH\ (+O_2) \rightarrow CBr_3O_2 + H_2O \qquad \text{R3.1}$$

$$CHBr_3 + Cl\ (+O_2) \rightarrow CBr_3O_2 + HCl \qquad \text{R3.2}$$

$$CHBr_3 + h\nu\ (+O_2) \rightarrow CHBr_2O_2 + Br \qquad \text{R3.3}$$

3.2.2 Removal of Peroxy Species

The two peroxy radicals formed in R3.1-R3.3 are assumed to be removed via reaction with NO and HO_2 (R3.4-R3.9). Self-reaction of these species is deemed slow and is therefore not considered here. The CBr_3O_2 + NO reaction (R3.4) is assumed to produce CBr_2O, an

expected major product of bromoform degradation (Ko and Poulet, 2003). Excited intermediates, such as CBr_3OONO^* (not considered here), are expected to fragment rapidly to form CBr_3O, which itself would undergo a rapid decomposition to CBr_2O (e.g. McGivern et al., 2002). The rate constant for R3.4 (k_4) is calculated using the recommended JPL06 expression for the analogous chlorine-containing species CCl_3O_2. Similarly, rate constants for the CBr_3O_2 + HO_2 reactions (k_5, k_6) are assumed equal (i.e. equal branching ratio of products) and taken from the MCM. These reactions produce CBr_2O and the minor hydroperoxide product CBr_3OOH, respectively.

$$CBr_3O_2 + NO \rightarrow CBr_2O + NO_2 + Br \quad \text{R3.4}$$

$$CBr_3O_2 + HO_2 \rightarrow CBr_2O + OH + O_2 + Br \quad \text{R3.5}$$

$$CBr_3O_2 + HO_2 \rightarrow CBr_3OOH \quad \text{R3.6}$$

The reaction of $CHBr_2O_2$ + NO (R3.7) is assumed to produce a second major product of bromoform degradation, namely formyl bromide (CHBrO). Similar to R3.4, it is likely that R3.7 would proceed via an excited intermediate (not considered here as sufficiently short-lived) such as $CHBr_2OOH^*$. The rate constant for this reaction (k_3.7) is assumed equal to the analogous species $CHCl_2O_2$ and taken from the MCM. This is also the case for the $CHBr_2O_2$ + HO_2 reactions (R3.8, R3.9) which produce CHBrO and the minor hydroperoxide, $CHBr_2OOH$, respectively.

$$CHBr_2O_2 + NO \rightarrow CHBrO + NO_2 + Br \quad \text{R3.7}$$

$$CHBr_2O_2 + HO_2 \rightarrow CHBrO + OH + O_2 + Br \quad \text{R3.8}$$

$$CHBr_2O_2 + HO_2 \rightarrow CHBr_2OOH + O_2 \quad \text{R3.9}$$

3.2.3 Removal of Minor End Products

Removal of the two hydroperoxide species produced in R3.6 and R3.9 is assumed to be achieved via reaction with OH (R3.10, R3.12) and also by photolysis (R3.11, R3.13).

Rate constants for the OH reactions are assumed equal to that of the analogous chlorine-containing species, CCl_3OOH and $CHCl_2OOH$, from the MCM. The photolysis rates are calculated using the absorption cross sections of methylhydroperoxide (CH_3OOH). Reaction of these hydroperoxides with OH leads to the reformation of the respective peroxy radical (initially formed in R3.1 and R3.3).

$$\mathrm{CBr_3OOH + OH} \rightarrow \mathrm{CBr_3O_2 + H_2O} \qquad \text{R3.10}$$

$$\mathrm{CBr_3OOH + h\nu} \rightarrow \mathrm{CBr_2O + OH + Br} \qquad \text{R3.11}$$

$$\mathrm{CHBr_2OOH + OH} \rightarrow \mathrm{CHBr_2O_2 + H_2O} \qquad \text{R3.12}$$

$$\mathrm{CHBr_2OOH + h\nu} \rightarrow \mathrm{CHBrO + OH + Br} \qquad \text{R3.13}$$

3.2.4 Removal of Major End Products and Br_y

Removal of the major products of bromoform degradation, CBr_2O and CHBrO, is assumed to occur via photolysis (R3.14, R3.15). For $CBr_2O + h\nu$ we assume a yield of two Br atoms; other photolysis pathways, such as that leading to HBr production, are not considered. Similarly, for $CHBrO + h\nu$ it is assumed the quantum yield for Br atoms is unity. Photolysis rates for both reactions are calculated using the recommended JPL06 cross section data.

$$\mathrm{CBr_2O + h\nu} \rightarrow \mathrm{CO + 2Br} \qquad \text{R3.14}$$

$$\mathrm{CHBrO + h\nu} \rightarrow \mathrm{CHO + Br} \qquad \text{R3.15}$$

In the basic scheme all inorganic bromine species produced are grouped together as Br_y without any further partitioning. For idealised experiments with a chemical transport model (CTM, Chapter 4), Br_y is removed in the troposphere (by washout) according to a fixed uniform loss rate (R3.16). In later chapters, the removal of Br_y is modelled explicitly.

$$\mathrm{Br_y} \rightarrow \text{washout} \qquad \text{R3.16}$$

3.3 Degradation of Dibromomethane

The degradation of CH_2Br_2 has also been examined in previous theoretical studies (McGivern et al., 2004). The surface lifetime of CH_2Br_2 is ∼120 days with oxidation by OH being the dominant loss process (Ko and Poulet, 2003). The scheme developed here (Figure 3.2) considers six organic species, CH_2Br_2, $CHBr_2O_2$, CH_2BrO_2, CHBrO, $CHBr_2OOH$ and CH_2BrOOH. The major products of CH_2Br_2 degradation are expected to be CHBrO and Br_y with $CHBr_2OOH$ being a minor product.

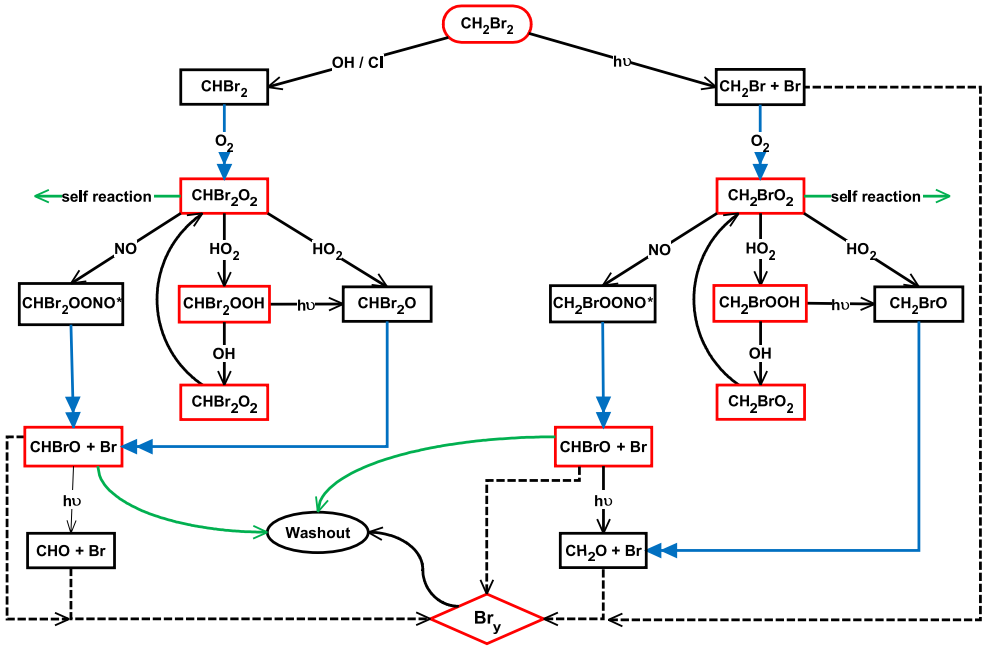

FIGURE 3.2: As Figure 3.1 but for CH_2Br_2.

3.3.1 Removal of Source Gas

The scheme assumes removal of CH_2Br_2 is achieved via reaction with OH/Cl radicals and also, less rapidly, by photolysis (R3.17-3.19). The rates of reaction with OH and Cl ($k_{3.17}$, $k_{3.18}$) are calculated using the JPL06 temperature-dependent expressions. The rate of photolysis ($j_{3.19}$) is calculated using JPL06 absorption cross section data at 295-298 K. For CH_2Br_2, (unlike $CHBr_3$) photolysis is only a minor tropospheric sink. The temperature-dependence of the crosss sections are not considered here. The quantum yield for Br atoms is assumed to be unity. As for the $CHBr_3$ scheme, it is assumed that following H abstraction and photolysis, the immediate products of source gas degradation

($CHBr_2$, CH_2Br) will be rapidly oxidised under tropospheric conditions forming associated peroxy radicals.

$$CH_2Br_2 + OH\ (+O_2) \rightarrow CHBr_2O_2 + H_2O \qquad \text{R3.17}$$

$$CH_2Br_2 + Cl\ (+O_2) \rightarrow CHBr_2O_2 + HCl \qquad \text{R3.18}$$

$$CH_2Br_2 + h\nu\ (+O_2) \rightarrow CH_2BrO_2 + Br \qquad \text{R3.19}$$

3.3.2 Removal of Peroxy Species

The two peroxy radicals formed in R3.17-R3.19 are assumed to be removed via reaction with NO and HO_2. Loss of $CHBr_2O_2$ via these reactions (R3.20-3.22) is treated in the same way as in the bromoform scheme.

$$CHBr_2O_2 + NO \rightarrow CHBrO + NO_2 + Br \qquad \text{R3.20}$$

$$CHBr_2O_2 + HO_2 \rightarrow CHBrO + OH + O_2 + Br \qquad \text{R3.21}$$

$$CHBr_2O_2 + HO_2 \rightarrow CHBr_2OOH + O_2 \qquad \text{R3.22}$$

The CH_2BrO_2 + NO reaction (R3.23) is assumed to produce NO_2 and Br_y. The rate constant for this reaction ($k_{3.23}$) is calculated using the recommended JPL06 expression. For reactions with HO_2 (R3.24, R3.25), rate constants are taken from the MCM. The products of these reactions are Br_y and the hydroperoxide CH_2BrOOH, respectively.

$$CH_2BrO_2 + NO \rightarrow CH_2O + NO_2 + Br \qquad \text{R3.23}$$

$$CH_2BrO_2 + HO_2 \rightarrow CH_2O + OH + O_2 + Br \qquad \text{R3.24}$$

$$CH_2BrO_2 + HO_2 \rightarrow CH_2BrOOH + O_2 \qquad \text{R3.25}$$

3.3.3 Removal of End Products

Removal of CHBrO (R3.30, Table 3.2), produced in R3.20 and R3.21, is achieved via photolysis as discussed in the bromoform scheme. Similarly removal of $CHBr_2OOH$ (R3.26, R3.27, Table 3.2) produced in R3.22 is analogous to removal in R3.12 and R3.13 (i.e. by reaction with OH and by photolysis). Removal of CH_2BrOOH, produced in R3.25, has yet to be considered and is also assumed to be removed via reaction with OH (R3.28) and also by photolysis (R3.29). The rate constant for the OH reaction ($k_{3.28}$) is taken from the MCM and the reaction products are expected to be the peroxy species CH_2BrO_2 and water. The photolysis rate ($j_{3.29}$) is calculated using the cross sections of CH_3OOH.

$$CH_2BrOOH + OH \rightarrow CH_2BrO_2 + H_2O \qquad \text{R3.28}$$

$$CH_2BrOOH + h\nu \rightarrow CH_2O + OH + Br \qquad \text{R3.29}$$

3.4 Summary

This chapter has described schemes for the tropospheric degradation of $CHBr_3$ and CH_2Br_2. Certain mechanistic approximations have been made and have been discussed. A number of kinetic assumptions were also necessary due to the limited availability of kinetic data (e.g. rate constants). These schemes are to be used within a global model in order to predict the abundance of organic product gases such as carbonyl dibromide and formyl bromide. In previous modelling work, these gases have been ignored; i.e. it has been assumed that the degradation of a source gas produces Br_y instantaneously. This work should allow this assumption to be tested and should prove useful given that there are no atmospheric observations of these gases. In Chapter 4, CTM simulations that incorporate these schemes are described.

TABLE 3.1: Summary of bromoform chemistry scheme. **[a]** Photolysis rates calculated from (where available) recommended absorption cross section data. **[b]** Parameterisation for the temperature dependence of SG absorption cross sections included. **[c]** Br_y first-order loss due to washout adjusted to give required lifetime. **[d]** Rate constant estimated from reactions of analogous chlorine-containing species or generalised expression.

	Reaction	Rate / $cm^3molecule^{-1}s^{-1}$	Comment	Ref.
R3.1	$CHBr_3$ + OH	k(T)= 1.35E-12.exp(-600/T)	-	JPL06
R3.2	$CHBr_3$ + Cl	k(T)= 4.85E-12.exp(-850/T)	-	JPL06
R3.3	$CHBr_3$ + hν	**a**, **b**	Assume quantum yield of 1 for Br	JPL06
R3.4	CBr_3O_2 + NO	k(T)= 7.30E-12.exp(-270/T)	**d**	JPL06
R3.5	CBr_3O_2 + HO_2	k(T)= 3.30E-13.exp(820/T)	**d**	MCM
R3.6	CBr_3O_2 + HO_2	k(T)= 3.30E-13.exp(820/T)	As (R3.5) and equal partitioning of products	MCM
R3.7	$CHBr_2O_2$ + NO	k(T)= 2.54E-12.exp(360/T)	**d**	MCM
R3.8	$CHBr_2O_2$ + HO_2	k(T)= 3.30E-13.exp(820/T)	**d**	MCM
R3.9	$CHBr_2O_2$ + HO_2	k(T)= 3.30E-13.exp(820/T)	As (R3.8) and equal partitioning of products	MCM
R3.10	CBr_3OOH + OH	k(T)= 1.90E-12.exp(190/T)	**d**	MCM
R3.11	CBr_3OOH + hν	**a**	Assume cross sections of CH_3OOH	JPL06
R3.12	$CHBr_2OOH$ + OH	k(T)= 1.90E-12.exp(190/T)	**d**	MCM
R3.13	$CHBr_2OOH$ + hν	**a**	Assume cross sections of CH_3OOH	JPL06
R3.14	CBr_2O + hν	**a**	Assume quantum yield of 2 for Br	JPL06
R3.15	CHBrO + hν	**a**	Assume quantum yield of 1 for Br	JPL06
R3.16	Br_y washout	**c**	Variable in model - see Chapter 4	

TABLE 3.2: As Table 3.1 but for dibromomethane.

	Reaction	Rate / $cm^3molecule^{-1}s^{-1}$	Comment	Ref.
R3.17	CH_2Br_2 + OH	k(T)= 2.00E-12.exp(-840/T)	-	JPL06
R3.18	CH_2Br_2 + Cl	k(T)= 6.30E-12.exp(-800/T)	-	JPL06
R3.19	CH_2Br_2 + hν	**a**	Assume quantum yield of 1 for Br	JPL06
R3.20	$CHBr_2O_2$ + NO	k(T)= 2.54E-12.exp(360/T)	As Table 3.1 (R3.7)	
R3.21	$CHBr_2O_2$ + HO_2	k(T)= 3.30E-13.exp(820/T)	As Table 3.1 (R3.8)	
R3.22	$CHBr_2O_2$ + HO_2	k(T)= 3.30E-13.exp(820/T)	As Table 3.1 (R3.9)	
R3.23	CH_2BrO_2 + NO	k(T)= 4.00E-13.exp(300/T)	**d**	MCM
R3.24	CH_2BrO_2 + HO_2	k(T)= 3.30E-13.exp(820/T)	**d**	MCM
R3.25	CH_2BrO_2 + HO_2	k(T)= 3.30E-13.exp(820/T)	As (R3.24) and equal partitioning of products	MCM
R3.26	$CHBr_2OOH$ + OH	k(T)= 1.90E-12.exp(190/T)	As Table 3.1 (R3.12)	
R3.27	$CHBr_2OOH$ + hν	**a**	As Table 3.1 (R3.13)	
R3.28	CH_2BrOOH + OH	k(T)= 1.90E-12.exp(190/T)	**d**	MCM
R3.29	CH_2BrOOH + hν	**a**	Assume cross sections of CH_3OOH	JPL06
R3.30	CHBrO + hν	**a**	As Table 3.1 (R3.15)	
R3.31	Br_y washout	**c**	As Table 3.1 (R3.16)	

Chapter 4

Modelling the Transport and Chemistry of $CHBr_3$ & CH_2Br_2

4.1 Introduction

Chapter 3 described a tropospheric degradation scheme for bromoform ($CHBr_3$) and dibromomethane (CH_2Br_2). This chapter incorporates that scheme within a numerical model, in order to investigate the transport and chemistry of these source gases (SGs), from the tropical marine boundary layer (MBL) to the stratosphere. Specifically, the aims of this chapter are to:

1. Quantify the source gas injection (SGI), product gas injection (PGI) and total bromine (SGI + PGI) loading to the stratosphere from $CHBr_3$ and CH_2Br_2.
2. Determine the relative importance of the SGI and PGI pathways. Also, determine the fraction of PGI that is due to organic product gases (PGs).
3. Determine the sensitivity of the SGI and PGI pathways to hydroxyl radical (OH) concentration, lifetime of inorganic bromine (Br_y) and convective transport.
4. Using aircraft observations, assess the performance of the model in simulating the vertical distribution of $CHBr_3$ and CH_2Br_2 in the tropical tropopause layer (TTL).

The chapter is structured as follows. Section 4.2 contains a basic description of the model dynamics and chemistry. Simulations that were performed are also described here. The main results begin in Section 4.3, where the photochemistry of $CHBr_3$ and CH_2Br_2 is discussed. Section 4.4 considers SGI and its sensitivity to various model parameters. Here, the modelled distribution of $CHBr_3$ and CH_2Br_2 is validated with aircraft observations. In addition, trajectory calculations examine the transport of VSLS through the TTL. Section 4.5 considers the PGI pathway and assesses the importance of organic degradation products on the total stratospheric PGI from VSLS. Section 4.6 presents a modelled estimate of the total input of Br_y from $CHBr_3$ and CH_2Br_2 into the lower stratosphere. Finally, a summary of this chapter's work is given in Section 4.7. The work in this chapter has been published in the journal Atmospheric Chemistry and Physics (Hossaini et al., 2010).

4.2 TOMCAT/SLIMCAT Chemical Transport Model

TOMCAT/SLIMCAT is a three-dimensional (3-D) chemical transport model (CTM) (Chipperfield, 2006). The model is forced using offline winds and temperature fields taken from, for example, the European Centre for Medium-Range Weather Forecasts (ECMWF). The CTM in "TOMCAT" mode uses a hybrid sigma-pressure (σ-p) vertical coordinate and diagnoses the large-scale vertical motion from divergence of the horizontal winds. For this study, the vertical resolution of the model has been increased to 38 levels from 31 with additional levels in the TTL. The CTM also includes parameterisations of cumulus convection, based on the Tiedtke (1989) mass flux scheme (Stockwell and Chipperfield, 1999), and also boundary layer mixing (Holtslag and Boville, 1993).

The CTM has an option ("SLIMCAT") for running with isentropic (θ) levels in the upper troposphere and stratosphere ($\theta \geq 350$ K) where vertical motion is calculated from heating rates. The SLIMCAT model only considers transport by large-scale advection; there is no parameterisation of convection and boundary layer mixing. For tracer advection, the CTM uses a conservation of second-order moments scheme (Prather, 1986). The CTM also includes a scheme to calculate trajectories (Monge-Sanz et al., 2007). Of particular relevance to this thesis is the model's treatment of convection and associated precipitation. The stratospheric SGI of VSLS is likely sensitive to the frequency/magnitude of convective updrafts, while PGI will be sensitive to removal of soluble gases in convective rain.

The parameterised moist convection in TOMCAT considers cumulus updrafts, entrainment of environmental air into, and detrainment of cloud air out of the convective column, in both shallow and deep convection. Before moist convection can occur, three criteria must be met. First, a parcel must become supersaturated as it is lifted along the dry adiabat. Secondly, the parcel must also be buoyant with respect to the environment at the lifting condensation level. Thirdly, for deep convection, moisture convergence must be present below the cloud base. If there is divergence, shallow convection is possible if the surface evaporative flux is sufficiently large. The updraft tracer mass flux (Tr_u) can be calculated using equations 4.10 and 4.20, where M_u is the mass flux of air, E_u and D_u are entrainment/detrainment rates, and SM and S0 are the mass of air/mass of tracer in the grid box, respectively. Subscripts u and e represent updraft and environmental fields (Stockwell and Chipperfield, 1999). Turbulent entrainment and detrainment in and out of the cloud is parameterised using equations 4.30 and 4.40.

$$\frac{\delta M_u}{\delta z} = E_u - D_u \qquad \text{E4.1}$$

$$\frac{\delta Tr_u}{\delta z} = E_u \frac{S0e}{SM_e} - D_u \frac{Tr_u}{M_u} \qquad \text{E4.2}$$

$$E_u = M_u.\varepsilon_u \qquad \text{E4.3}$$

$$D_u = M_u.\delta_u \qquad \text{E4.4}$$

The fractional entrainment and detrainment rates (ε_u and δ_u) are assumed equal. For deep convection they are assumed as $1{\times}10^{-4}$ m^{-1} and for shallow convection $3{\times}10^{-4}$ m^{-1} (Tiedtke, 1989). Convective fluxes are calculated every 6 hours and applied to the tracer fields at each dynamical time step (30 minutes). Convective precipitation (CP) occurs only above 1.5 km and its rate is calculated using equation 4.50. Here, C is a constant ($2.0{\times}10^{-3}$ s^{-1}) (Tiedtke, 1989), LWC is the cloud liquid water content, ϱ is the environmental air density and dz is the vertical depth of the model level.

$$CP = C \times LWC \times \varrho \times dz \qquad \text{E4.5}$$

4.2.1 Simulations

In all simulations described here (see Table 4.1), the resolution of the model was 5.6° × 5.6° with 38 (or 31) vertical levels (∼1km deep in mid troposphere), extending from the surface to ∼35 km. The model was forced using ECMWF 6-hourly operational analyses. The TOMCAT version of the model was initialised on 01/01/2006 and run for 2 years. Year 1 was treated as model spin-up and year 2 output (2007) was saved every 3.75 days for analysis. SLIMCAT simulations differed in that the model was spun up for 3 years prior to analysis of 2007 output.

For the 'base run' (run **B**), the TOMCAT model included specified oxidant fields along with the $CHBr_3$ and CH_2Br_2 degradation schemes described in Chapter 3. Monthly mean diurnal mean fields of the concentration of fixed species (e.g. OH, NO, HO_2) were read from a previous TOMCAT full chemistry run. The background concentration of atomic chlorine, which was not calculated in the full tropospheric chemistry run, was set to 1×10^4 atom cm^{-3}. The model chemistry scheme uses a climatological tropical ozone profile for photolysis calculations (Chipperfield, 2006). Figure 4.1 shows example tropical mean profiles of temperature and the primary oxidant OH.

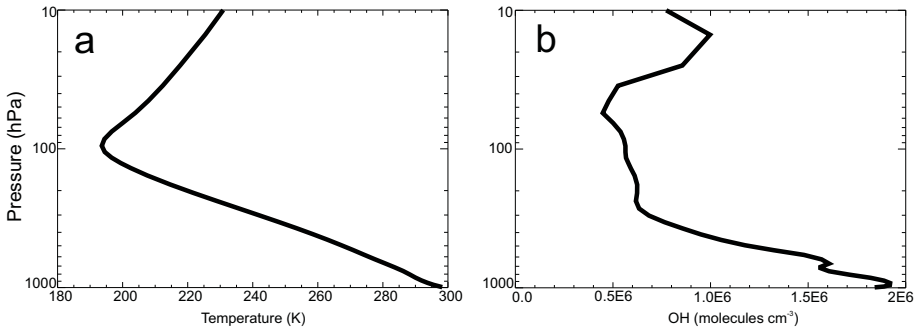

FIGURE 4.1: Tropical (±20° latitude) annual mean profiles of (a) temperature (K) from model run **B** (i.e. ECMWF analyses) and (b) specified (24-hr mean) OH concentration (molecule cm^{-3}) used in CTM experiments.

The volume mixing ratio (vmr) of $CHBr_3$ and CH_2Br_2 was fixed uniformly in space and time at 1.2 parts per trillion (ppt) in the bottom two layers of the model and in tropical regions (±20°) only. This value is typical of mean $CHBr_3$ and CH_2Br_2 observed in the MBL. Quack and Wallace (2003) report background MBL $CHBr_3$ in the range 0.5-1.5 ppt. Similarly for CH_2Br_2, Butler et al. (2007) report CH_2Br_2 in the range 0.6-1.3 ppt.

Furthermore, an assumed SG vmr of 1.2 ppt at the surface provides a good fit to observed profiles (see Section 4.4.2). In this chapter, of interest is the relative mixing ratio of brominated species in the TTL (compared with the surface). Therefore, introducing the complication of specifying uncertain emission fluxes is not required yet. For this work, the TTL base is defined as the level of mean convective outflow (∼12 km). The top of the TTL is defined as the cold-point tropopause (CPT) (Law and Sturges, 2007).

All advected tracers (apart from $CHBr_3$ and CH_2Br_2) were initialised at zero at the start of the simulation. The lifetime of Br_y was assumed to be infinite for run **B**. A number of sensitivity runs were also performed. Run $\mathbf{S}_{NOCONV}$ differed from run **B** in that model convection was switched off. Runs $\mathbf{S}_{10}$, $\mathbf{S}_{20}$ and $\mathbf{S}_{40}$ differed from run **B** in that the lifetime of Br_y was set to 10, 20 and 40 days below the CPT, respectively. Run $\mathbf{S}_{2OH}$ differed from the base run in that model [OH] was doubled. Run $\mathbf{S}_{L31}$ differed in that the model employed coarser vertical resolution (∼factor of 2) above ∼300 hPa and therefore used only 31 levels.

Table 4.1: Summary of CTM experiments performed.

Run	Convection	Br_y lifetime	Vertical levels	[OH]
B	yes	Infinite	38	1x
$\mathbf{S}_{NOCONV}$	no	Infinite	38	1x
$\mathbf{S}_{10}$	yes	10 days below cold-point	38	1x
$\mathbf{S}_{20}$	yes	20 days below cold-point	38	1x
$\mathbf{S}_{40}$	yes	40 days below cold-point	38	1x
$\mathbf{S}_{2OH}$	yes	Infinite	38	2x
$\mathbf{S}_{L31}$	yes	Infinite	31	1x
$\mathbf{S}_{SLIMCAT}$	no	Infinite	38 (σ-θ)	1x
$\mathbf{S}_{SLIMCAT10}$	no	10 days below cold-point	38 (σ-θ)	1x
$\mathbf{S}_{SLIMCAT20}$	no	20 days below cold-point	38 (σ-θ)	1x
$\mathbf{S}_{SLIMCAT40}$	no	40 days below cold-point	38 (σ-θ)	1x

In addition, SLIMCAT simulations were also carried out in which artificial mixing in the tropical troposphere was assumed by fixing both $CHBr_3$ and CH_2Br_2 in the lower 8 levels of the SLIMCAT σ-θ model (surface to ∼10 km). For run $\mathbf{S}_{SLIMCAT}$, the assumed lifetime of Br_y due to washout was infinite. For runs $\mathbf{S}_{SLIMCAT10}$, $\mathbf{S}_{SLIMCAT20}$ and $\mathbf{S}_{SLIMCAT40}$, the assumed Br_y lifetime was 10, 20 and 40 days, respectively. Note, for SLIMCAT simulations (due to the artificial mixing in the troposphere) the assumed washout is only "switched on" between ∼10-17 km.

4.3 Photochemistry of Source Gases

Figure 4.2 shows the mean modelled loss rate (due to reaction with OH and photolysis) of $CHBr_3$ and CH_2Br_2 and also their local lifetime in the tropics (See Chapter 2).

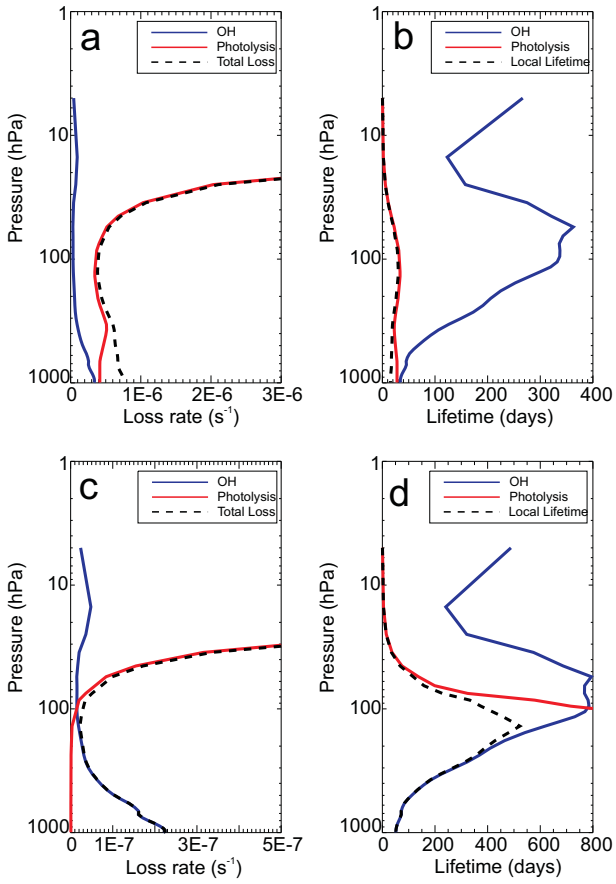

FIGURE 4.2: Tropical (±20° latitude) annual mean zonal mean profiles of (a) $CHBr_3$ loss rate (s^{-1}) due to photolysis (red line), reaction with OH (blue line), and the overall total (black dashed line), and (b) $CHBr_3$ lifetime (days) due to the same processes from TOMCAT model runs. Panels (c) and (d) are the equivalent plots for CH_2Br_2.

For $CHBr_3$, the dominant sink is photolysis and the local lifetime (τ_{local}) ranges from ∼15 days at the surface, to between ∼25-30 days in the TTL - consistent with previous model estimates (e.g., Warwick et al., 2006; Sinnhuber and Folkins, 2006). For CH_2Br_2, in the mid-troposphere loss is dominated by reaction with OH and photolysis is relatively slow. However, at the CPT (∼100 hPa) the two are roughly equal. For CH_2Br_2, τ_{local} ranges from ∼50 days at the surface to a maximum of ∼520 days in the TTL. This is large given the working definition of a VSLS is one whose lifetime is less than 6 months (Law and Sturges, 2007). Table 4.2 summarises the modelled lifetimes of these SGs.

TABLE 4.2: Mean modelled lifetime of $CHBr_3$ and CH_2Br_2 in the tropics (±20°), from the surface to the cold-point tropopause (∼17 km, ∼100 hPa) and with respect to photolysis ($\tau_{h\nu}$), OH (τ_{OH}) and overall total lifetime (days).

Source Gas	Pressure (hPa)	$\tau_{h\nu}$ (days)	τ_{OH} (days)	τ_{local} (days)
$CHBr_3$	1000	28	35	16
$CHBr_3$	1000-500	28	42	17
$CHBr_3$	500-200	25	132	21
$CHBr_3$	200-95	33	292	29
CH_2Br_2	1000	21004	53	52
CH_2Br_2	1000-500	20495	66	65
CH_2Br_2	500-200	13231	243	237
CH_2Br_2	200-95	2535	655	453

4.4 Source Gas Injection

Figure 4.3 shows tropical zonal mean profiles of $CHBr_3$ and CH_2Br_2 from the base run **B** and sensitivity runs $\mathbf{S}_{NOCONV}$ (no convection), $\mathbf{S}_{2OH}$ (2×[OH]) and $\mathbf{S}_{SLIMCAT}$. The results here show that with the full TOMCAT model transport (run **B**), the mean $CHBr_3$ vmr at the CPT (∼17 km) is ∼0.13 ppt, resulting in an SGI contribution of ∼0.39 ppt of Br_y to the lower stratosphere. This is in general agreement with the SGI value of 0.5 ppt estimated by Sinnhuber and Folkins (2006). Similarly for CH_2Br_2, run **B** predicts a mean SG vmr of 0.80 ppt at the CPT, resulting in an SGI input of ∼1.60 ppt of Br_y - over 4× that supplied from $CHBr_3$.

Without convection (run $\mathbf{S}_{NOCONV}$), SGI from $CHBr_3$ and CH_2Br_2 reduces to 0.32 ppt and 1.57 ppt, i.e. ∼84% and ∼98% of that from run **B** . This suggests that the SGI at the CPT, from both species, is not overly sensitive to the model's parameterised convection. For $CHBr_3$, this apparently contradicts the findings of Nielsen and Douglass (2001) who report a treatment of convection required in order for $CHBr_3$ to reach the tropical lower stratosphere in their model simulations. Similarly, from a 3D model study, Warwick et al. (2006) find $CHBr_3$ in the tropical upper troposphere to be highly dependent on convection. Without further details on the experiments performed in these other studies further comments on the differences cannot be made. In experiments here, although convection is switched off, the parameterisation of mixing in the PBL, which causes mixing of surface-emitted tracers in the bottom few kilometres, is still included. If PBL mixing

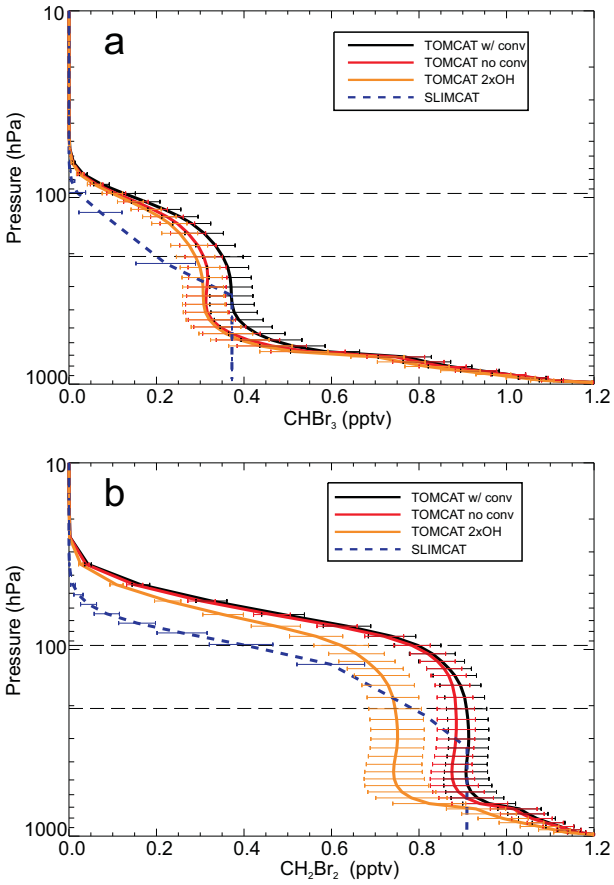

FIGURE 4.3: Tropical (±20° latitude) annual mean modelled profiles of (a) $CHBr_3$ and (b) CH_2Br_2. Black line denotes output from the run **B** (i.e. with convection), red line denotes output from sensitivity run $\mathbf{S}_{NOCONV}$ (no convection), orange line from run $\mathbf{S}_{2OH}$ and dashed blue line from run $\mathbf{S}_{SLIMCAT}$. Variability in time and space shown with ±1 standard deviation. The location of the cold-point tropopause (CPT) and the base of the TTL (black dashed lines) are shown for reference.

is switched off, $CHBr_3$ especially is found to be largely confined to the lowest model level (∼100 m), resulting in a large decrease in its abundance in the upper troposphere (UT). It may be that the studies of Nielsen and Douglass (2001) and Warwick et al. (2006) also included transport due to this process in their definition of convection. Given that turbulent mixing in the PBL can transport tracers to the lower free troposphere, then the lifetimes of $CHBr_3$ and CH_2Br_2 would indicate that resolved vertical advection by the analysed winds could still cause some transport to the UT.

As model OH fields are uncertain in the UT, a sensitivity run was performed to investigate the impact of a large (×2) change in [OH] on the modelled SG profiles. From the run $\mathbf{S}_{2OH}$ profile in Figure 4.3, it is clear the abundance of CH_2Br_2 (and associated SGI) is more sensitive to changes in [OH] than that of $CHBr_3$. This is expected given the

dominance of the CH_2Br_2 + OH reaction over photolysis, relative to that of $CHBr_3$ + OH. For the SLIMCAT run $\mathbf{S}_{SLIMCAT}$, SG profiles have been scaled to approximately mimic that of the TOMCAT base run in the mid-troposphere. It can be seen that SLIMCAT simulates a lower abundance of both SGs in the TTL and near-tropopause regions.

TOMCAT runs with ECMWF winds have previously been noted to exhibit too rapid vertical motion in the upper troposphere/lower stratosphere (UTLS) region (Chipperfield, 2006; Monge-Sanz et al., 2007). The problem is more obvious with ERA-40 winds than with the more recent ECMWF data sets and is mainly related to the noisy analysed wind fields. This is known to affect all CTMs using wind velocities or divergence to obtain their vertical motion (e.g., Scheele et al., 2005; Wohltmann and Rex, 2008). SLIMCAT runs are not affected by the same problem as, in this case, above 350 K potential temperature vertical motion is computed from diagnosed heating rates. For this reason, the spurious vertical transport present in TOMCAT runs (due to analyses noise) is eliminated from SLIMCAT runs. In addition, SLIMCAT uses isentropic levels in the stratosphere, which help to separate vertical/horizontal motion, and has shown to provide more realistic transport in the UTLS than TOMCAT (Chipperfield, 2006).

Krueger et al. (2008) performed a Lagrangian model study in the TTL using ECMWF operational winds and found use of the vertical wind field resulted in significantly faster motion over the use of computed heating rates. A study by Wohltmann and Rex (2008) (also with ECMWF winds) has also shown improvements in model vertical velocities when obtained from diagnosed heating rates with respect to the vertical velocity field from the analyses. Note, the vertical velocity field from the analyses is not used in directly in TOMCAT/SLIMCAT (see Section 4.2).

4.4.1 Transport through the TTL

The trajectory calculation inside the TOMCAT/SLIMCAT CTM has been used to estimate the mean vertical velocity of tracers in the TTL for runs **B** and $\mathbf{S}_{SLIMCAT}$. Trajectories were initialised at 80 hPa (run **B**) and 380 K (run $\mathbf{S}_{SLIMCAT}$) and advected backwards in time using vertical winds from the analysed divergence field and also the diagnosed heating rates, respectively. The mean vertical motion calculated from the trajectory displacement was 0.64 mm/s in run **B** and 0.324 mm/s in run $\mathbf{S}_{SLIMCAT}$. Analysis

of CO_2 data shows a similar transit time, which corresponds to a range in vertical velocities, between the lower boundary of the TTL and the tropopause of 0.5-0.14 mm/s (Park et al., 2010).

Krueger et al. (2008) find residence times in the winter TTL (2001/02) of 36 days using diagnosed heating rates, and only 20 days when using the corresponding operational ECMWF vertical winds. Calculations here show a residence time in the 360-380 K region of 20 days based on the TOMCAT run and 52 days based on the SLIMCAT run for the period November-December 2005. The slower vertical motion in the SLIMCAT θ-coordinate model seems realistic, which leads to overall better agreement with observations (see Section 4.4.2). The residence times in the TTL calculated here are within the range, 20-80 days, as published (Law and Sturges, 2007). More recently, analysis of hydrochlorofluorocarbon (HCFC) and hydrofluorocarbon (HFCs) data from the WB-57 aircraft during the National Aeronautics and Space Administration (NASA) TC4 campaign indicates a transit time from 360 K to 380 K of about 3-4 months (Elliot Atlas, unpublished data, 2010). This estimate is somewhat larger than the 80 day upper limit quoted in (Law and Sturges, 2007) and may, in part, be due to the calculation being performed for summer months.

4.4.2 Model Versus Observations

Modelled profiles of $CHBr_3$ and CH_2Br_2 have been compared with observations taken on board research aircraft. For the campaigns discussed herein, whole air samples were collected using evacuated canisters on board both the DC-8 and WB-57 aircraft, prior to laboratory analysis. This was carried out using a 5-column 5-detector gas chromatography (GC) system along with two flame ionization detectors, two electron capture detectors, coupled with a quadrupole mass spectrometer (MS). For the PEM TROPICS-B campaign, the precision on $CHBr_3$ and CH_2Br_2 measurements is reported at 1.6%. The accuracy is estimated to be between 1-10% at 1σ (Colman et al., 2001).

Figure 4.4 shows modelled profiles of $CHBr_3$ and CH_2Br_2 versus tropospheric observations from the PEM TROPICS-B (http://www-gte.larc.nasa.gov/pem/) and INTEX-B (http://www.espo.nasa.gov/intex-b/) campaigns. The modelled profiles here are averaged spatially over the flight domain and are also averaged for the same months (but for 2007).

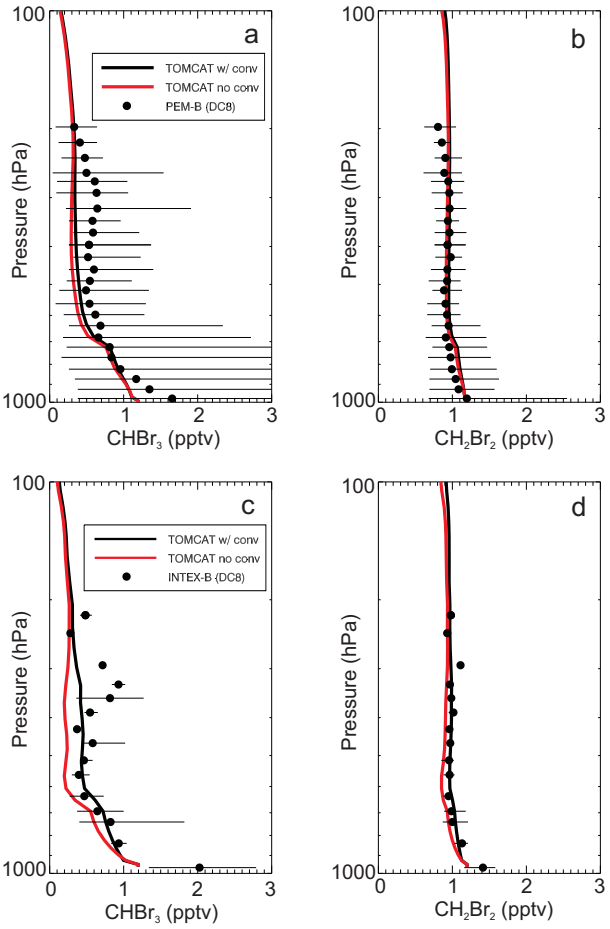

FIGURE 4.4: Comparison of modelled profiles of (a) $CHBr_3$ and (b) CH_2Br_2 versus observations made on board the DC-8 aircraft during the PEM TROPICS-B mission (March-April 1999). The observations are averaged vertically in ∼0.5 km bins for tropical latitudes and between 84° and 211°W longitude. The model (runs **B** and $\mathbf{S}_{NOCONV}$) is sampled over the same spatial domain and over the same months (for 2007). Panels (c) and (d) are similar plots for the NASA INTEX-B campaign (March 2006). The observations have been averaged at tropical latitudes and between 95° and 99°W longitude. Horizontal lines on all observations denote min-max variability.

TOMCAT, constrained by 1.2 ppt of both SGs at the surface, provides a good agreement with the observations in the mid troposphere. For $CHBr_3$, whose lifetime is relatively short, variability can be large. The difference between runs **B** and $\mathbf{S}_{NOCONV}$ here is small, suggesting minor modelled convection in the region.

Figure 4.5 shows model profiles of $CHBr_3$ and CH_2Br_2 against high-altitude observations which extend into the TTL. The following NASA aircraft campaigns are used; 2007 Tropical Composition, Cloud and Climate Coupling (TC4, http://www.espo.nasa.gov/tc4/), 2006 Pre-Aura Validation Experiment (PRE-AVE, http://espoarchive.nasa.gov/archive

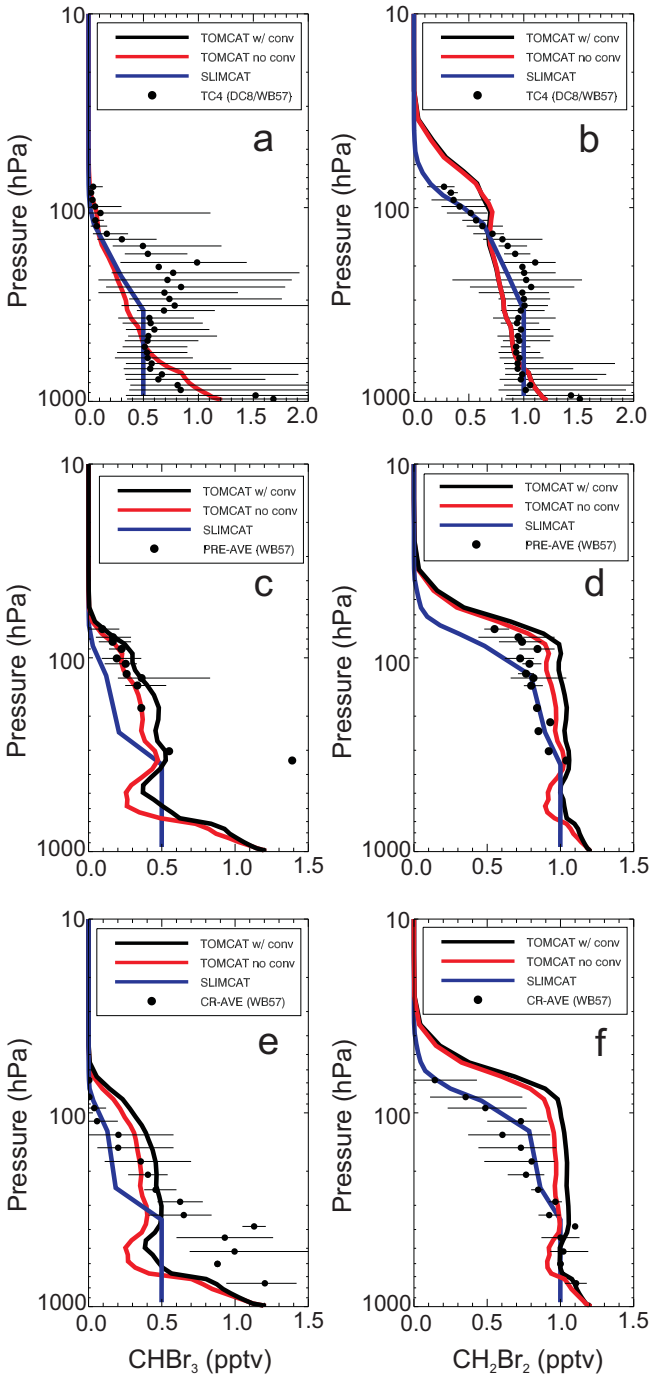

FIGURE 4.5: Comparison of modelled profiles of (a) $CHBr_3$ and (b) CH_2Br_2 versus observations made on board the DC-8 and WB-57 aircraft during the NASA TC4 campaign (July-August 2007). Panels (c) and (d) are similar comparisons for the PRE-AVE campaign (January-February 2004). Panels (e) and (f) are similar comparisons for the CR-AVE campaign (January-February 2006). TC4 observations are averaged in tropical latitudes and between 70° and 106°W longitude. PRE-AVE observations are averaged in tropical latitudes and between 81° and 85°W longitude. Similarly, the CR-AVE observations are averaged at tropical latitudes and between 79° and 86°W longitude. Horizontal lines on all observations denote min-max variability.

/arcs /pre) and the 2004 Costa Rica Aura Validation Experiment (CR-AVE, http://www.espo.nasa.gov/ave-costarica2/).

For $CHBr_3$, the base model **B** performs reasonably well and is generally within the variability of the observations. Of importance is the model's ability to simulate $CHBr_3$ in the UTLS. A number of previous model studies have significantly overestimated $CHBr_3$ in this region (e.g. Warwick et al., 2006; Nielsen and Douglass, 2001). TOMCAT generally does well reproducing the low $CHBr_3$ mixing ratio around the tropopause (∼100 hPa), although it is slightly overestimated during CR-AVE. In the mid troposphere, TOMCAT profiles do not capture the signature "C-shape" of convection as observed during TC4. However, it should be noted that DC-8 flights targeted recent convective outflow during most TC4 flights. The observations provide a *snapshot* and may not be representative of this region as a whole.

For CH_2Br_2, there is significantly less variability observed. This SG is relatively long-lived and thus also relatively well mixed near the surface. In the lower troposphere, TOMCAT profiles seem reasonable, however in the UTLS, CH_2Br_2 is overestimated. This will be in part due to the (too) rapid vertical transport through the TTL region in run **B** (see earlier discussion). The TOMCAT overestimation of CH_2Br_2 in the TTL is not due to the model vertical resolution. The SG profiles from runs **B** (38 levels) and $\mathbf{S}_{L31}$ (31 levels) are almost identical (not shown). Therefore, it is deduced that the vertical transport is controlled by the vertical winds and not by numerical diffusion. From Figure 4.5 it can be seen that run $\mathbf{S}_{SLIMCAT}$, with slower TTL transport, gives much better agreement with observed CH_2Br_2 in the UTLS. The improvement over the TOMCAT simulation is most striking for the CR-AVE comparison (panel [f]).

Figure 4.6 shows a tracer-tracer plot of $CHBr_3$ versus CH_2Br_2 in the 350-80 hPa region from runs **B**, $\mathbf{S}_{NOCONV}$, $\mathbf{S}_{2OH}$ and $\mathbf{S}_{SLIMCAT}$. Mean observations from the TC4 data set (also in this region, see Figure 4.5) are included along with a power line of best fit on all data sets. The origins of the model lines (high SG mixing ratios) are arbitrary and the plot tests the ability of the different model runs to fit both SG profiles simultaneously. The model lines here indicate that with the current model setup (chemistry and transport), both tracers cannot be simulated correctly at the same time. Run $\mathbf{S}_{SLIMCAT}$ performs the best, as can be seen in the gradient relative to that of the observations. Run $\mathbf{S}_{SLIMCAT}$ has

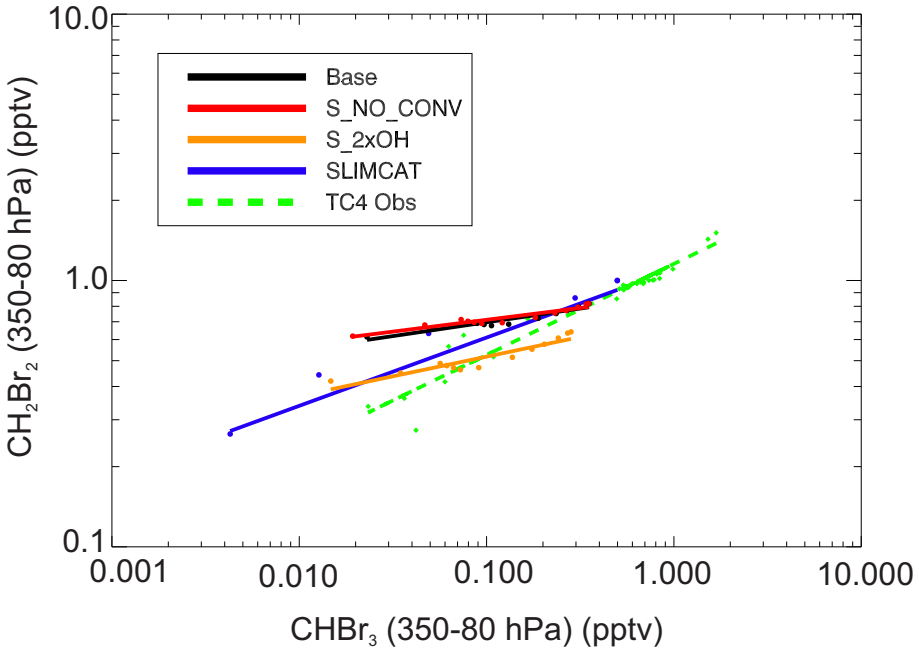

FIGURE 4.6: Correlation plot of observed CH_2Br_2 versus observed $CHBr_3$ between 350 and 80 hPa from the TC4 campaign (Figure 4.5). Also shown are modelled correlations from runs $\mathbf{B}$, $\mathbf{S}_{2OH}$, and $\mathbf{S}_{SLIMCAT}$ in the same region. Power lines of best fit are included on all data sets of the form, $Y=(aX)^b$.

the slowest transport through the TTL and allows more loss of CH_2Br_2 (relative to $CHBr_3$) in the lower TTL, where loss by OH is faster (Figure 4.2).

Given the simulated (and observed) UTLS mixing ratios of $CHBr_3$ and CH_2Br_2, the latter SG seems more important for the stratospheric SGI of bromine. Wamsley et al. (1998) reported CH_2Br_2 to have an atmospheric lifetime long enough to reach the stratosphere. The authors deduce $CHBr_3$, with its shorter lifetime, to contribute a negligible amount of bromine to the stratosphere. This may be the case via SGI, however bromine loading can also occur via PGI and with 3 Br atoms per molecule, PGI from $CHBr_3$ may be large. Other observation-based studies include Laube et al. (2008) who deduce CH_2Br_2 to be the "dominant" very short-lived SG. Their results, along with Schauffler et al. (1999), find CH_2Br_2 to be present up to ~18.5 km (~0.15 ppt). The modelling work in this chapter shows ~0.5 ppt and ~0.16 ppt of CH_2Br_2 at this altitude from runs $\mathbf{B}$ and $\mathbf{S}_{SLIMCAT}$, respectively. The latter mixing ratio seems more reasonable given the overestimation of CH_2Br_2 by the TOMCAT version of the model.

4.5 Product Gas Injection

Figure 4.7 shows the annual tropical zonal mean abundance of the organic product gases arising from $CHBr_3$ and CH_2Br_2 degradation. For bromoform, the major degradation products are carbonyl dibromide (CBr_2O) and formyl bromide (CHBrO). The hydroperoxy species CBr_3OOH and $CHBr_2OOH$ are found to be minor products - consistent with the suggestions of Ko and Poulet (2003). The mixing ratios of these species in the TTL are very low (<0.03 ppt) and have been scaled so that here they are relative to an assumed 1.0 ppt of the SG at the surface. It is unlikely that these organic products contribute significantly to the PGI of bromine into the stratosphere from $CHBr_3$. The mixing ratios of the peroxy radicals CBr_3O_2 and $CHBr_2O_2$, which were also considered in the degradation schemes, were found to be near zero throughout the profile (not shown).

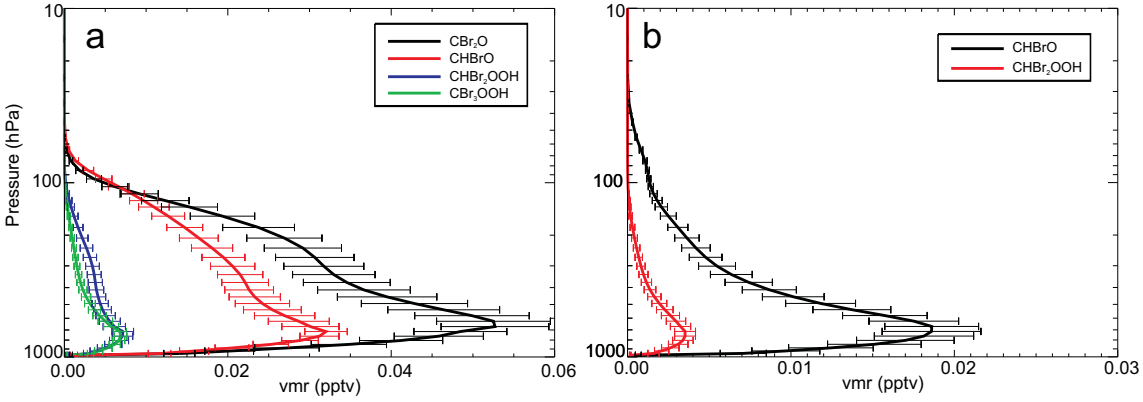

FIGURE 4.7: Modelled tropical (±20° latitude) annual mean zonal mean profiles of the principal organic PGs arising from (a) $CHBr_3$ and (b) CH_2Br_2 degradation in the tropics. The assumed surface mixing ratio of both SGs was 1 ppt. The output is from run **B** with variability in time and space shown with ±1 standard deviation.

Similarly, for dibromomethane the model predicts the major organic degradation products to be CHBrO and a minor product to be $CHBr_2OOH$. Again, this is consistent with the suggestions of Ko and Poulet (2003). The mixing ratios of these species are also very low throughout the troposphere. As for $CHBr_3$, it seems likely that organic products arising from CH_2Br_2 degradation form only a very small fraction of PGI. Furthermore, although poorly quantified, organic PGs would be expected to be removed from the atmosphere by washout processes due to their solubility. The model work described in this paper has not accounted for this and thus the extremely low near-tropopause mixing ratios reported here for CBr_2O, CHBrO and other products could indeed be overestimates.

Figure 4.8 shows the calculated loss rates and lifetimes of major organic products CBr_2O and CHBrO, with respect to photolysis in the tropics. CBr_2O is the longest lived with a lifetime peaking at ∼7 days. For CHBrO, its lifetime with respect to photolyis is short at ∼1 day. Both products are therefore significantly shorter-lived than their respective parent source gases.

Ultimately, the results here suggest that PGI of bromine (from VSLS) into the stratosphere is likely dominated by inorganic products such as HBr and BrO. In addition, the assumption made in previous modelling work of instantaneous conversion between organic bromine PGs and Br_y seems reasonable. To validate this result, an attempt at observation of CBr_2O and CHBrO could be made. To my knowledge there are currently no atmospheric observations of these species. Locally, in regions of high or low HO_x and NO_x, the partioning of organic products could change.

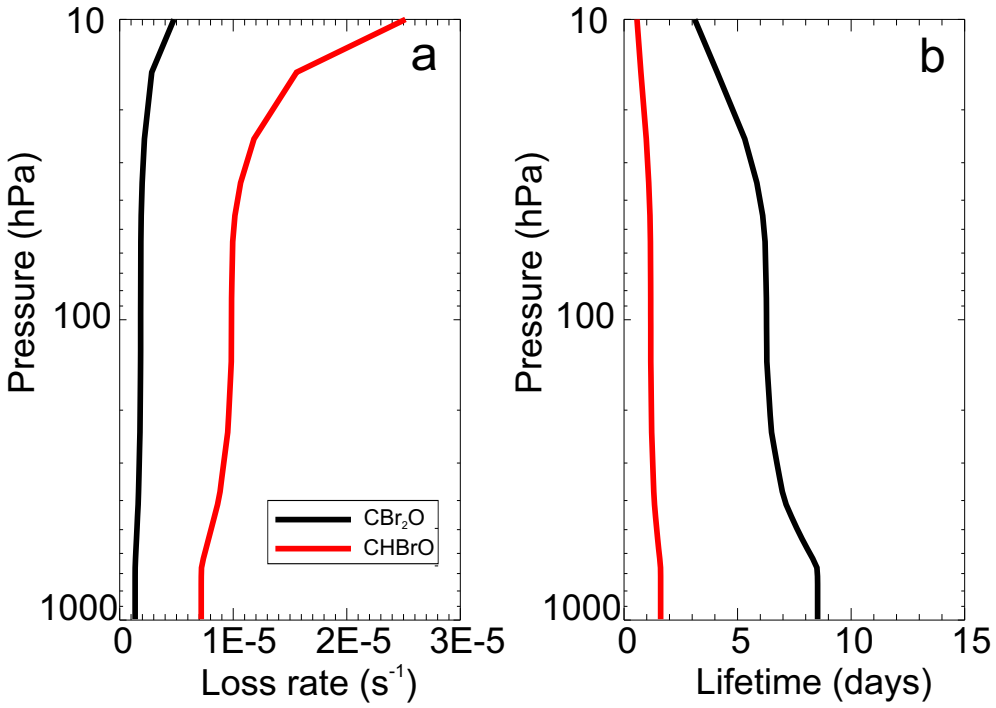

FIGURE 4.8: Modelled tropical (±20°) annual mean zonal mean profiles of (a) the loss rate with respect to photolysis (s^{-1}) and (b) the lifetime (days) with respect to photolysis of CBr_2O (black line) and CHBrO (red line).

4.6 Total Bromine

Figures 4.9 and 4.10 show the modelled contribution of SGI and PGI to the total bromine delivered to the lower stratosphere from $CHBr_3$ and CH_2Br_2, respectively. Results are shown for sensitivity runs S_{10}, S_{20} and S_{40} (i.e. Br_y lifetimes of 10, 20 and 40 days). See Table 4.3 also.

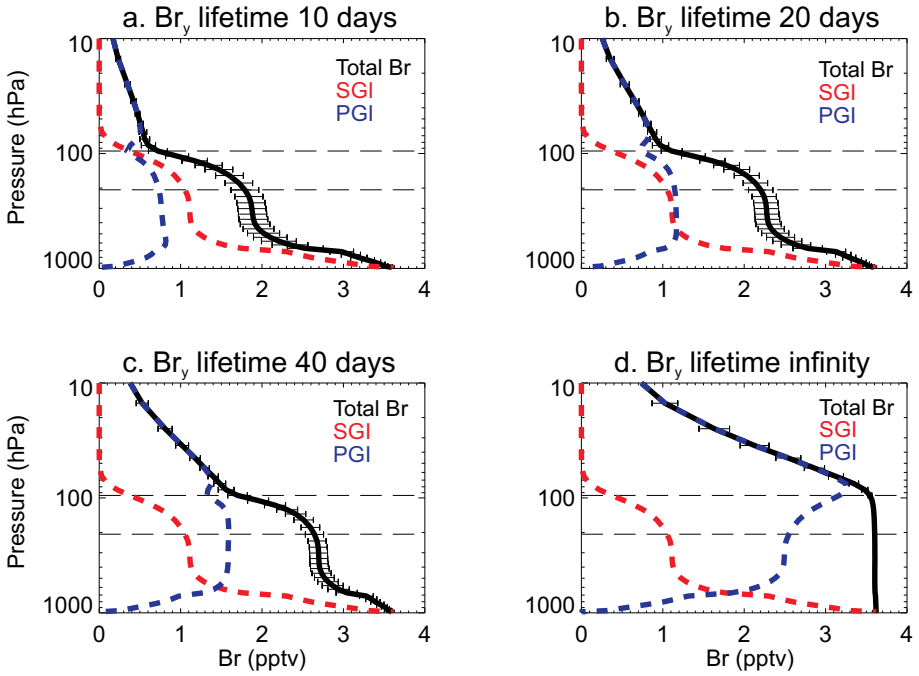

FIGURE 4.9: Modelled tropical (±20°) annual mean zonal mean profiles of SGI, PGI and total (SGI+PGI) bromine from $CHBr_3$ for runs (a) **B**, (b) $\mathbf{S}_{10}$, (c) $\mathbf{S}_{20}$ and (d) $\mathbf{S}_{40}$. These runs assume a $CHBr_3$ surface mixing ratio of 1.2 ppt. The location of the cold-point tropopause (CPT) and base of the TTL (black dash lines) are shown for reference. Variability of total Br in time and space shown with ±1 standard deviation (horizontal bars).

Assuming a Br_y lifetime of 10 days, a resonable assumption based on previous modelling work (Sinnhuber and Folkins, 2006), the modelled total bromine from $CHBr_3$ (SGI+PGI) is ∼0.72 ppt. The contribution to this total from the SGI and PGI pathways is approximately equal at the CPT. This is in general agreement with the work of Dvortsov et al. (1999) and Nielsen and Douglass (2001) who report similar values of ∼1 ppt. These studies also find the SGI and inorganic PGI pathways to be approximately equal. The results here are in good agreement with the work of Sinnhuber and Folkins (2006), who report a 0.8 ppt total bromine contribution from $CHBr_3$ whilst also using an assumed 10 day Br_y lifetime

in their calculations. Their estimated PGI contribution (0.3 ppt) is in good agreement with the modelled PGI here (0.35 ppt).

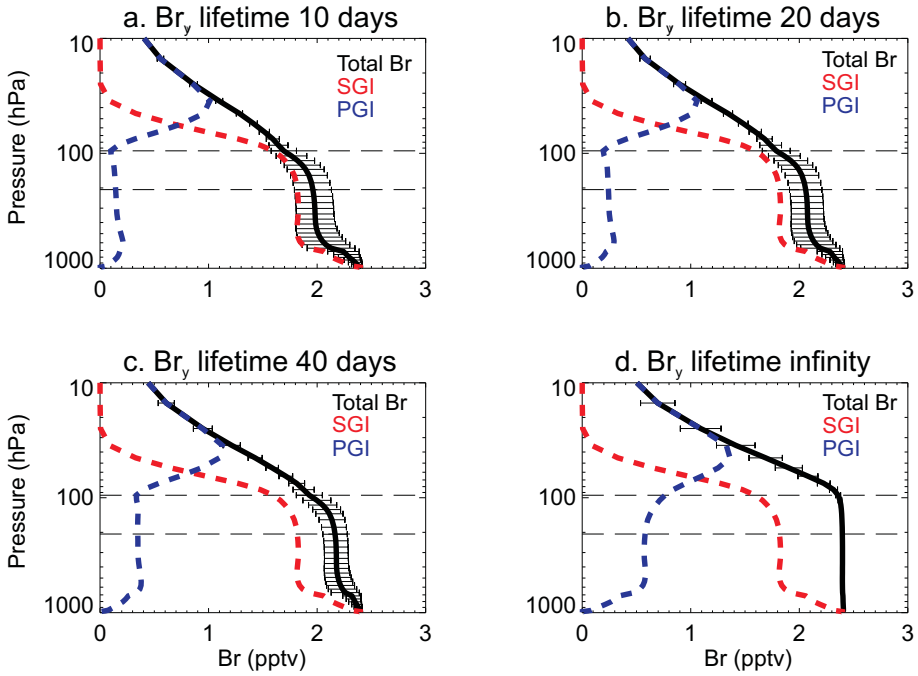

FIGURE 4.10: As Figure 4.9 but for CH_2Br_2.

Also, assuming a 10 day Br_y lifetime, the bromine loading due to CH_2Br_2 is ~1.69 ppt at the CPT. Of this total, SGI accounts for ~94%. Despite containing two Br atoms per molecule, the PGI contribution from CH_2Br_2 is small. This is due to the relatively long CH_2Br_2 lifetime (Table 4.2) and thus relatively little tropospheric loss of SG/formation of product gases occurs. The modelled SGI from CH_2Br_2 may constitute an upper limit as the TOMCAT CTM was shown to overestimate the SG in the tropical UTLS region (Figure 4.5).

Overall, the total bromine loading from both $CHBr_3$ and CH_2Br_2 is ~2.4 ppt. Increasing the assumed tropospheric Br_y lifetime to 20 and 40 days naturally raises this value to ~2.9 and ~3.6 ppt. The mean lifetime of Br_y in the troposphere, and in particular the TTL region, is uncertain at present.

SLIMCAT sensitivity runs indicate lower values of total bromine from $CHBr_3$ and CH_2Br_2 reaching the stratosphere (compared with TOMCAT)(see Table 4.4). The results here are derived assuming a fixed 0.5 ppt $CHBr_3$ and 1 ppt CH_2Br_2 in the lower 8 levels of the model (surface to ~10 km). These values are chosen as they mimic the mid-tropospheric

TABLE 4.3: Summary of TOMCAT modelled stratospheric SGI, PGI and total (SGI+PGI) bromine loading from $CHBr_3$ and CH_2Br_2 for assumed Br_y lifetimes of 10, 20, 40 and ∞ days below the cold-point tropopause.

Source Gas	Br_y Lifetime	SGI / ppt	PGI / ppt	Total Br / ppt	%SGI
$CHBr_3$	10 days	0.377	0.345	0.722	53
CH_2Br_2	10 days	1.594	0.099	1.693	94
Total	10 days	1.971	0.434	**2.415**	81
$CHBr_3$	20 days	0.377	0.732	1.109	34
CH_2Br_2	20 days	1.594	0.194	1.788	89
Total	20 days	1.971	0.92	**2.891**	68
$CHBr_3$	40 days	0.377	1.323	1.700	22
CH_2Br_2	40 days	1.594	0.334	1.928	82
Total	40 days	1.971	1.657	**3.628**	54
$CHBr_3$	∞	0.377	3.168	$\sim$3.6	11
CH_2Br_2	∞	1.594	0.763	$\sim$2.4	66
Total	∞	1.971	3.931	$\sim$**6.0**	33

values of the TOMCAT profiles and also provide the best fit with aircraft observations (e.g. Figure 4.5). From $CHBr_3$, assuming a 10 day Br_y lifetime, total bromine reaching the stratosphere is found to be $\sim$0.2 ppt. For CH_2Br_2, the total bromine contribution is $\sim$1.0 ppt. The lower values (relative to TOMCAT) result from the slower vertical motion in the TTL (as discussed previously) reducing the SGI contribution. The slower transport also causes a decrease in PGI as soluble Br_y remains in the troposphere, where washout is possible, for longer.

SLIMCAT simulations, which do not model all aspects of tropospheric tracer transport, can only be seen as sensitivity tests. Furthermore, SLIMCAT simulations have been performed over a period of 6 years which is not long enough for the model to spin up and reach equilibrium in the stratosphere. This can be seen from the values quoted in Table 4.4 for the run $\mathbf{S}_{SLIMCAT}$ (infinite Br_y lifetime). Total bromine from $CHBr_3$ and CH_2Br_2 has not yet reached equilibrium at 1.5 ppt and 2.0 ppt. This is likely due to the strong quasi-horizontal mixing of extra-tropical stratospheric air with low Br_y content into the TTL. This is not the case for the equivalent TOMCAT simulations where the model has been spun up sufficiently (Table 4.3) and total bromine from $CHBr_3$ and CH_2Br_2 has settled at 3.6 ppt and 2.4 ppt, respectively.

TABLE 4.4: As Table 4.3 but for SLIMCAT simulations.

Source Gas	Br_y Lifetime	SGI / ppt	PGI / ppt	Total Br / ppt	%SGI
$CHBr_3$	10 days	0.074	0.156	0.230	32
CH_2Br_2	10 days	0.867	0.127	0.994	87
Total	10 days	0.941	0.283	**1.224**	77
$CHBr_3$	20 days	0.074	0.287	0.361	20
CH_2Br_2	20 days	0.867	0.204	1.071	81
Total	20 days	0.941	0.491	**1.432**	66
$CHBr_3$	40 days	0.074	0.463	0.537	14
CH_2Br_2	40 days	0.867	0.295	1.162	75
Total	40 days	0.941	0.758	**1.699**	56
$CHBr_3$	∞	0.074	0.976	1.05	7
CH_2Br_2	∞	0.867	0.532	1.399	62
Total	∞	0.941	1.508	**2.449**	38

4.7 Summary

In this chapter, the TOMCAT/SLIMCAT CTM has been used in order to quantify first, the contribution of $CHBr_3$ and CH_2Br_2 to the stratospheric bromine budget and, secondly, the relative magnitude of source gas injection and product gas injection. A chemical scheme describing the tropospheric degradation of both source gases, along with simple product gas chemistry, has been included in CTM experiments. The major degradation products of $CHBr_3$ and CH_2Br_2 are found to be CBr_2O and CHBrO, whose local lifetimes are calculated to be ~7 and ~2 days, respectively. Simulations here show their contribution to stratospheric bromine is likely to be negligible. The previously used model assumption of instantaneous production of Br_y, following $CHBr_3/CH_2Br_2$ degradation, therefore seems reasonable. It is likely that this assumption will also be valid for other short-lived source gases (e.g. $CHBr_2Cl$, $CHBrCl_2$), whose degradation products are comparably short-lived. However, an attempt at measurement of CBr_2O and CHBrO in the tropical UTLS would be useful.

The CTM has been shown to perform reasonably well against aircraft observations of $CHBr_3$ and CH_2Br_2 in the tropical UTLS. The σ-θ level model (SLIMCAT) tends to agree better with high-altitude aircraft observations than the σ-p level model (TOMCAT). This

is likely due to a more realistic vertical transport in the TTL. Sensitivity simulations have shown a treatment of convection is not required in TOMCAT in order to transport significant quantities of VSLS to the lower stratosphere. In future work the convective transport parameterisation could be included in SLIMCAT to investigate the impact of this against the background of slower resolved advection.

The total contribution from $CHBr_3$ and CH_2Br_2 to stratospheric bromine loading is found to be ∼2.4 ppt. However, a number of assumptions have been made in model experiments. First, a single Br_y tracer has been used and was removed from the model with an assumed 10 day lifetime (due to washout) below the tropopause. Secondly, a uniform surface mixing ratio of 1.2 ppt for both source gases has been used to constrain their abundance at the surface. If the total contribution from all VSLS (Br_y^{VSLS}) is ∼5 ppt (Dorf et al., 2008), then a shortfall of ∼2.6 ppt remains. This may in part be supplied from other bromine-containing source gases such as CH_2BrCl, $CHBr_2Cl$ and $CHBrCl_2$ (local lifetimes of 150, 69 and 78 days respectively, Law and Sturges (2007)). However, it seems unlikely that these species can account for such a shortfall, given their relatively low abundance at the surface and in the UTLS (Kerkweg et al., 2008). Based on compiled observations, Law and Sturges (2007) report mixing ratios of CH_2BrCl, $CHBr_2Cl$ and $CHBrCl_2$ in the UTLS of 0.32 (0.26-0.35) ppt, 0.08 (0.03-0.12) ppt and 0.12 (0.05-0.15) ppt, respectively. The contribution of these minor VSLS to stratospheric bromine will be investigated in Chapter 5. In addition, although not quantified, it is possible "additional bromine source gases", currently unknown, may also contribute (Laube et al., 2008).

Sensitivity simulations using the SLIMCAT σ-θ model have shown a smaller overall contribution from $CHBr_3$ and CH_2Br_2 to stratospheric bromine. From these runs we infer a value of 1.2 ppt (∼0.5× the TOMCAT estimate) when assuming a 10 day lifetime of Br_y. Naturally this increases the discrepancy between the model and the Br_y^{VSLS} value of ∼5 ppt (Dorf et al., 2008).

Chapter 5

Stratospheric Bromine Loading due to Very Short-Lived Species

5.1 Introduction

In Chapter 4, the transport and chemistry of bromoform ($CHBr_3$) and dibromomethane (CH_2Br_2) was examined using the TOMCAT/SLIMCAT three-dimensional (3-D) chemical transport model (CTM). Simulations showed that these source gases (SGs) may contribute ∼2.4 parts per trillion (ppt) of additional inorganic bromine (Br_y) to the tropical lower stratosphere. However, the total contribution from all bromine-containing (Br-containing) very short-lived species (VSLS, Br_y^{VSLS}) is estimated to be 6 (3-8) ppt (Montzka and Reimann, 2011). Therefore, the results of Chapter 4 suggest $CHBr_3$ and CH_2Br_2 alone can only account for 40 (30-80)% of this total. In this chapter, the modelling work of Chapter 4 is extended to include other known biogenic Br-containing VSLS; dibromochloromethane ($CHBr_2Cl$), bromodichloromethane ($CHBrCl_2$) and bromochloromethane (CH_2BrCl).

Some VSLS have a predominately anthropogenic source; e.g. *n*-propyl bromide (*n*-C_3H_7Br, nPB), *i*-propyl bromide (*i*-C_3H_7Br, iPB), ethyl bromide (C_2H_5Br) and ethylene dibromide (CH_2BrCH_2Br, EDB). nPB is currently used as a replacement compound for some chlorofluorocarbons (CFCs, e.g., CFC-113) and for methyl chloroform (CH_3CCl_3). It is used for industrial metal degreasing and electronic part cleaning (Montzka and Reimann, 2011). C_2H_5Br is used in chemical synthesis, as a refrigerant and as a flame retardant.

Observations show surface mixing ratios of <0.3 ppt (Low et al., 2003) and 0.09-0.49 ppt (Carpenter et al., 1999). EDB is used as a fumigant and has been observed at ∼5 ppt in urban areas (Pratt et al., 2000).

In general these *minor* VSLS are poorly studied and observations are sparse. Laube et al. (2008) have suggested unidentified peaks in their chromatogram from air sampled at 15.2 km point towards the presence of C_2H_5Br, nPB and EDB. These balloon-borne measurements were made in 2005 in the tropics (Teresina, Brazil). These species are estimated to currently contribute <0.2 ppt of organic bromine in the tropical tropopause region (Montzka and Reimann, 2011). Although likely small, quantifying the present-day contribution of these unregulated anthropogenic VSLS on stratospheric Br_y is important in order to accurately assess stratospheric bromine loading due to VSLS. The work described in this chapter uses the TOMCAT/SLIMCAT chemical transport model (CTM), as described in Chapter 4, but with some key changes. The aims of this chapter are to:

1. Evaluate modelled distribution of Br-containing VSLS with new observations from the 2009 NSF HIAPER Pole-to-Pole (HIPPO-1) campaign (Wofsy et al., 2011) and ongoing National Oceanic and Atmospheric Administration / Earth System Research Laboratory (NOAA/ESRL) measurement programs.

2. Calculate the local atmospheric lifetimes of poorly studied anthropogenic VSLS C_2H_5Br, CH_2BrCH_2Br, n-C_3H_7Br and i-C_3H_7Br.

3. Estimate Br_y^{VSLS} in the tropical lower stratosphere. Given convection is an uncertainty in a global model, the sensitivity of Br_y^{VSLS} to two treatments of convection is examined.

The chapter is structured as follows. Section 5.2 describes the model simulations that have been performed. Improvements on the previous model set up (Chapter 4) are discussed here also. A comparison of model versus observations along with a description of the HIPPO-1 aircraft data is in Section 5.3. Section 5.4 examines the transport of VSLS in modelled convection and Section 5.6 examines their contribution to stratospheric bromine. Section 5.7 contains a summary of the chapter. This work has been published in the journal Atmospheric Chemistry and Physics (ACP) (Hossaini et al., 2012b).

5.2 Simulations

This section describes simulations performed with the TOMCAT/SLIMCAT 3-D CTM (See Chapter 4). Some aspects of the model set up were identical to that of the previous chapter. The model was again run with a resolution of 5.6° × 5.6° and with 38 vertical levels from the surface to ∼35 km. However, for simulations here the model was forced with analysed winds from the European Centre for Medium-Range Weather Forecasts (ECMWF) ERA-Interim reanalysis (as opposed to operational). This was so the large-scale forcing winds were consistent with a new treatment of convection (see Section 5.4). The number of advected tracers was increased to include all significant Br-containing very short-lived (VSL) SGs. In addition, four long-lived Br-containing SGs were also considered; methyl bromide (CH_3Br), Halon-1211 (H1211), Halon-1301 (H1301) and Halon-2402 (H2402). A summary of the these tracers is given in Table 5.1.

There is significant uncertainty in the surface emissions of natural (and anthropogenic) VSLS. There is likely to be considerable spatial variation in the location of emission (e.g., Law and Sturges, 2007). Warwick et al. (2006) found significant variation in modelled $CHBr_3$ profiles depending on source region. While use of spatially varying emissions for $CHBr_3$ and CH_2Br_2 is possible (e.g., Liang et al., 2010), emissions of minor VSLS (e.g., $CHBr_2Cl$) are poorly quantified. For simplicity, and to overcome some of this uncertainty, the model runs in this chapter again did not use emission fluxes. Rather, as in Chapter 4, the surface volume mixing ratio (vmr) of the Br-containing SGs was overwritten. This constraint is constant with latitude and longitude within the tropics and was scaled so that the model gave good agreement with observations in the free troposphere, where available. This approximation is better for longer-lived species which will be mixed by transport processes and are the species which are potentially more important for transport to the stratosphere. For VSLS, this approach will not capture potential *hot spot* regions where surface fluxes may be relatively large.

For most SGs, the surface vmr was constrained by HIPPO-1 observations in tropical regions. For $CHBrCl_2$ and CH_2BrCl, the model was constrained by the estimated marine boundary layer (MBL) mixing ratios, based on a compilation of observations, provided in Law and Sturges (2007). Observations of EDB, nPB and iPB are sparse. For these gases, the model surface mixing ratio cannot be constrained by observations and thus had

TABLE 5.1: Br-containing source gases and assumed surface volume mixing ratio (ppt).

Source gas	Formula	Source	Surface vmr
Methyl bromide	CH_3Br	N(A)	7.50[a]
Halon 1211 (H1211)	CF_2BrCl	A	4.23[a]
Halon 1301 (H1301)	$CBrF_3$	A	3.15[a]
Halon 2402 (H2402)	$C_2Br_2F_4$	A	0.46[a]
Bromoform	$CHBr_3$	N(A)	1.20[a,b]
Dibromomethane	CH_2Br_2	N	1.0[a,b]
Dibromochloromethane	$CHBr_2Cl$	N(A)	0.20[a]
Bromodichloromethane	$CHBrCl_2$	N(A)	0.33[c]
Bromochloromethane	CH_2BrCl	N	0.47[c]
Ethyl bromide	C_2H_5Br	A	0.30[a]
Ethylene dibromide (EDB)	CH_2BrCH_2Br	A	–
n-propyl bromide (nPB)	n-C_3H_7Br	A	–
i-propyl bromide (iPB)	i-C_3H_7Br	A	–

[a] Best fit to HIPPO observations (this work).
[b] Best fit to observations (Chapter 4).
[c] Estimated tropical MBL mixing ratio (Law and Sturges, 2007).
Source data both natural (N) and/or anthropogenic (A) taken from Law and Sturges (2007).

an arbitrary value at the surface. These gases were not considered in the calculation of Br_y^{VSLS}. Additional tracers added to the CTM included methyl iodide (CH_3I) and also an idealised tracer with a 6 hour lifetime (i6hr). These shorter lived species are useful for assessing troposphere-stratosphere transport in modelled convection. For i6hr, the assumed surface vmr was 1 ppt - an arbitrary value. For CH_3I, the assumed surface vmr was also 1 ppt. This provides a reasonable fit to observations and is also within the estimated range of 0.3-1.9 ppt for the MBL reported by Montzka and Reimann (2011).

Similarly to the CTM set up described in Chapter 4, loss of VSL SGs occurs via OH oxidation and photolysis. Rate constants and absorption cross sections were taken from Sander et al. (2006), where available. SG degradation was assumed to release Br_y immediately (i.e. $CHBr_3 + OH \rightarrow 3\times Br_y$). This assumption, which ignores any organic product gases (e.g. CBr_2O), has been shown to be reasonable for $CHBr_3$ and CH_2Br_2 (See Chapter 4 summary). Henry's law constants needed for calculating the wet deposition of soluble Br_y products were taken from Law and Sturges (2007). Two model simulations have been performed; run $\mathbf{S}_{\text{diagnosed}}$, where convective transport is diagnosed and run $\mathbf{S}_{\text{archived}}$, where convective transport is forced by archived mass fluxes (see Section 5.2.2) Both simulations were initialised on 1 January 2005 and run for 3 years.

5.2.1 Treatment of Soluble Br_y

Two improvements were made to the CTM set up described in Chapter 4. First, the removal of soluble Br_y by wet deposition (washout) in both large-scale dynamic, and also convective, precipitation was considered. The previously employed approach of assuming a uniform 10, 20 or 40 day tropospheric lifetime of Br_y is an oversimplification. This approximation has recently been shown to result in too much scavenging of Br_y (e.g., Liang et al., 2010; Aschmann et al., 2011). The fraction of Br_y available for wet deposition was altitude-dependent. Here Br_y was partitioned among non-soluble products (e.g BrO) and highly soluble HBr using a HBr:Br_y ratio from a previous full chemistry TOMCAT integration (Breider et al., 2010).

Figure 5.1 shows modelled annual tropical mean profiles of primary Br_y species, BrO, HBr, Br_2, Br and HOBr. The CTM output here is taken from a full chemistry integration of the TOMCAT CTM (data provided by T.J. Breider, personal communication). The right panel shows the annual tropical mean HBr:total Br_y ratio. For simulations described here, this profile was interpolated on to the 38 CTM levels and used to determine the mean fraction of Br_y in (soluble) HBr form.

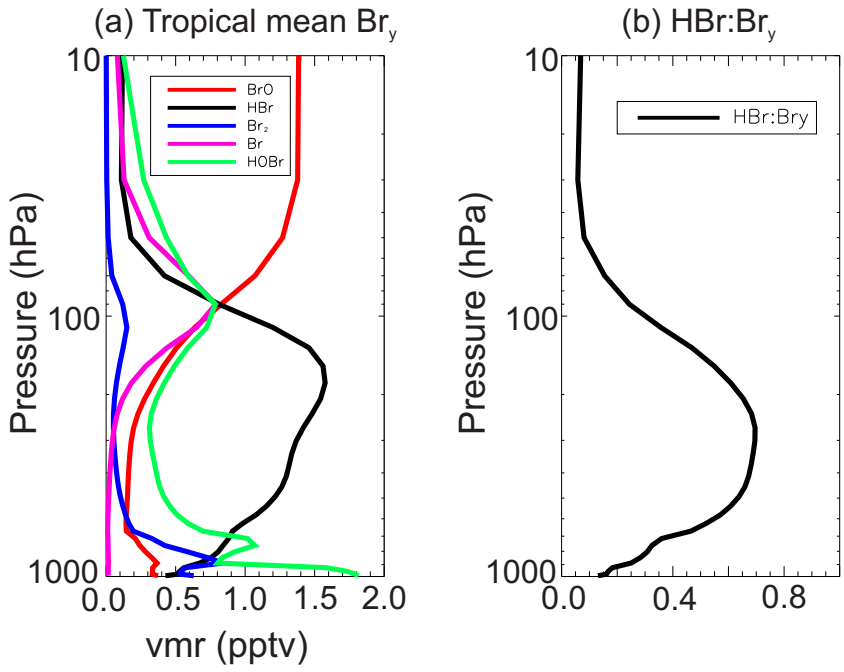

FIGURE 5.1: Annual tropical mean profiles of (a) primary Br_y species and (b) HBr: total Br_y ratio from a full chemistry integration of the TOMCAT CTM.

5.2.2 Treatment of Convection

The second improvement on the Chapter 4 CTM set up concerns model convection. Many offline CTMs, including TOMCAT, diagnose convection from the large-scale meteorological fields of the (ECMWF or other) analyses. This approach requires convection to be re-diagnosed from fields that may have already experienced its effects. Therefore, use of these stable fields may result in too little convection being diagnosed (Feng et al., 2011) and hence an underestimation of short-lived tracers in the upper troposphere.

The standard CTM includes an online parameterisation of cumulus convection based on the Tiedtke (1989) mass flux scheme (Stockwell and Chipperfield, 1999). This version of the CTM set up has been shown to simulate the vertical distribution of short-lived tracers reasonably well in the troposphere; for example see Figure 4.4 of Chapter 4. However, as parameterised convection is an uncertainty, the CTM can also use an offline approach, where convective updraft (and downdraft) mass fluxes are taken from archived ERA-Interim fields. This offline approach is described in Feng et al. (2011) and has been shown to give more tropical convection, which extends to higher altitudes, than that diagnosed using the using the Tiedtke (1989) scheme. A comparison of these two schemes for the transport of VSLS has yet to be performed.

Figure 5.2 shows seasonal zonal mean updraft convective mass fluxes diagnosed from the CTM using the Tiedtke (1989) scheme. Similarly, the same field from the archived ERA-Interim reanalysis (interpolated to CTM levels) is shown in Figure 5.3. The archived mass fluxes are non-zero at ∼100 hPa (∼17 km). The online diagnosed convection does not extend to this level and is only significant up to ∼200 hPa (∼12.5 km), penetrating the bottom of the TTL only. Furthermore, the diagnosed convection also shows a weaker updraft mass flux in the boundary layer.

For run $\mathbf{S}_{\text{diagnosed}}$, the removal of soluble Br_y products in convective precipitation (*washout*) was calculated according to the standard TOMCAT scheme of Giannakopoulos et al. (1999). This scheme is coupled to the Tiedtke (1989) parameterisation, which provides the convective precipitation rates needed to calculate wet deposition rates (see Section 4.2, Chapter 4 also).

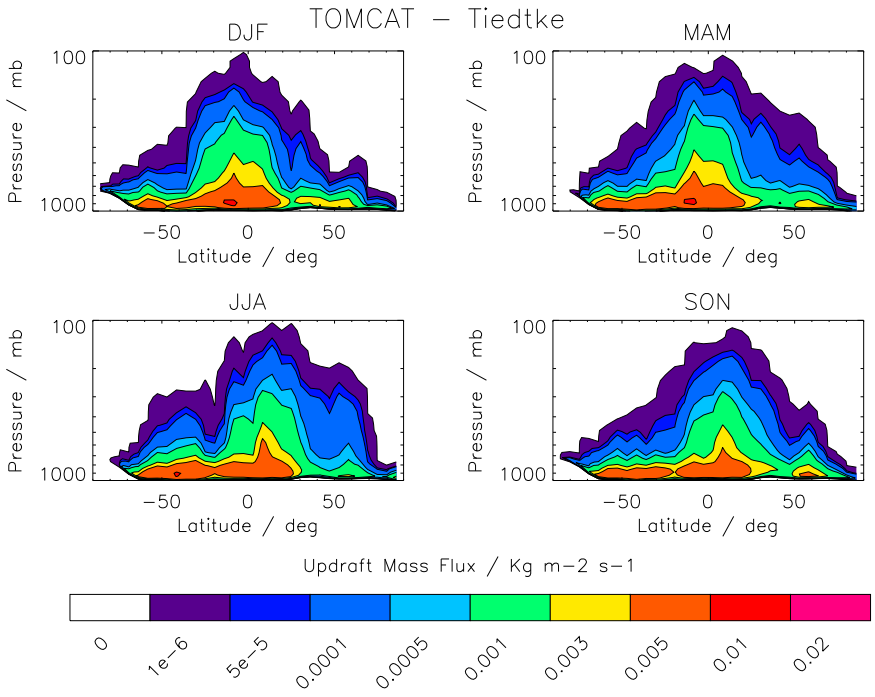

FIGURE 5.2: 2006 seasonal zonal mean updraft convective mass flux (Kg $m^{-2}s^{-1}$) diagnosed from the TOMCAT CTM with the Tiedtke (1989) mass flux scheme.

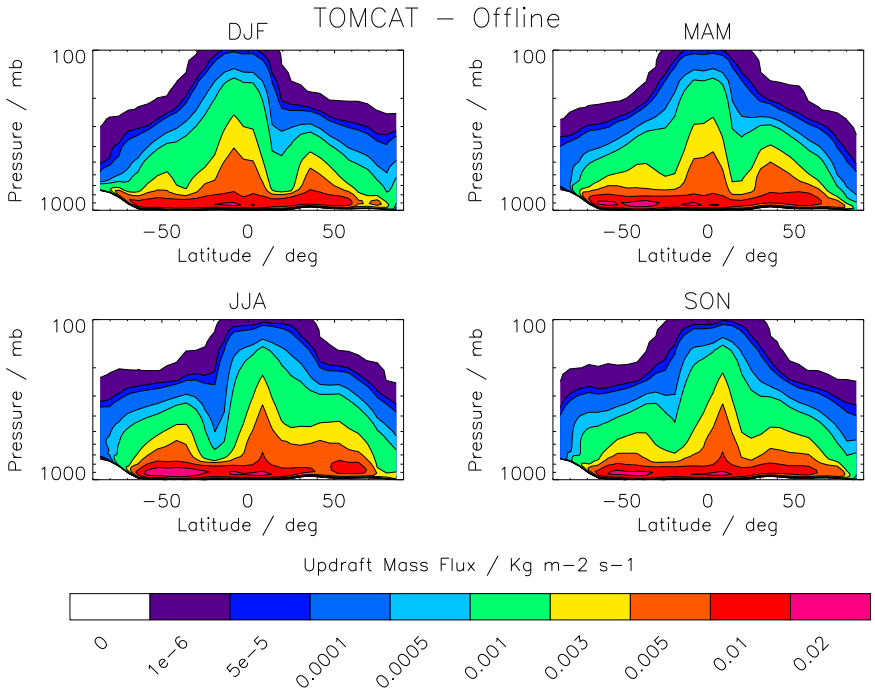

FIGURE 5.3: 2006 seasonal zonal mean updraft convective mass flux (Kg $m^{-2}s^{-1}$) from ECMWF ERA-Interim reanalysis interpolated onto CTM levels.

For this study, the model was adapted to allow convective precipitation and the removal of soluble products to occur whilst using the archived mass fluxes also. Figure 5.4 shows the modelled convective precipitation rate from run $\mathbf{S}_{\text{diagnosed}}$ and from run $\mathbf{S}_{\text{archived}}$. The peak local convective precipitation rate ($\sim$10 mm day^{-1}) occurs in the tropics for run $\mathbf{S}_{\text{archived}}$. However, over all tropical latitudes, the mean rate is largest for $\mathbf{S}_{\text{diagnosed}}$, which overalls shows more convection - particularly over the tropical Western Pacific region.

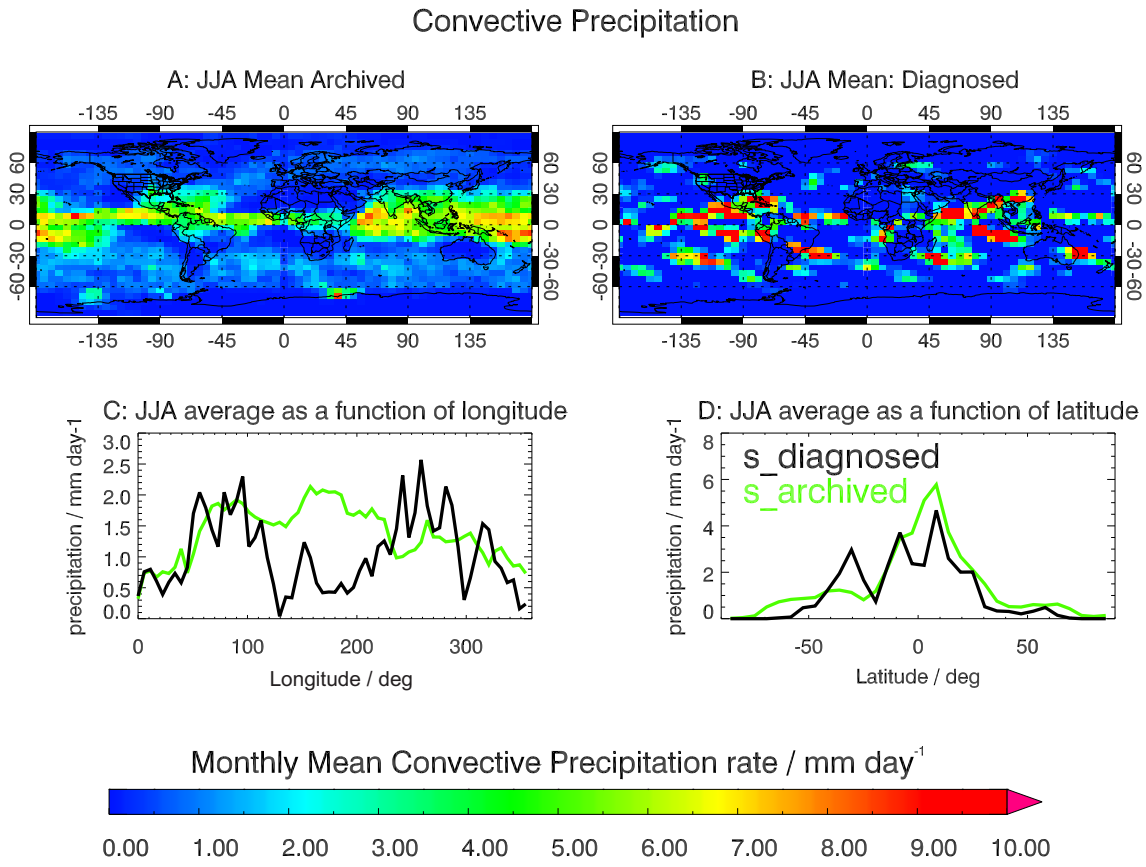

FIGURE 5.4: Modelled convective precipitation rate (mm day^{-1}). (a) JJA mean from run $\mathbf{S}_{\text{archived}}$. (b) JJA mean from run $\mathbf{S}_{\text{diagnosed}}$. (c) JJA mean and latitudinal mean. (d) JJA mean and longitudinal mean.

5.3 Modelled Tracer Profiles

HIPPO-1 was a National Science Foundation (NSF) funded aircraft campaign (http://hippo.ornl.gov/) that took place in January 2009. Flight tracks from the campaign are shown in Figure 5.5. The ongoing HIPPO program spans the globe, from the Arctic circle to coastal Antarctica. The NSF Gulfstream V aircraft is used to sample the atmosphere from the surface to ∼14 km. Numerous trace gases have been measured including major greenhouse gases CO_2, CH_4, N_2O and also CO, SF_6, CFCs, VSLS etc. (Wofsy et al., 2011). The modelled source gas profiles of CH_3Br, H1211, H1301, H2402, $CHBr_3$, CH_2Br_2, $CHBr_2Cl$, C_2H_5Br and CH_3I are shown in Figure 5.6. These are compared with HIPPO-1 aircraft observations in the tropics (±20°). Whole air samples, collected in stainless steel and glass flasks, from 5 flights were analysed using gas chromatography/mass spectrometry (GC-MS) in two different laboratories; the University of Miami and NOAA/ESRL (Schauffler et al., 1999). Mixing ratios reported by the Miami laboratory were multiplied by factors of 0.90, 0.94, 0.98, 0.94, 0.81 and 1.01 for CH_3Br, H1301, H1211, H2402, CH_2Br_2 and $CHBr_3$, respectively, to be consistent with the NOAA/ESRL laboratory calibration scale (S. Montzka, personal communication).

Monthly mean (January 2009) surface observations from an ongoing NOAA/ESRL program at three sites in the Pacific Basin are also considered; American Samoa (SMO, 14.3°S, 170.6°W), Mauna Loa (MLO, 19.5°N, 155.6°W) and Cape Kumukahi (KUM, 19.5°N, 154.8°W). See Figure 5.5 for their location. Whole air samples were collected weekly into paired steel or glass flasks and were analysed (GC-MS) in the same laboratory as the HIPPO measurements. Aircraft observations up to ∼6.5 km above sea level (a.s.l) over Rarotonga (21.5°N, 160.0°W) are also considered. These additional observations are consistent in space/time with the HIPPO-1 observations. Further description of the NOAA/ESRL surface network is in Montzka et al. (2003). For this comparison, the model is averaged over the flight days and spatially over flight tracks. The TTL base is defined as the level of main convective outflow (∼ 12 km) and the top as the cold-point tropopause (CPT, ∼ 17 km). The *upper TTL* is defined as beyond the level of zero radiative heating, where slow radiatively-driven ascent dominates (Law and Sturges, 2007).

Both runs $\mathbf{S}_{\text{diagnosed}}$ and $\mathbf{S}_{\text{archived}}$ show good agreement with observations. Model profiles of $CHBr_3$ and CH_2Br_2 give good agreement when constrained by 1–1.2 ppt at the surface.

This is consistent with the previous aircraft comparisons in Chapter 4. The profiles indicate ∼0.5 and 0.8 ppt of $CHBr_3$ and CH_2Br_2 in the lower TTL, respectively. This is consistent with the lower TTL (12–14 km) mean mixing ratio and range of 0.61(0.3–1.1) ppt and 0.92 (0.77–1.15) ppt reported by Montzka and Reimann (2011), based on a compilation of previous measurements. The HIPPO-1 observations show $CHBr_2Cl$ mixing ratios of 0.1–0.2 ppt in the lower TTL. This is again consistent with previously observed mixing ratios of 0.1(0.06–0.15) ppt (Montzka and Reimann, 2011). The anthropogenic short-lived substance, C_2H_5Br, was also detected in the TTL (∼0.4 ppt). nPB was below the detection limit of ∼0.5 ppt (E. Atlas, personal communication, 2012).

Overall, run $\mathbf{S}_{\text{archived}}$ shows more tracer transported to the upper TTL. This can be expected given that the archived mass fluxes show strong convection in the tropics (e.g., Hoyle et al., 2011; Feng et al., 2011). However, the averaged profiles in Figure 5.6 show only small differences between runs $\mathbf{S}_{\text{diagnosed}}$ and $\mathbf{S}_{\text{archived}}$, particularly for the relatively longer-lived gases for which vertical transport in convective cells is less important. The differences between the two model runs is discussed further in Section 5.4.

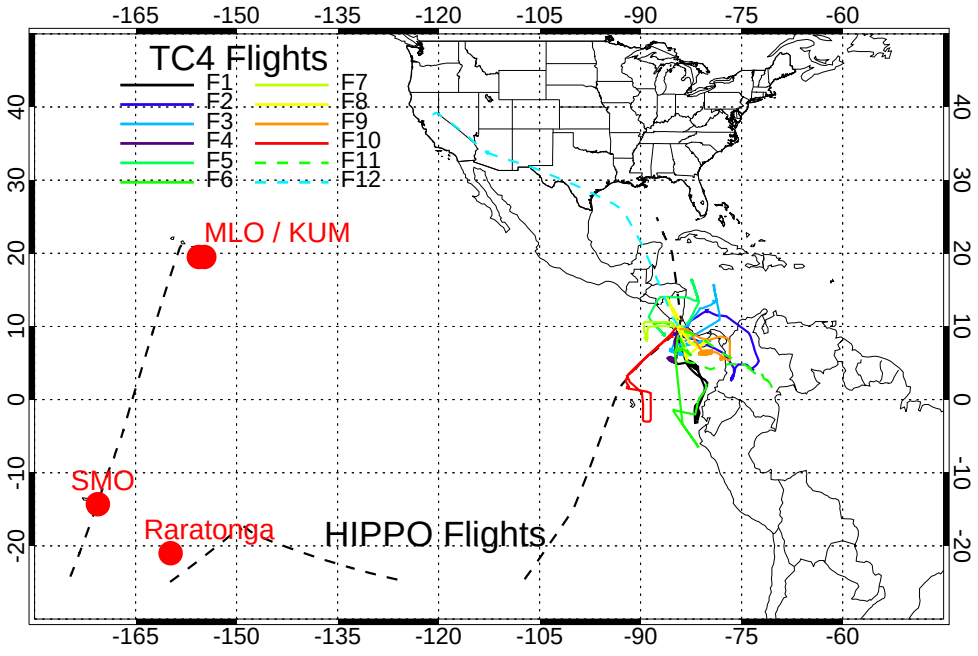

FIGURE 5.5: Location of NOAA/ESRL ground-based stations and aircraft flight tracks (tropics) from the NSF HIPPO-1 and NASA TC4 mission.

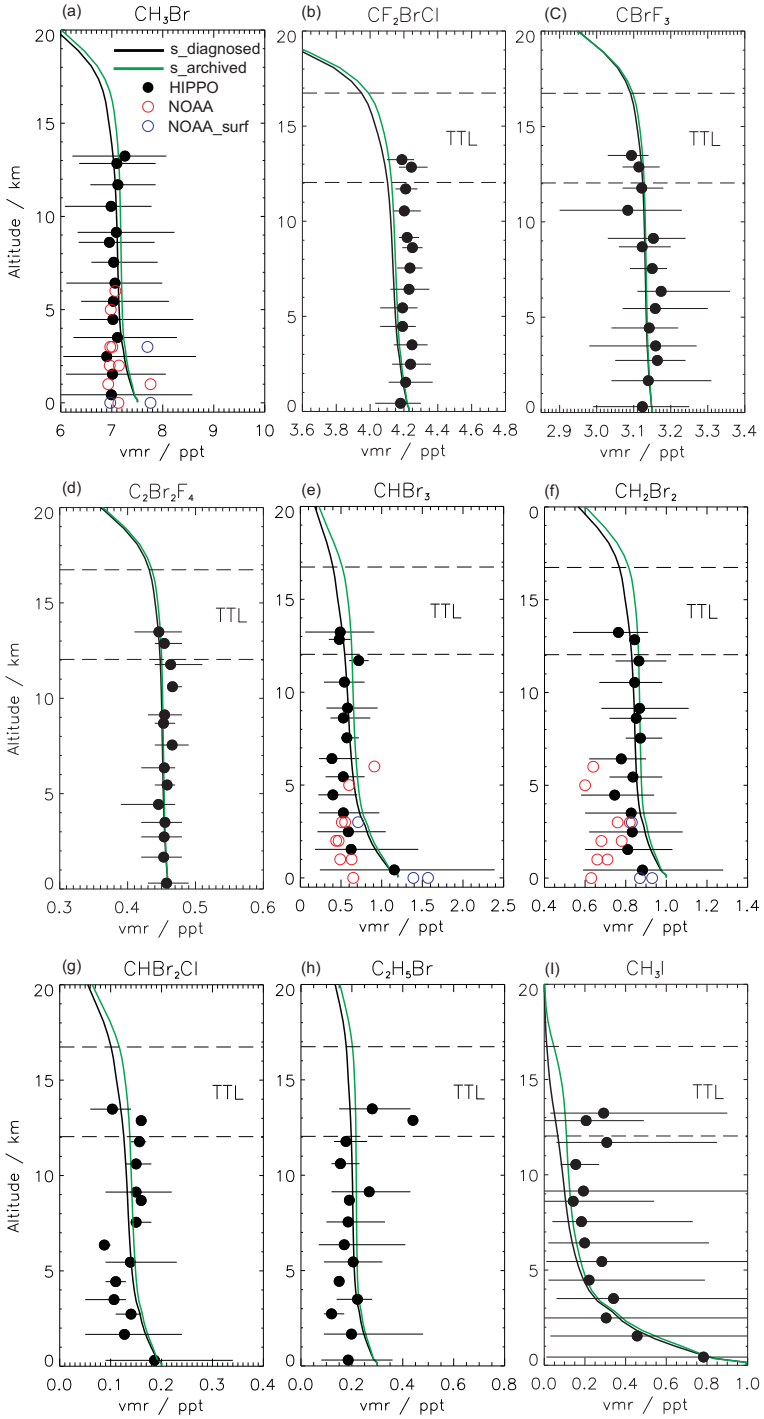

FIGURE 5.6: Mean observed and modelled tropical (±20°) mixing ratio (ppt) of **(a)** CH_3Br, **(b)** CF_2BrCl (H1211), **(c)** $CBrF_3$ (H1301), **(d)** $C_2Br_2F_4$ (H2402), **(e)** $CHBr_3$, **(f)** CH_2Br_2, **(g)** $CHBr_2Cl$, **(h)** C_2H_5Br and **(i)** CH_3I. Observations (filled circles) taken from the NSF HIPPO-1 campaign (January 2009). Horizontal bars denote min-max variability of observations at given level. Open circles denote observations during January 2009 from three NOAA/ESRL surface sites (blue points from SMO, 14.3°S, 170.6°W, 77 m a.s.l.; MLO, 19.5°N, 155.6°W, 3397 m a.s.l.; KUM, 19.5°N, 154.8°W, 3 m a.s.l.) or from vertical profiles (red points sampled over Rarotonga, 21°S, 159.8°W).

5.4 Archived Versus Diagnosed Convection

The implementation of 6-hourly ECMWF archived convective mass fluxes in the TOMCAT CTM is described in Feng et al. (2011). Here, observations of short-lived halogen species in the mid-upper troposphere are used to examine the performance of these fluxes compared to fluxes diagnosed within the model. The archived convective updraft mass flux shows non-zero values at 100 hPa ($\sim$17 km). The diagnosed convection typically does not extend above 200 hPa ($\sim$12.5 km) and this does not capture deep convective events (Feng et al., 2011). To investigate the differences between runs $\mathbf{S}_{\text{diagnosed}}$ and $\mathbf{S}_{\text{archived}}$ further, CH_3I is also considered; a trace gas with a local lifetime of $\sim$7 days and thus shorter lived than any of the bromine-containing VSLS previously discussed (Law and Sturges, 2007). Figure 5.7 shows modelled profiles of CH_3I in the tropics from both runs $\mathbf{S}_{\text{diagnosed}}$ and $\mathbf{S}_{\text{archived}}$ versus observations made on board the DC-8 aircraft during the 2007 NASA TC4 campaign (see Chapter 4 for campaign description).

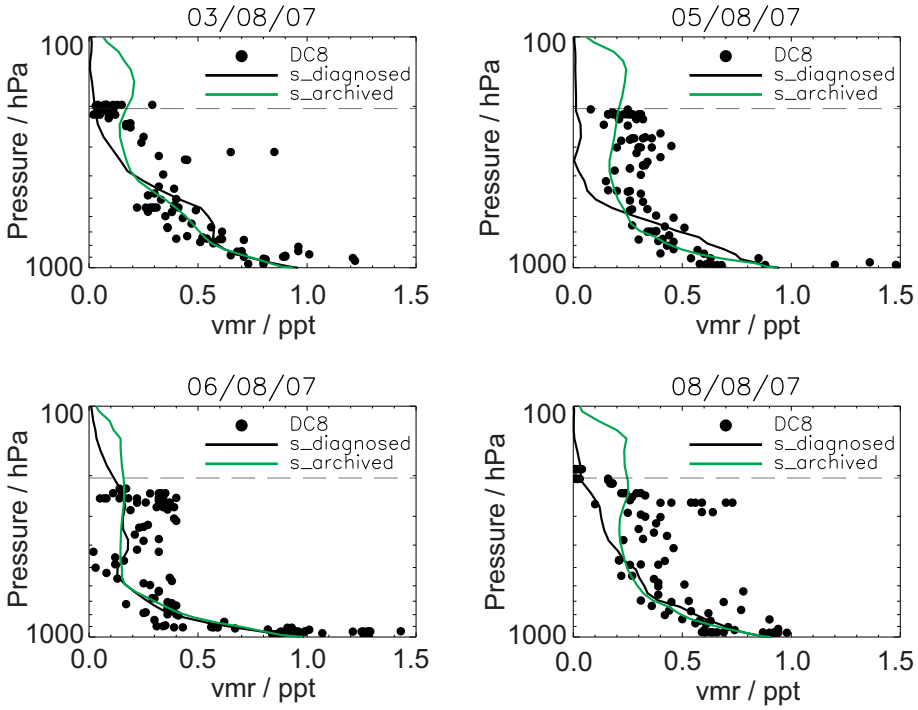

FIGURE 5.7: Comparison of modelled CH_3I profiles with observations made on board 12 DC-8 flights during the NASA TC4 campaign (July–August 2007, http://www.espo.nasa.gov/tc4/). The CTM profiles are from both runs $\mathbf{S}_{\text{diagnosed}}$ and $\mathbf{S}_{\text{archived}}$. The approximate base of the TTL is indicated with a dashed line.

In Figure 5.7, the difference due to the two treatments of convection is more pronounced on the tracer distribution. With an assumed uniform surface mixing ratio of 1 ppt in the tropics, both runs $\mathbf{S}_{\text{diagnosed}}$ and $\mathbf{S}_{\text{archived}}$ give reasonable agreement with the observations. A surface mixing ratio of 1 ppt is within the estimated range of 0.3–1.9 ppt for the marine boundary layer reported by Montzka and Reimann (2011). Run $\mathbf{S}_{\text{archived}}$ shows significantly more CH_3I in the TTL. This appears to provide a better fit to observations, particularly for flights on the 5/8 August 2007. However, more comparison with observations is required in order for a quantitative assessment. The zonally averaged mixing ratios of the idealised tracer with a 6 h lifetime (i6hr), CH_3I, $CHBr_3$ and CH_2Br_2 at the approximate base of the TTL ($\sim$200 mb) and the tropical cold point tropopause (CPT, $\sim$100 mb) are shown in Figure 5.8.

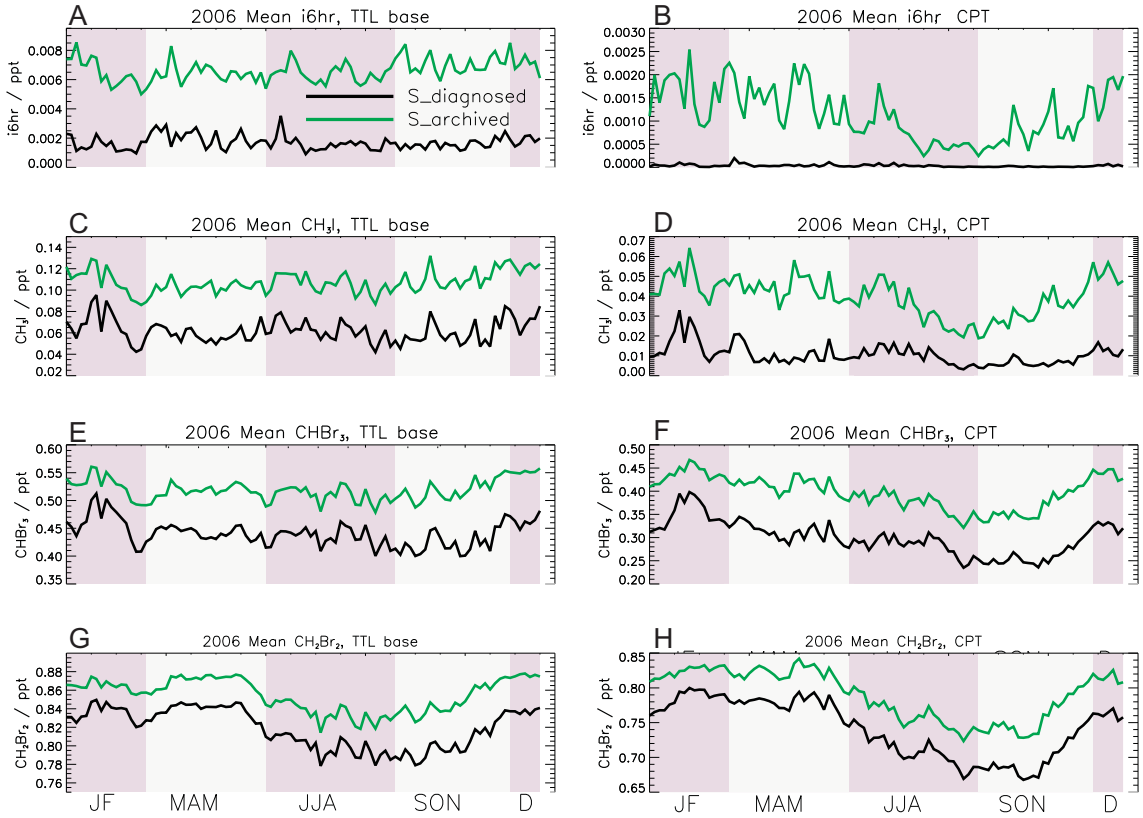

FIGURE 5.8: Zonally averaged volume mixing ratio of **(A,B)** i6hr, **(C,D)** CH_3I, **(E,F)** $CHBr_3$ and **(G,H)** CH_2Br_2 as a function of time (2006) at the TTL base and the tropical cold point tropopause, respectively, for CTM runs $\mathbf{S}_{\text{diagnosed}}$ and $\mathbf{S}_{\text{archived}}$.

i6hr was initialised at 1 ppt at the surface at the start of the simulation. Run $\mathbf{S}_{\text{archived}}$ transports more tracer to higher altitudes in all seasons with the largest difference between runs

$\mathbf{S}_{\text{diagnosed}}$ and $\mathbf{S}_{\text{archived}}$ being for the relatively shortest lived species (e.g. i6hr, CH_3I). For CH_3I, CPT mixing ratios are within the estimated range of 0.02–0.18 ppt reported by Law and Sturges et al. (2007) for the tropical upper troposphere. The CPT CH_3I mixing ratios from $\mathbf{S}_{\text{diagnosed}}$ are up to $\sim 6\times$ lower. For $CHBr_3$ and CH_2Br_2, both the TTL and CPT mixing ratios are less sensitive to the choice of convection scheme.

Figure 5.9 shows the annual mean mixing ratio of i6hr at the CPT for runs $\mathbf{S}_{\text{diagnosed}}$ and $\mathbf{S}_{\text{archived}}$. Clearly, stronger convection with run $\mathbf{S}_{\text{archived}}$ leads to a larger modelled mixing ratio at this level. Here, the strongest convection occurs over the Western Pacific, indicating a strong source region for the troposphere-stratosphere of VSLS – consistent with Aschmann et al. (2009). For studying the troposphere-stratosphere transport of relatively short lived gases (including species whose lifetime is equal to or less than that of CH_3I), the choice of convection scheme will clearly be important.

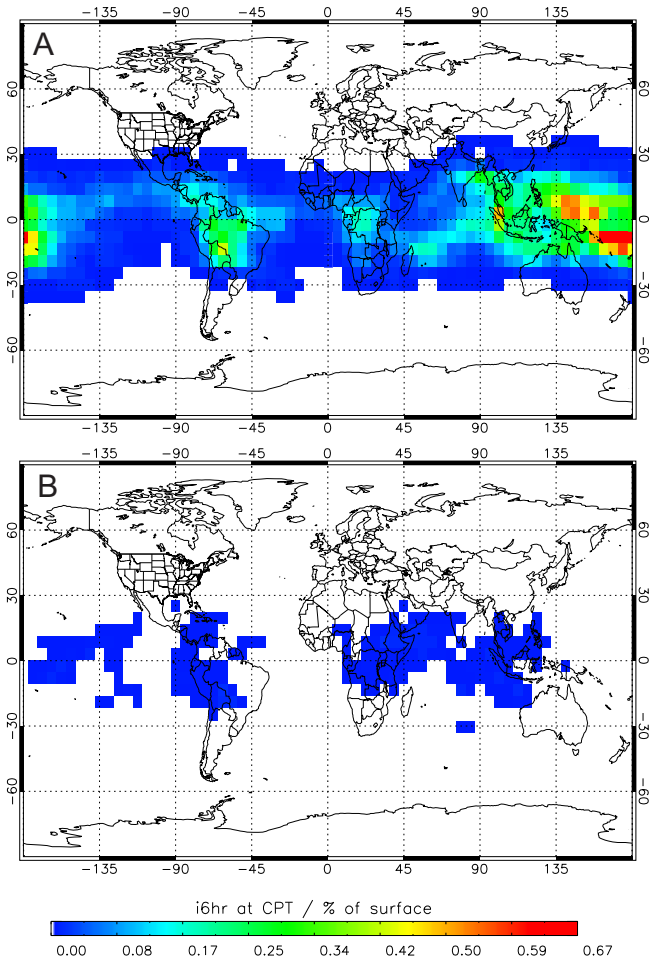

FIGURE 5.9: Percentage (%) of the surface vmr of i6hr at the cold point tropopause from **(a)** $\mathbf{S}_{\text{archived}}$ and **(b)** $\mathbf{S}_{\text{diagnosed}}$. Initial uniform surface vmr of 1 ppt.

5.5 Source Gas Local Lifetimes

The local lifetimes (τ_{local}) of source gases have been calculated with:

$$\tau_{\text{local}}^{-1} = \tau_{OH}^{-1} + \tau_{h\nu}^{-1}$$

Here τ_{OH} and $\tau_{h\nu}$ are the lifetimes with respect to OH oxidation and photolysis, respectively. The annual tropical mean profiles of these fields for C_2H_5Br, EDB, nPB and iPB are shown in Figure 5.10. The equivalent lifetime plots for $CHBr_3$ and CH_2Br_2 can be found in Chapter 4 (Figure 4.2).

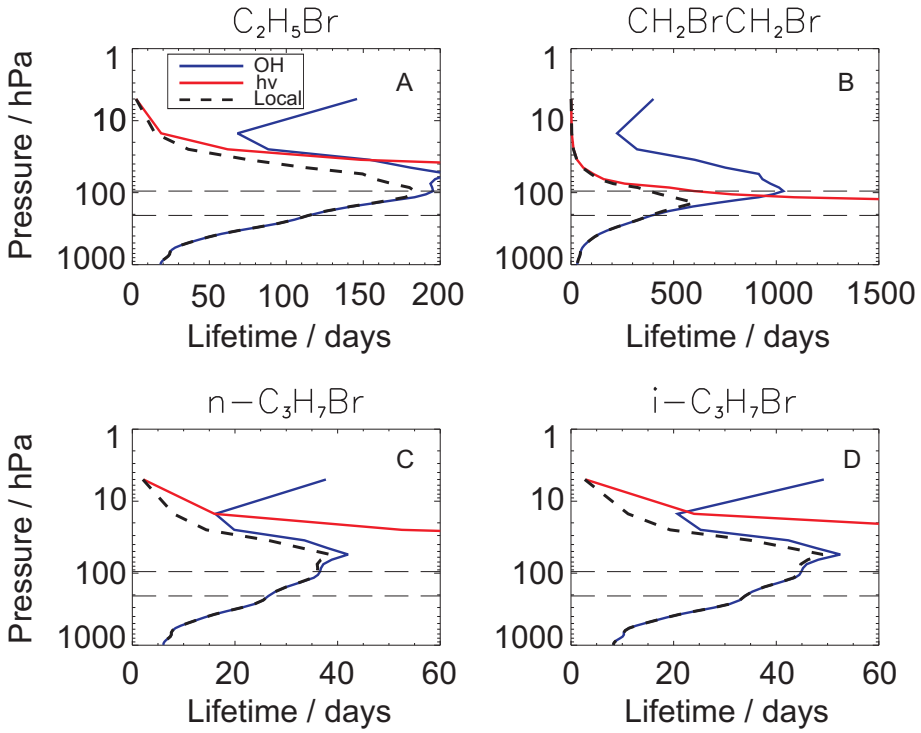

FIGURE 5.10: Modelled tropical mean local lifetime (days) with respect to OH oxidation, photolysis and total for **(a)** C_2H_5Br, **(b)** CH_2BrCH_2Br, **(c)** n-C_3H_7Br and **(d)** i-C_3H_7Br. Horizontal lines denote the approximate TTL.

For these species OH oxidation is the dominant sink in the troposphere. For C_2H_5Br, the simulated local lifetime is $\sim$18 days at the surface and up to $\sim$183 days in the TTL. Similarly for EDB, the local lifetime is $\sim$30 and up to $\sim$603 days at the surface and in the TTL, respectively. The long local lifetime in the cold TTL is due to the strong temperature dependence of the OH sink reaction. Once in the TTL, C_2H_5Br and EDB are thus potentially important carriers of bromine to the stratosphere.

It is clear that local lifetimes of VSLS can vary substantially with altitude. The simulated local lifetime of nPB is $\sim$6 days at the surface and up to 38 days in the TTL. Similarly for iPB, a local lifetime of 8 (surface) and 49 days (TTL) is found. For these species with relatively shorter lifetimes at the surface, rapid convective transport to the TTL is likely required for their source gas injection of stratospheric bromine to be significant. The mean tropospheric local lifetimes of VSLS have also been calculated. These values are shown in Table 5.2.

The simulated local lifetimes in the TTL reported here vary from those quoted in the recent World Meteorological Organisation (WMO) Assessment Report (Montzka and Reimann et al., 2010). The reason for this is that the WMO values are based on OH loss rates calculated using a uniform tropospheric OH concentration (1×10^6 molecule cm^{-3}) and for a temperature of 275 K, i.e. representative of the surface. The simulated local lifetimes here are derived using a spatially/temporally varying OH field (and photolysis) and can be quoted as a function of temperature/altitude. A direct comparison of the two is therefore not appropriate, but if a gas is sufficiently long-lived to be transported away from the surface then the WMO lifetimes may not be applicable.

5.6 Modelled Total Bromine

The calculated stratospheric source gas injection (SGI), product gas injection (PGI) and total bromine (SGI + PGI) for VSLS, CH_3Br and the halons is shown in Table 5.2. SGI is the organic bromine resulting from direct transport of a source gas to the lower stratosphere (i.e. for CH_2Br_2, 2$\times$ the SG mixing ratio at the tropopause). Similarly, PGI is the contribution from the inorganic products, formed following SG degradation.

The total bromine contribution from *major* VSLS $CHBr_3$ and CH_2Br_2 is $\sim$2.09 and 1.69 ppt (tropical mean), respectively from simulation $\mathbf{S}_{\text{diagnosed}}$. The contribution is larger (2.32 and 1.74 ppt) from simulation $\mathbf{S}_{\text{archived}}$. The larger SGI values from simulation $\mathbf{S}_{\text{archived}}$ are due to deeper model convection from the ECMWF ERA-Interim fields. This allows more rapid tracer transport to the cold TTL where the lifetime of most SGs is relatively long. As noted previously (see Section 5.2.2), the enhanced upwelling due to stronger convection in simulation $\mathbf{S}_{\text{archived}}$ is most significant for the shortest lived tracers. For CH_3I (PGI not considered), expressed as a tropical mean, $\sim$1.0% and 3.6% of the

TABLE 5.2: 2007 tropical mean source gas injection (SGI), product gas injection (PGI) and total bromine (SGI + PGI) loading from VSLS, CH_3Br and the halons in the lower stratosphere. Results are from simulations $\mathbf{S}_{\text{diagnosed}}$ and $\mathbf{S}_{\text{archived}}$.

	SGI (ppt)		PGI (ppt)		Total[b]	
Species[a]	S_{diag}	S_{arch}	S_{diag}	S_{arch}	S_{diag}	S_{arch}
CH_3Br	6.77	6.90	0.33	0.29	7.11 [95]	7.19 [96]
H1211	3.94	3.98	0.21	0.19	4.15 [98]	4.17 [99]
H1301	3.09	3.09	0.04	0.04	3.13 [99]	3.13 [99]
H2402	0.86	0.87	0.04	0.04	0.90 [98]	0.91 [99]
$CHBr_3$ {21}	1.06	1.41	1.03	0.91	2.09 [58]	2.32 [64]
CH_2Br_2 {212}	1.49	1.58	0.20	0.16	1.69 [85]	1.74 [87]
$CHBr_2Cl$ {42}	0.19	0.22	0.10	0.08	0.29 [73]	0.30 [75]
$CHBrCl_2$ {35}	0.14	0.17	0.09	0.07	0.23 [70]	0.24 [73]
CH_2BrCl {274}	0.37	0.39	0.04	0.03	0.41 [87]	0.42 [89]
$C2H_5Br$ {72}	0.17	0.19	0.04	0.03	0.21 [70]	0.22 [73]
EDB {200}	–	–	–	–	– [80]	– [85]
nPB {17}	–	–	–	–	– [40]	– [50]
iPB {21}	–	–	–	–	– [50]	– [60]
$\sum$ **VSLS**	**3.42**	**3.96**	**1.50**	**1.28**	**4.92**	**5.24**
$\sum$ **ALL**	**18.08**	**18.80**	**2.12**	**1.84**	**20.21**	**20.64**

[a] Curly brackets ({ }) give the mean species-weighted tropical tropospheric lifetime (days).
[b] Square brackets ([ ]) give the fraction of total boundary layer bromine reaching the lower stratosphere (%).

source gas surface vmr (1 ppt) reaches the lower stratosphere from runs $\mathbf{S}_{\text{diagnosed}}$ and $\mathbf{S}_{\text{archived}}$, respectively.

As run $\mathbf{S}_{\text{archived}}$ experiences more spatially widespread convection, the associated precipitation is also greater. This increases the likelihood of wet deposition of soluble Br_y in these regions and acts to reduce PGI. Overall, convection is a significant uncertainty in global models and significant variation exits between parameterisations of cumulus convection. Here the Tiedtke (1989) scheme is used but different parameterisations that provide more (less) frequent/intense convective upwelling would likely increase (decrease) the modelled SGI. As the removal of soluble products are coupled to the convective precipitation this could also lead to a decrease (increase) in the delivery of Br_y from VSLS reaching the stratosphere via the PGI route. Physical atmospheric removal of Br_y in the TTL is also possible from adsorption on to ice. However, according to recent model work, this process (not considered here) represents only a small sink (Aschmann et al., 2011).

The modelled Br_y^{VSLS} from $CHBr_3$ and CH_2Br_2 alone ($\sim$ 4 ppt) is slightly lower than the

5 ppt reported by Liang et al. (2010) but larger than the 2.4 ppt calculated in Chapter 4. This is due to the explicit modelling of wet deposition, resulting in a larger contribution from the PGI route in this present work. For $CHBr_3$, 0.97 ppt of Br_y is found to reach the tropical lower stratosphere via the PGI route. This is $\sim 3\times$ larger than the 0.3 ppt reported in Chapter 4.

The *minor* VSLS individually provide a modest amount of total bromine to the lower stratosphere. The largest contributor, CH_2BrCl, provides about one fifth that of $CHBr_3$. However, their accumulated total (~ 1.2 ppt from $\mathbf{S}_{\text{archived}}$) is significant and is likely a lower limit due to nPB, iPB and EDB not considered in the calculation. The contribution of all VSLS considered here and also the long-lived species to the total stratospheric bromine is shown in Figure 5.11. The model ($\mathbf{S}_{\text{archived}}$) shows ~ 21 ppt of total bromine in the stratosphere. The total Br_y^{VSLS} supply is found to be ~ 4.9–5.2 ppt for runs $\mathbf{S}_{\text{diagnosed}}$ and $\mathbf{S}_{\text{archived}}$, respectively. This range is consistent with the inferred Br_y^{VSLS} supply of $5.2(\pm 2.5)$ ppt by Dorf et al. (2008). This study used ballon-borne DOAS (Differential Optical Absorption Spectroscopy) measurements of BrO in the stratosphere. Combined with modelling work, the authors were able to infer the VSLS Br_y contribution (from the BrO/Br_y ratio). The modelled Br_y^{VSLS} estimate of ~ 4.9–5.2 ppt is also in reasonable agreement with estimates based on ground-based BrO observations; for example, 6 (3-9) ppt (Schofield et al., 2006). However, it is significantly lower than the estimate of 8.4 (6.4-10.4) ppt of Sioris et al. (2006) from SCIAMACHY satellite BrO profiles.

Of the VSLS with a solely anthropogenic source, only C_2H_5Br was considered in the calculated value of Br_y^{VSLS}. These results may therefore have a low bias due to EDB, nPB and iPB not being included in the calculation. Montzka and Reimann (2011) estimate that minor anthropogenic VSLS including C_2H_5Br, EDB and nPB species contribute < 0.2 ppt via the SGI pathway. The model shows C_2H_5Br and EDB are sufficiently long-lived to be potentially important carriers of bromine to the stratosphere. Simulations show, regardless of the surface vmr, ~ 70–73 % and 80–85 % of total surface bromine from C_2H_5Br and EDB in the tropics can reach the lower stratosphere.

Tropospheric loss of the major long-lived SGs have also been quantified. Tropospheric loss of the halons in the model was found to be negligible. For CH_3Br, ~ 0.7 ppt of source gas is found to be removed in the troposphere from $\mathbf{S}_{\text{diagnosed}}$; 9 % of the assumed 7.5 ppt surface boundary condition. This is consistent with the estimated CH_3Br gradients of

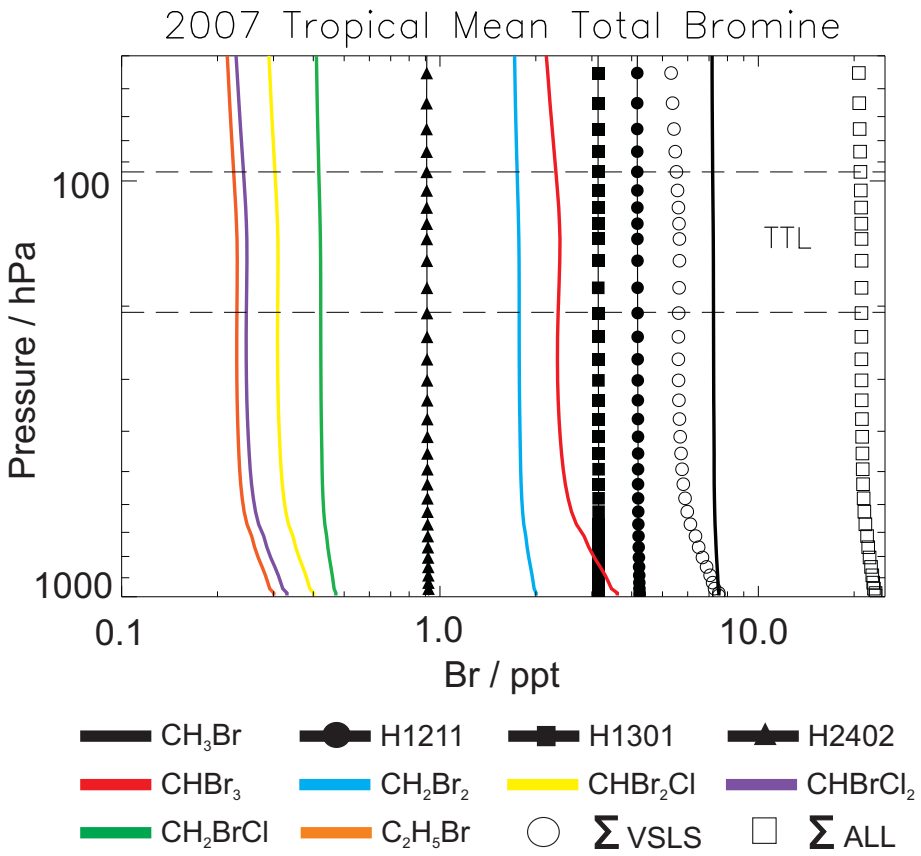

FIGURE 5.11: Modelled tropical mean total bromine (ppt) for 2007 and from simulation $\mathbf{S}_{\text{archived}}$. Dashed horizontal lines denote the approximate base of the TTL and the cold-point tropopause (CPT).

0–15 % reported by Schauffler et al. (1999). The PGI route still allows ∼0.33 ppt of the resulting Br_y to enter the stratosphere. Therefore, ∼0.4 ppt of bromine is physically removed from the atmosphere (∼5 % of the surface boundary condition). This result implies that estimates of Br_y^{VSLS} that ignore tropospheric gradients of CH_3Br may have a low bias of 0.4 ppt or so (though this may be compensated for by omission of minor VSLS). This result is likely sensitive to the model OH field and also treatment of wet deposition; both of which carry some uncertainty. For OH, the model reads monthly averaged 24-hour mean values from a previous full chemistry integration. Tropospheric variability in OH is large and observations are sparse. However, comparison of OH profiles from the 1999 NASA PEM TROPICS-B campaign with modelled profiles (not shown), show reasonable agreement. The model OH field in this case was found to be within the min-max variability of the available observations from the surface to 200 hPa. However, it is acknowledged that model [OH] is still a potential source of error.

5.7 Summary

A 3-D offline CTM has been used to calculate the contribution of VSLS to the stratospheric bromine budget. In total, 9 VSLS, methyl bromide and also four halon source gases have been considered. Modelled profiles of these gases give good agreement with tropical observations from the recent 2009 HIPPO-1 aircraft campaign. Both model and observations reiterate that a significant amount of total stratospheric bromine may arise from naturally-emitted VSLS. The observations did not detect significant levels of anthropogenic-VSLS. However, ethyl bromide (C_2H_5Br) was detected at ~ 0.4 ppt in the TTL. Anthropogenic VSLS likely contribute only a small amount of bromine to the present day stratosphere. However, observations of these species are limited and more data is needed to support this conclusion.

Both ethyl bromide and ethylene dibromide (EDB) are long-lived in the tropical tropopause layer and thus are potentially efficient carriers of bromine to the stratosphere. The simulated local atmospheric lifetime of these anthropogenic gases are up to ~ 183 and 603 days in the TTL, respectively. Therefore, locally these gases may breach the WMO working definition of a very short-lived species (i.e. lifetimes less than 6 months). Other anthropogenic gases considered, *n*-propyl bromide and *i*-propyl bromide are shorter-lived. The maximum simulated local lifetimes in the TTL are ~ 39 and 49 days.

Model simulations show the contribution of the VSLS $CHBr_3$, CH_2Br_2, $CHBr_2Cl$, $CHBrCl_2$, CH_2BrCl and C_2H_5Br to stratospheric Br_y is 4.9–5.2 ppt for the present day, consistent with balloon-borne estimates. This may represent a lower limit as three anthropogenic gases, EDB, *n*-propyl bromide and *i*-propyl bromide are not included in the calculation. Approximately 76 % of this supply comes from $CHBr_3$ and CH_2Br_2. To date, most model work has focused on these species. This study shows *minor* VSLS (e.g. $CHBr_2Cl$, CH_2BrCl) individually contribute modest amounts. However, their overall total is significant and comparable to that of one of the *major* VSLS (e.g. CH_2Br_2). Omission of these *minor* species in model simulations may result in an underestimate of stratospheric Br_y by $\sim$1.2 ppt. More observations of these gases, particularly in the upper TTL, are required to further constrain estimates of their contribution to stratospheric Br_y.

Chapter 6

The Impact of Very Short-Lived Species on Stratospheric Ozone

6.1 Introduction

The importance of active bromine radicals (Br_x = Br + BrO) in the catalytic destruction of stratospheric ozone (O_3) is well established (e.g., Wofsy et al., 1975). Due to a lack of stable reservoirs, BrO is the dominant inorganic bromine (Br_y) species in the stratosphere. Coupled cycles, involving analogous chlorine radicals, account for a significant total of seasonal O_3 loss observed in polar regions (WMO, 2011). At mid-latitudes, the BrO-ClO cycle is enhanced during periods of high aerosol loading due to heterogeneous halogen activation (e.g., Feng et al., 2007). A coupled BrO-HO_2 cycle is also important for O_3 loss in the mid-latitude lower stratosphere (Salawitch et al., 2005).

In Chapter 5, a chemical transport model (CTM), with varying treatments of convection, was used to quantify stratospheric bromine (Br) loading due to very short-lived species (VSLS). The CTM results suggest VSLS may contribute ∼5.0 parts per trillion (ppt) of inorganic bromine (Br_y^{VSLS}) to the tropical lower stratosphere - consistent with balloon borne estimates (e.g., Dorf et al., 2008) and within the currently accepted range of 6 (3-8) ppt (Montzka and Reimann, 2011). In this chapter, the impact of Br_y^{VSLS} on stratospheric (O_3) is examined using a chemistry-climate model (CCM). Specifically, the aims of this chapter are to:

1. Describe the treatment of Br-containing VSLS in a 3-D CCM. Use the CCM to quantify stratospheric Br_y^{VSLS} and compare with previous CTM estimates.

2. Assess the CCM performance in reproducing observed bromoform ($CHBr_3$) and dibromomethane (CH_2Br_2) at various ground-based stations and also in the tropical tropopause layer (TTL).

3. Perform (1) and (2) using a range of available emission estimates for major VSLS bromoform ($CHBr_3$) and dibromomethane (CH_2Br_2). Determine the suitability of each emission scenario.

4. Determine the impact of Br_y^{VSLS} on global stratospheric O_3.

The chapter is structured as follows. Section 6.2 contains a brief description of the key dynamics and chemistry within the CCM. This section also describes the experiments that have been performed with the model and the different VSLS emission scenarios considered. In Section 6.3, the model is evaluated against a range of observations from both ground-based and aircraft platforms. In Section 6.4, the CCM is used to quantify Br_y^{VSLS} and compared with the previous CTM estimate of Chapter 5. The impact of Br_y^{VSLS} on global O_3 is evaluated in Section 6.5. Finally, a summary of this chapter's work is given in Section 6.6.

6.2 UKCA Chemistry Climate Model

The UK Chemistry and Aerosols (UKCA) model is a CCM based on the Met Office Unified Model (UM) version 7.3. The model has previously been used for studies of stratospheric O_3 (e.g., Morgenstern et al., 2008; Braesicke et al., 2011) and recently took part in the Stratospheric Processes and their Role in Climate (SPARC) Chemistry-Climate Model Validation Activity (CCMVal, 2010). The dynamical core of the model is based on the middle atmosphere version of the UM and is described in Davies et al. (2005). The model is non-hydrostatic and employs a terrain-following hybrid height vertical coordinate. Advection follows the semi-Lagrangian scheme of Priestley (1993) and the model boundary layer scheme is that of Lock et al. (2000).

The version of the model used here contains a detailed stratospheric chemistry scheme based on Chipperfield and Pyle (1998). A list of reactions can be found in Morgenstern et al. (2009). Photolysis rates are computed online using the FAST-JX scheme [P. Telford, manuscript in preparation, 2012] and O_3 chemistry is coupled to the radiation scheme of Edwards and Slingo (1996) which considers 9 bands in the longwave and 6 in the shortwave part of the spectrum. The following radiatively important gases are also coupled: carbon dioxide (CO_2), methane (CH_4), nitrous oxide (N_2O), chlorofluorocarbons (CFCs), CFC-11 (CCl_3F), CFC-12 (CCl_2F_2), CFC-113 ($C_2Cl_3F_3$) and hydrochlorofluorocarbons (HCFCs), HCFC-22 ($CHClF_2$), HCFC-125 (C_2HF_5) and HCFC-134a (CH_2FCF_3).

6.2.1 Simulations

For all simulations described here UKCA was run with a horizontal resolution of 3.75° longitude × 2.5° latitude and with 60 hybrid-height levels extending from the surface to ∼80 km. The model was run in *atmosphere-only* mode and forced with prescribed sea surface temperatures (SSTs) and sea ice fields. These were taken from the Hadley Centre Sea Ice and Sea Surface Temperature (HadISST) data set (Rayner et al., 2003).

Five 30-year time-slice experiments corresponding to 2000 conditions ($\mathbf{S}_{2000N}$, $\mathbf{S}_{2000F}$, $\mathbf{S}_{2000L}$, $\mathbf{S}_{2000W}$ and $\mathbf{S}_{2000Ord}$) were performed. For each of these runs the greenhouse gas (GHG) loading was prescribed according to the World Meteorological Organization (WMO) A1 scenario (Law and Sturges, 2007). For the long-lived and well-mixed bromocarbons, a prescribed uniform volume mixing ratio (vmr), also based on WMO A1, is applied at the surface (χ_{2000}). In this study, 5 Br-containing very short-lived (VSL) source gases (SGs) were added to the CCM; $CHBr_3$, CH_2Br_2, dibromochloromethane ($CHBr_2Cl$), bromodichloromethane ($CHBrCl_2$) and bromochloromethane (CH_2BrCl). For run $\mathbf{S}_{2000N}$, these VSLS are switched off, i.e. long-lived bromine SGs only.

For run $\mathbf{S}_{2000F}$ a fixed vmr was used to constrain the surface abundance of VSL SGs (χ_{2000}). This simple, idealised approach, which is better for long-lived gases, has been shown in the CTM work of Chapters 4 and 5 to give reasonable agreement between modelled and measured profiles of $CHBr_3$ and CH_2Br_2 in the mid-upper troposphere. However, as the imposed surface boundary condition is uniform, the model will not capture spatial variability and potential regional *hot spots*. For VSLS, χ_{2000} was based on compiled aircraft

TABLE 6.1: UKCA Br-containing source gases and product gases. The values of the fixed surface boundary mixing ratios (χ_{2000}) are given in parts per trillion (ppt).

Species	Formula	χ_{2000} (ppt)
Long-lived		
Methyl bromide	CH_3Br	8.66
Halon 1211	CF_2BrCl	4.04
Halon 1202	CBr_2F_2	0.05
Halon 1301	$CBrF_3$	2.73
Halon 2402	$C_2Br_2F_4$	0.41
VSLS		
Bromoform	$CHBr_3$	1.20 [1]
Dibromomethane	CH_2Br_2	1.20 [1]
Dibromochloromethane	$CHBr_2Cl$	0.30 [1]
Bromodichloromethane	$CHBrCl_2$	0.30 [1]
Bromochloromethane	CH_2BrCl	0.50 [1]
Inorganic		
Hydrogen bromide	HBr	-
Hypobromous acid	HOBr	-
Bromine monoxide	BrO	-
Bromine atom	Br	-
Bromine nitrate	$BrONO_2$	-
Bromine chloride	BrCl	-

[1] $\mathbf{S}_{2000F}$ only.

observations in the marine boundary layer (MBL) (Montzka and Reimann, 2011). Table 6.1 summarises the UKCA Br-containing SGs, including the 5 VSLS added for this work, along with values of χ_{2000}.

In UKCA, loss of VSL SGs occurs via oxidation with OH or by photolysis, calculated using the recommended rate constants and absorption cross section data of Sander et al. (2006). As was concluded in Chapter 4, it is likely that organic product gases from $CHBr_3$ and CH_2Br_2 degradation make a negligible contribution to the total Br_y^{VSLS} in the lower stratosphere. Therefore, for UKCA experiments here, instantaneous production of Br_y was assumed (i.e. $CHBr_3 + OH \rightarrow 3\times Br_y$), ignoring intermediates such as CBr_2O and CHBrO. For soluble Br_y (e.g., HOBr, HBr), wet deposition occurs in both dynamic and convective precipitation (Giannakopoulos et al., 1999), with the effective Henry's law constants taken from Yang et al. (2005).

6.2.2 Emissions

Emissions of VSLS are highly variable in both space and time (e.g Quack and Wallace, 2003). The global source strengths of major VSLS $CHBr_3$ and CH_2Br_2 are uncertain, with compiled estimates in the range 430-1400 Gg Br yr^{-1} and 57-280 Gg Br yr^{-1}, respectively (Montzka and Reimann, 2011). Three further simulations, in which $CHBr_3$ and CH_2Br_2 emissions were specified from a range of previously published scenarios, were performed.

Run $\mathbf{S}_{2000L}$ was identical to run $\mathbf{S}_{2000F}$ but used the *top down* emission fluxes proposed by Liang et al. (2010) (hereafter "Liang2010"). This scenario is a *top down* estimate constrained by $CHBr_3$ and CH_2Br_2 observations from 8 National Aeronautics and Space Administration (NASA) aircraft campaigns between 1996 and 2008. Run $\mathbf{S}_{2000W}$ used the *bottom up* emission fluxes of F. Wittke (IFM-GEOMAR, personal communication, hereafter "Wittke2011"). The Wittke2011 scenario is a *bottom up* estimate based on a range of observed sea-air fluxes of VSLS. These observations form part of the Halocarbons in the Ocean and Atmosphere (HalOcAt) database (http://halocat.geomar.de/). Global emission fluxes were extrapolated from the available observations using an ordinary least squares method (F. Wittke, personal communication, 2011).

Finally, run $\mathbf{S}_{2000Ord}$ used the emission estimates of Ordóñez et al. (2012) (hereafter "Ordóñez2012"). This scenario is a top down estimate based on tropospheric aircraft observations. The emissions are weighted towards observations of chlorophyll-a in the ocean, a potential proxy for VSLS. The total source strength of $CHBr_3$ and CH_2Br_2 under each of these scenarios is summarised in Table 6.2 and Figure 6.1 shows the zonally averaged $CHBr_3$ emission field for each.

TABLE 6.2: UKCA CCM 30-year time-slice experiments and global source strength (Gg source gas yr^{-1}) of $CHBr_3$ and CH_2Br_2.

Run	VSLS	Emissions	$CHBr_3$	CH_2Br_2
$\mathbf{S}_{2000N}$	No	-	-	-
$\mathbf{S}_{2000F}$	Yes	Fixed vmr	-	-
$\mathbf{S}_{2000W}$	Yes	Wittke2011	183	64
$\mathbf{S}_{2000L}$	Yes	Liang2010	450	62
$\mathbf{S}_{2000Ord}$	Yes	Ordóñez2012	533	67

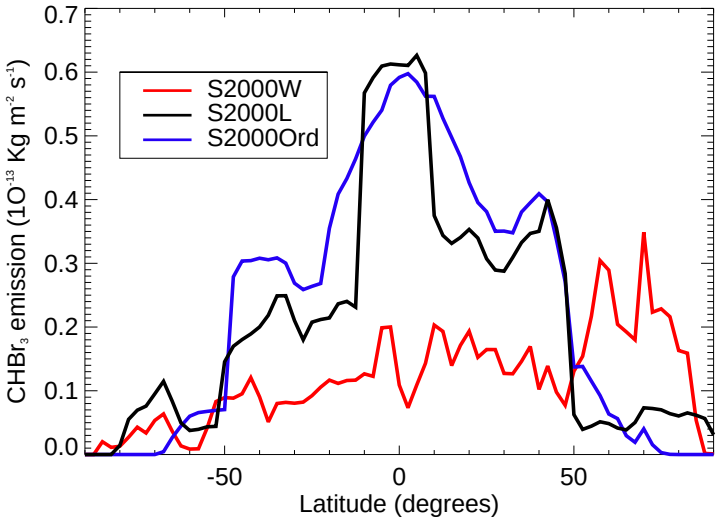

FIGURE 6.1: Zonal mean $CHBr_3$ emission field (10^{-13} Kg m^{-2} s^{-1}) from Wittke2011, Liang2010 and Ordóñez2012 scenarios.

The latitudinal dependence shows enhanced emissions in the tropics (±20°) for the Liang2010 and Ordóñez2012 scenarios. For the Wittke2011 scenario, which has the lowest global $CHBr_3$ source (Table 6.2), tropical emissions are considerably lower. However, at high northern hemisphere (NH) latitudes (>60°), emissions are relatively large.

Figure 6.2 shows the global maps of $CHBr_3$ emissions for each scenario. For Ordóñez2012, which includes monthly variability, January emissions are shown. Over the potentially important Western Pacific region, $CHBr_3$ emissions are largest in the Liang2010 scenario. For CH_2Br_2 (not shown), the total global emissions are much better constrained between scenarios (Table 6.2).

6.3 UKCA Versus Observations

Previous VSLS modelling studies have used aircraft data to validate modelled profiles of $CHBr_3$ and CH_2Br_2 in the upper troposphere (e.g., Liang et al., 2010; Ashfold et al., 2012). Observations from the NASA campaigns TC4 (2007), PRE-AVE (2004) and CR-AVE (2006) were discussed in Chapter 4 and compared with output from the TOMCAT/SLIMCAT CTM. In general, observations are sparse, particularly in upper troposphere where they are needed to help constrain estimates of the source gas injection (SGI) of VSLS

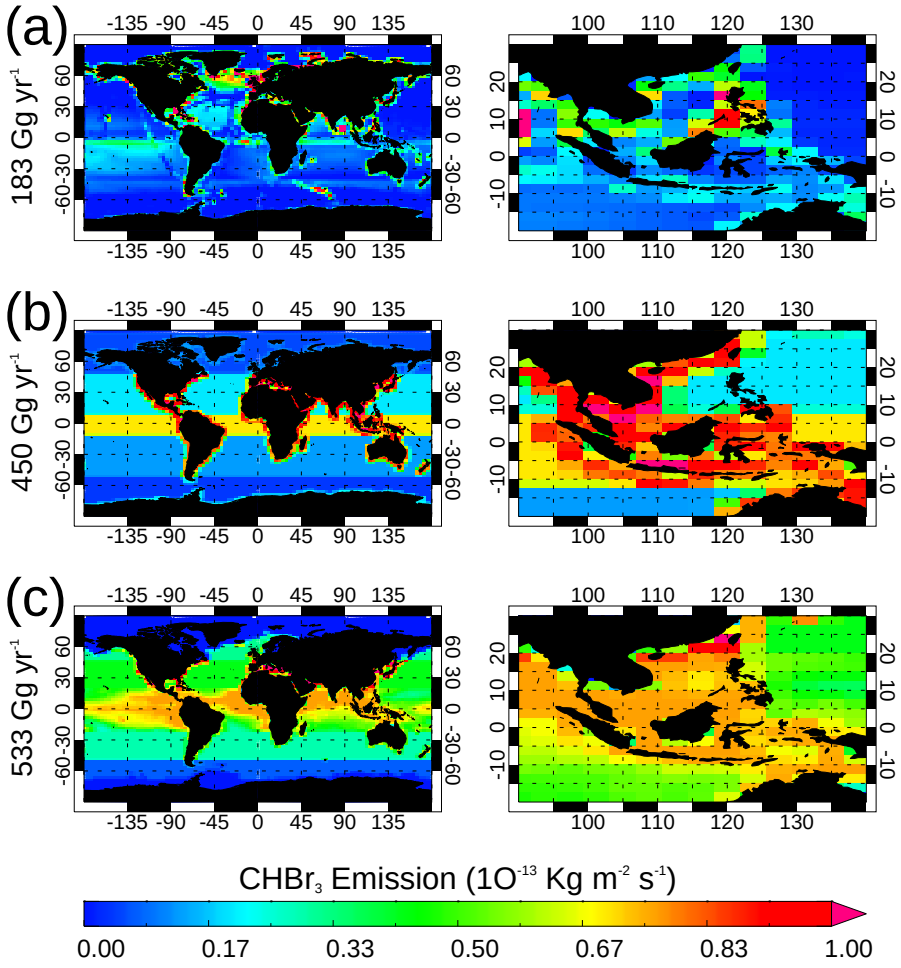

FIGURE 6.2: $CHBr_3$ emission field (10^{-13} Kg m^{-2} s^{-1}) on UKCA N48 (3.75°×2.5°) grid for global (left) and Western Pacific (right) regions. Emissions from (a) Wittke2011, (b) Liang2010 and (c) Ordóñez2012 scenarios.

into the stratosphere. However, these NASA campaigns provide good coverage in the tropics (±20°), where emissions of VSLS may be relatively large, and their troposphere-stratosphere transport rapid (e.g., Aschmann et al., 2009). Ideally, global models should also be validated with observations from other platforms, such as ground-based.

6.3.1 Ground-Based

Multi-annual observations of $CHBr_3$ and CH_2Br_2 at 14 ground-based stations (see Table 6.3) have been used to validate UKCA. The observed data is from an ongoing program of the National Oceanic and Atmospheric Administration/Earth System Research Laboratory (NOAA/ESRL) (Montzka et al., 2003).

TABLE 6.3: Summary and location of NOAA/ESRL ground-based stations. Arranged from north to south.

Station	Name	Lat	Lon
ALT	Alert, NW Territories, Canada	82.5°N	62.3°W
SUM	Summit, Greenland	72.6°N	38.4°W
BRW	Pt. Barrow, Alaska, USA	71.3°N	156.6°W
MHD	Mace Head, Ireland	53.0°N	10.0°W
LEF	Wisconsin, USA	45.6°N	90.2°W
HFM	Massachusetts, USA	42.5°N	72.2°W
THD	Trinidad Head, USA	41.0°N	124.0°W
NWR	Niwot Ridge, Colorado, USA	40.1°N	105.6°W
KUM	Cape Kumukahi, Hawaii, USA	19.5°N	154.8°W
MLO	Mauna Loa, Hawaii, USA	19.5°N	155.6°W
SMO	Cape Matatula, American Samoa	14.3°S	170.6°W
CGO	Cape Grim, Tasmania, Australia	40.7°S	144.8°E
PSA	Palmer Station, Antarctica	64.6°S	64.0°W
SPO	South Pole	90.0°S	-

Whole air samples were collected weekly into paired steel or glass flasks and were analysed using gas chromatography/mass spectrometry (GC-MS) (Montzka et al., 2003). Figure 6.3 shows the location of the NOAA/ESRL ground-based network.

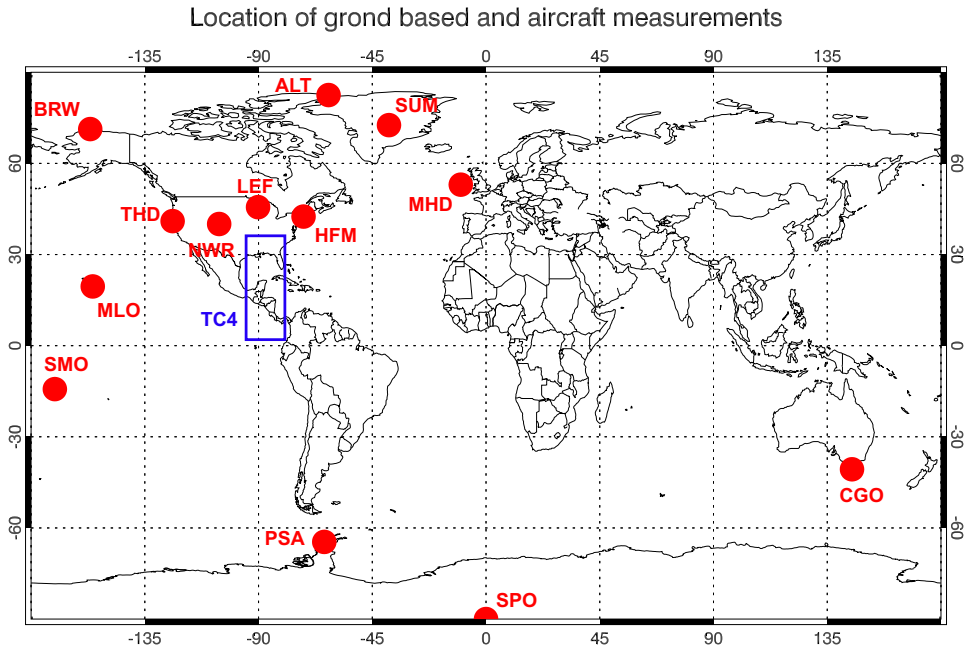

FIGURE 6.3: Location of NOAA/ESRL ground-based stations (red) and NASA aircraft campaigns (blue). Due to the close proximity of stations MLO and KUM (Table 6.3), KUM is omitted for clarity.

Figure 6.4 shows the modelled versus observed $CHBr_3$ mixing ratio from runs $\mathbf{S}_{2000W}$ and $\mathbf{S}_{2000Ord}$ (i.e. Wittke2011 & Ordóñez2012 emissions), arranged north-south by station location. For NOAA/ESRL stations, the observed data points are monthly mean fields that have been calculated from a larger 10-year monthly mean data set (i.e. taking the mean of a mean field). This approach will smooth out intra-monthly variability but can give a clear signal of inter-monthly and seasonal trends.

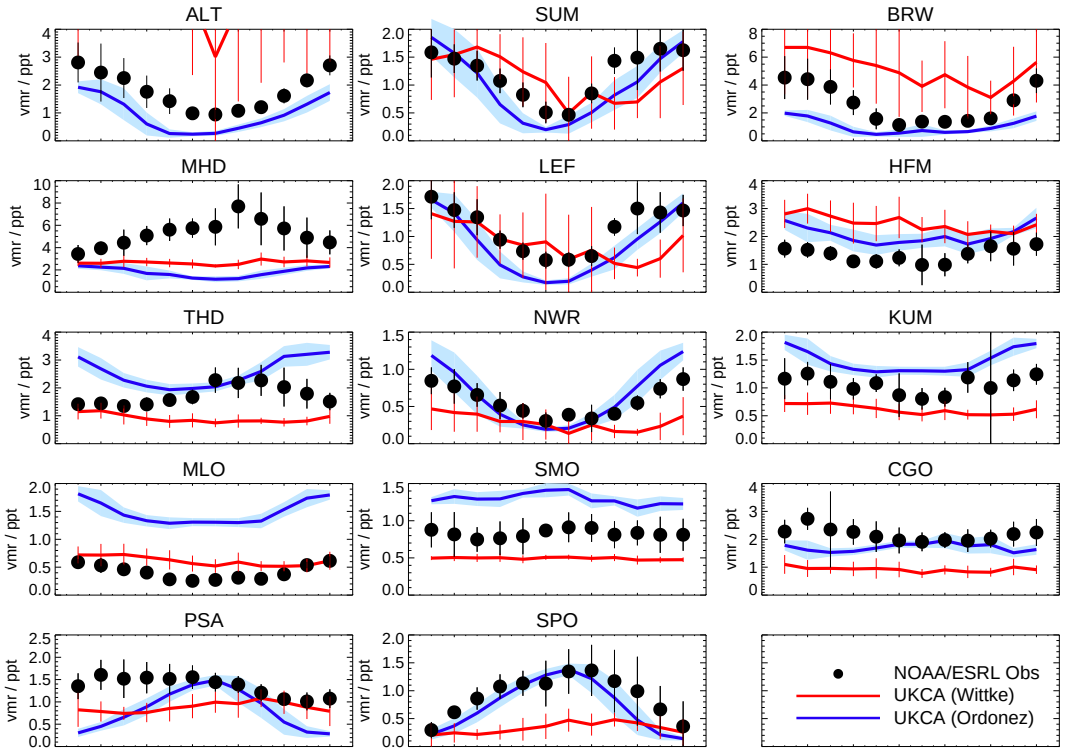

FIGURE 6.4: Comparison of monthly mean $CHBr_3$ mixing ratios (ppt) observed at 14 NOAA/ESRL ground stations versus UKCA runs $\mathbf{S}_{2000W}$ (Wittke2011 emissions) and $\mathbf{S}_{2000Ord}$ (Ordóñez2012 emissions). The vertical bars and the shading denote ± 1 standard deviation on the observed and modelled mean, respectively (see text for details). For clarity, the variability on run $\mathbf{S}_{2000W}$ is omitted at some stations.

For $CHBr_3$, the observations show a pronounced annual cycle at high latitude ($\geq 60°$) NH stations (ALT, SUM and BRW). Elevated mixing ratios occur during NH winter (DJF) and lower abundances are observed during summer months (JJA). A large seasonal variation in $CHBr_3$ at ALT has been previously reported by Yokouchi et al. (1996). At the surface, $CHBr_3$ has a relatively short local lifetime of $\sim$26 days with photolysis being the dominant sink (Law and Sturges, 2007). Relatively low $CHBr_3$ during NH summer will be, in part,

due to increased photochemical loss. At these stations, it is possible that transport also contributes to the observed seasonal cycle. However, from the runs here it is difficult to separate the two contributions.

The agreement between model and observation at these high latitude NH stations is varied. Overall, run $\mathbf{S}_{2000Ord}$, which includes seasonality in the emission field, is able to capture the shape of the annual cycle at ALT and SUM. However, the magnitude is too low at ALT and BRW. Run $\mathbf{S}_{2000W}$, which does not contain seasonality in the emission field, also captures the shape of the annual cycle. However, the magnitude is significantly overestimated at ALT and BRW (for all months), suggesting an excessive local $CHBr_3$ source. This Wittke2011 scenario has the largest emissions in the high latitude NH (see Figure 6.1).

At NH mid-latitudes stations (30-60°N, MHD, LEF, HFM, THD & NWR), modelled and observed $CHBr_3$ are in reasonable agreement. At stations LEF and NWR, the agreement is particularly good for both runs $\mathbf{S}_{2000Ord}$ and $\mathbf{S}_{2000W}$. However, elevated $CHBr_3$ at Mace Head (MHD), known as a strong VSLS source region (Carpenter et al., 1999), is not captured by either emission scenario. $CHBr_3$ seasonality at MHD is out of phase with that observed at ALT and SUM, i.e. minima occurring during winter months and maxima during summer. This is in agreement with Carpenter et al. (2005) who observe a similar seasonality and deduce that strong local emissions dominate over photochemical loss to control the local $CHBr_3$ abundance.

For tropical (±30°) stations (KUM, MLO and SMO), there is no clear signal of $CHBr_3$ seasonality and the agreement between model and observations is varied. Despite the close proximity of stations KUM and MLO, observed $CHBr_3$ is up to a factor of 2 different, indicating sharp spatial gradients. Run $\mathbf{S}_{2000Ord}$ (with top down emission estimate) overestimates $CHBr_3$, while run $\mathbf{S}_{2000W}$ (bottom up estimate) shows a low bias at KUM and SMO. AT MLO, $\mathbf{S}_{2000W}$ gives good agreement with the observations. Observations of $CHBr_3$ have also been made at two Antarctic stations (PSA & SPO). A clear seasonal cycle is apparent at SPO with maximum mixing ratios occurring during SH winter (JJA). This is consistent with Swanson et al. (2004) and Beyersdorf et al. (2010) who note a similar seasonality. Run $\mathbf{S}_{2000W}$ captures this SPO cycle extremely well.

Similarly for CH_2Br_2, Figure 6.5 compares the modelled versus observed source gas mixing ratio. At the surface, CH_2Br_2 has a lifetime of ∼120 days (Law and Sturges, 2007), significantly longer than that of $CHBr_3$. Horizontal gradients are therefore expected to be less pronounced. The observations show background mixing ratios of ∼1 ppt at most stations with generally little variability. A weak seasonal cycle is apparent at NH mid to high-latitude stations (e.g., LEF & SUM). Overall, runs $\mathbf{S}_{2000W}$, $\mathbf{S}_{2000Ord}$ and $\mathbf{S}_{2000L}$ (not shown) provide good agreement with observed CH_2Br_2. The global CH_2Br_2 source strength is relatively well constrained at 62-67 Gg yr^{-1} among the emission scenarios considered here. However, run $\mathbf{S}_{2000W}$ does show a high CH_2Br_2 bias, up to a factor of ∼2, at SH polar stations PSA and SPO.

Overall, UKCA run $\mathbf{S}_{2000W}$ is found to significantly overestimate $CHBr_3$ or CH_2Br_2 at some stations (e.g., ALT, PSA, SPO) when using the bottom up emission scenario. The most recent fluxes proposed by Ordóñez et al. (2012), which are monthly-varying and are weighted to observations of chlorophyll-a, provide generally good agreement with the observed data and are well suited for global modelling of VSLS.

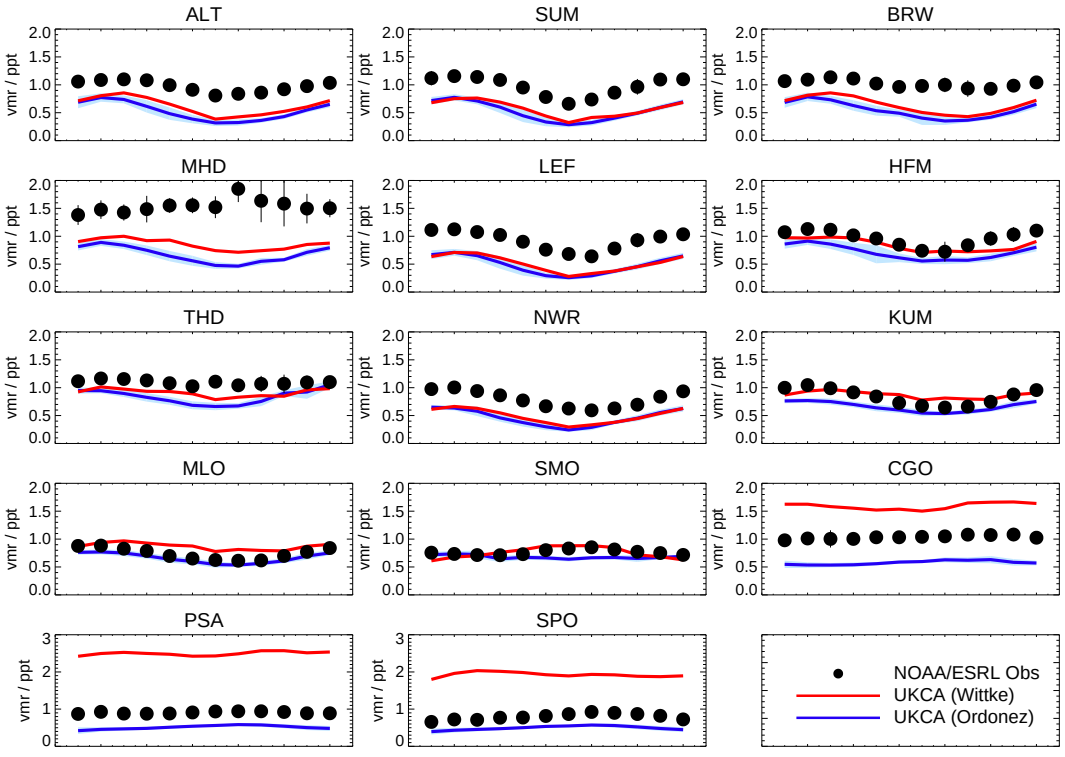

FIGURE 6.5: As Figure 6.4 but for CH_2Br_2.

6.3.2 Aircraft

UKCA-modelled profiles of $CHBr_3$ and CH_2Br_2 have also been compared with aircraft observations in the TTL (Figure 6.6). The observations were taken on board the high-altitude WB-57 aircraft during the 3 NASA campaigns listed at the beginning of Section 6.3. The location of these campaigns was discussed in Chapter 4.

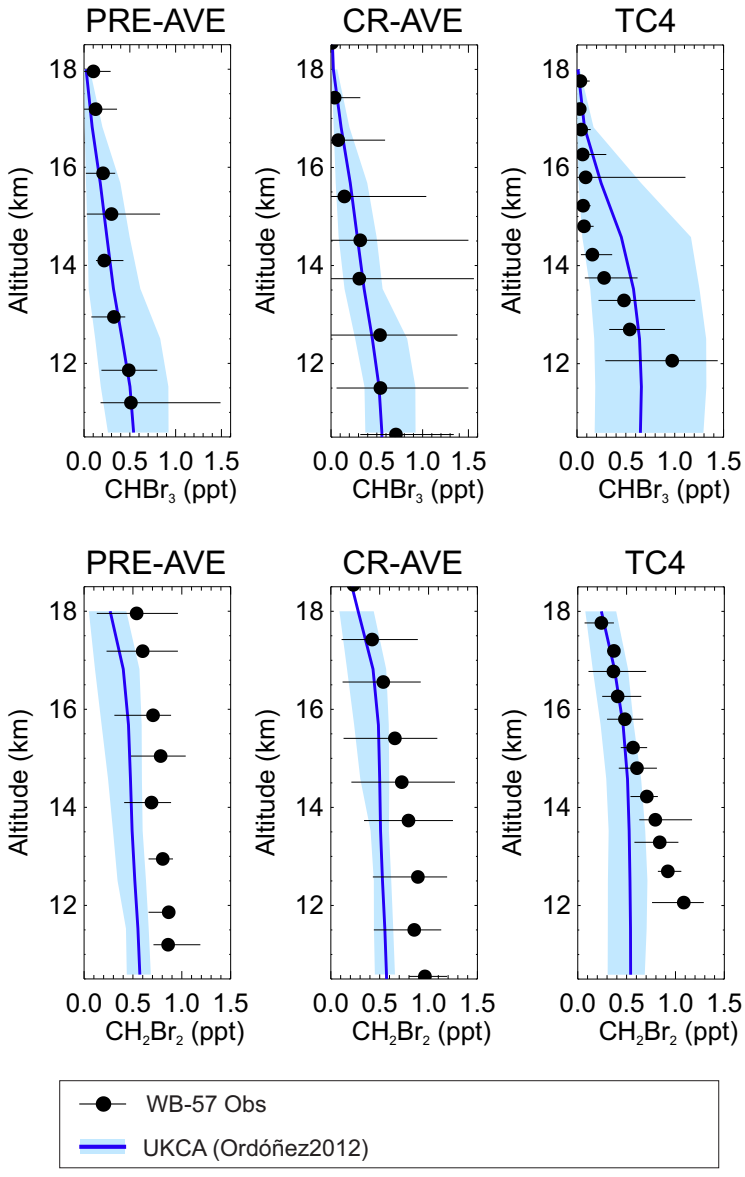

FIGURE 6.6: Comparison of modelled profiles of $CHBr_3$ (upper row) and CH_2Br_2 (lower row) with observations in the upper troposphere from the NASA TC-4 (Jul-Aug 2007), CR-AVE (Jan-Feb 2006) and PRE-AVE (Jan-Feb 2004) missions. The horizontal bars denote the min-max variability on the observations at a given level. Similarly, shaded regions denote the variability on the modelled profile (run $\mathbf{S}_{2000Ord}$).

In the TTL, the agreement between modelled and observed $CHBr_3$ and CH_2Br_2 is generally quite good. Run $\mathbf{S}_{2000Ord}$ captures the low $CHBr_3$ ($< \sim$0.25 ppt) and CH_2Br_2 observed in the upper TTL (15-17 km) well. A number of previous offline CTM studies, including the work described in Chapter 4, have been found to overestimate $CHBr_3$ and CH_2Br_2 in this region (e.g., Warwick et al., 2006). These models calculate vertical winds from meteorological analyses (e.g. ECMWF), an approach which may produce too rapid vertical motion in the upper troposphere (e.g., Wohltmann and Rex, 2008). Free running CCMs that generate their own wind fields (e.g. UKCA) and also CTMs that diagnose vertical motions from heating rates (e.g. SLIMCAT, Chapter 4) should not suffer this problem. Differences in transport schemes between models can lead to a significantly different modelled distribution of short-lived tracers in the tropical upper troposphere (Hoyle et al., 2011; Feng et al., 2011). For this reason, a multimodel estimate of VSLS transport to the stratosphere is desirable.

Figure 6.7 shows annual tropical mean profiles of $CHBr_3$ and CH_2Br_2 from UKCA and, for comparison, from the TOMCAT 3-D CTM (Chipperfield, 2006). The CTM set up here is identical to that described in Chapter 5; i.e. a fixed mixing ratio boundary condition was used to constrain the surface abundance of source gases. This approach is analogous to UKCA run $\mathbf{S}_{2000F}$ and therefore a direct comparison of these runs is most appropriate.

UKCA exhibits slower transport in the TTL, resulting in significantly less of each SG in the TTL and lower stratosphere. This difference, particularly for the most abundant gases $CHBr_3$ and CH_2Br_2, results in significantly different estimates for the total SGI (of bromine) across the tropopause. At 17 km, the CTM estimate is $\sim$3.25 ppt of bromine from the SGI of $CHBr_3$, CH_2Br_2, $CHBr_2Cl$ and CH_2BrCl and $CHBrCl_2$ (see Chapter 5 also). For UKCA this estimate is $\sim$1.7 ppt for the same five source gases. Both estimates are within the range of 1.5 (0.7-3.4) ppt reported by Montzka and Reimann (2011) based on a compilation of high-altitude aircraft observations. However, given the particularly good agreement of UKCA with the aircraft observations in the important upper TTL (shown in Figure 6.6), some confidence can be given to the UKCA estimate. Overall, more observations of these gases in the TTL are required in order to constrain estimates of SGI and to validate global models.

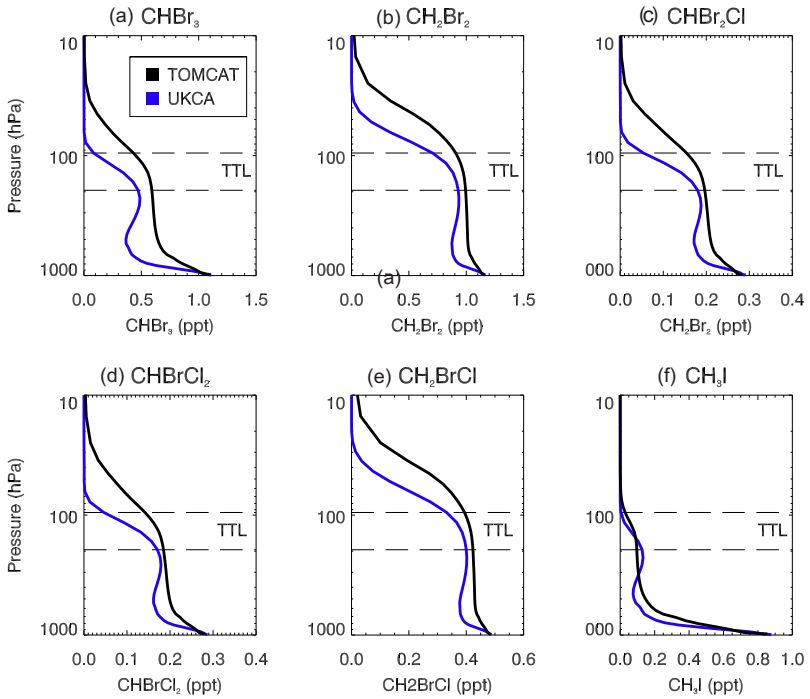

FIGURE 6.7: Annual tropical (±20°) mean profiles of (a) $CHBr_3$, (b) CH_2Br_2, (c), $CHBr_2Cl$, (d) $CHBrCl_2$, (e) CH_2BrCl and (f) CH_3I from UKCA run $\mathbf{S}_{2000F}$ and the TOMCAT chemical transport model.

6.4 Bromine Loading

Figure 6.8 shows the modelled zonally averaged total bromine field; i.e. the sum of long-lived and very short-lived SGs (organic bromine) plus inorganic product gases (e.g. BrO, HBr). The model was allowed to spin-up for 15 perpetual years and the subsequent 15 model years have been used for analysis here. The long-lived halons and methyl bromide (CH_3Br) together supply ∼16 ppt of this total - consistent with observed trends in their surface emission (WMO, 2007, 2011). Tropospheric gradients of these long-lived gases are small and they likely supply minimal Br_y below the tropopause.

UKCA is known to exhibit a wet bias in the tropical upper troposphere (Alex Archibald, personal communication, 2012). This bias, which affects all runs, is evident from Figure 6.8, which shows significant gradients in the total bromine field above the 380 K isentrope in the tropics (±20°). In the lower stratosphere, total bromine should not be subject to physical removal and should be vertically well mixed. However, gradients of to 0.5-1.0 ppt are present due to excessive removal of soluble Br_y. Therefore, based on the simulations here, the modelled PGI of soluble Br_y is likely underestimated and represents a lower limit.

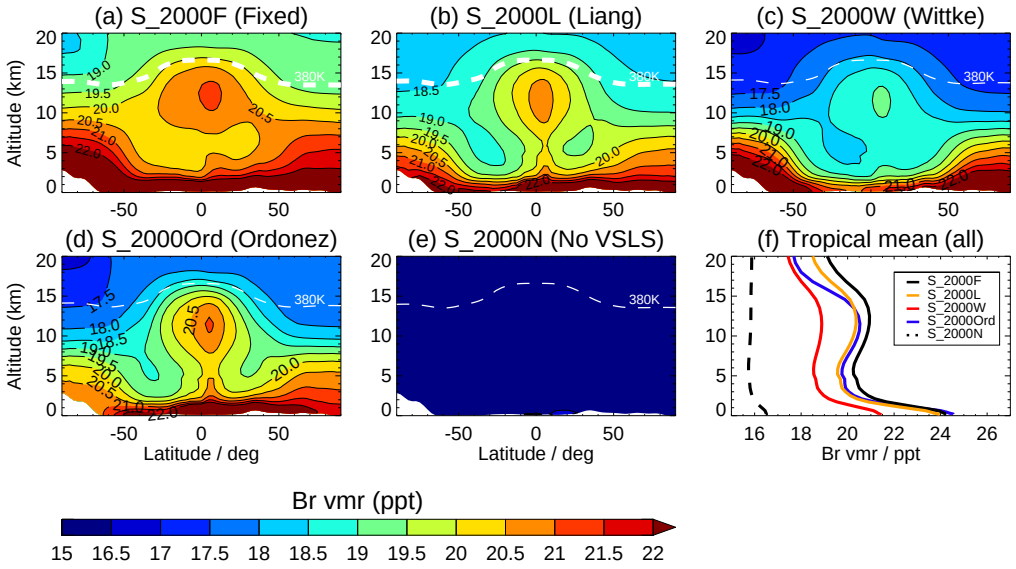

FIGURE 6.8: Zonally averaged total bromine (ppt) from runs (a) $\mathbf{S}_{2000F}$ (fixed VSLS), (b) $\mathbf{S}_{2000L}$ (Liang2010 VSLS), (c) $\mathbf{S}_{2000W}$ (Wittke2011 VSLS), (d) $\mathbf{S}_{2000Ord}$(Ordóñez2012 VSLS) and (e) $\mathbf{S}_{2000N}$ (no VSLS). For reference, the 380 K isentrope (approximate tropical tropopause) is shown with a dashed line. Also shown is (f) tropical mean profiles of total bromine from the above runs.

Inclusion of VSLS in the model provides a significant source of tropospheric bromine. The spatial distribution of which, particularly at the surface, can vary considerably with emission scenario. Quantifying the VSLS contribution to stratospheric bromine, via SGI and also product gas injection (PGI), is an area of active research. At the top of the TTL, this total (SGI + PGI) contribution (Br_y^{VSLS}) is ∼3 ppt for runs $\mathbf{S}_{2000F}$, $\mathbf{S}_{2000L}$ and also for $\mathbf{S}_{2000Ord}$ (Figure 6.9), therefore at the lower limit of the 6 (3-8) ppt range reported by Montzka and Reimann (2011) and lower than the CTM estimate reported in Chapter 5. Br_y^{VSLS} is even lower (∼2 ppt) for run $\mathbf{S}_{2000W}$, which used the Wittke2011 emission scenario and had the smallest tropical $CHBr_3$ source (Table 6.2).

The recent modelling work of Tegtmeier et al. (2012) also report a relatively low Br_y^{VSLS} contribution of up to 2.3 ppt ($CHBr_3$ and CH_2Br_2 only). It should be noted that due to the UKCA wet bias in the upper troposphere, modelled Br_y^{VSLS} is likely underestimated in all runs. Accounting for this bias would lower the discrepancy between the UKCA best estimate of ∼3 ppt of Br_y^{VSLS} and the ∼5 ppt modelled by the TOMCAT CTM. Furthermore, as noted in Chapter 4, TOMCAT may overestimate the SGI in the lower stratosphere. However, overall the two model estimates allow constraint on the contribution of VSLS to stratospheric bromine and are both considerably lower than estimates

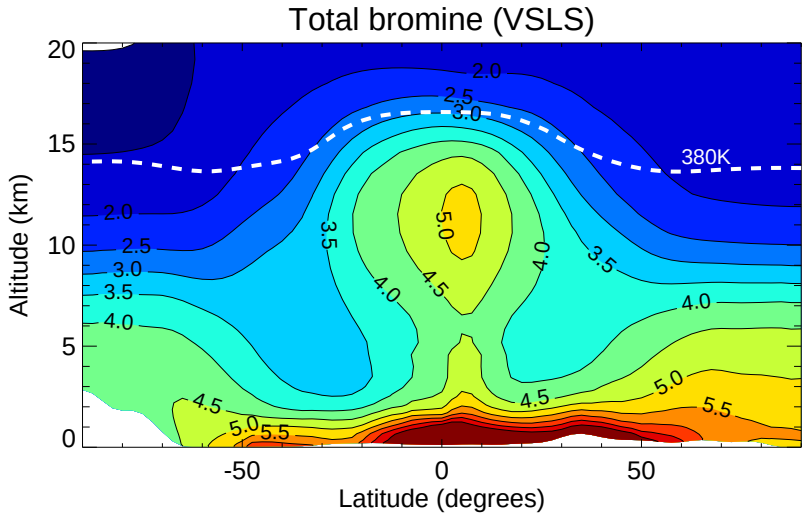

FIGURE 6.9: Zonally averaged total bromine (ppt) from VSLS for run $\mathbf{S}_{2000Ord}$ (Ordóñez2012 VSLS) under 2000 conditions.

based on satellite observations of BrO (e.g., Sioris et al., 2006; Kovalenko et al., 2007). Figure 6.10 shows the modelled partitioning of UKCA Br_y species in the troposphere and stratosphere. In the troposphere, HBr is the dominant Br_y species. Tracking the degradation products of individual source gases, in order to determine their relative contribution to the total PGI is not possible from these runs. However this was performed in Chapter 5 using the TOMCAT CTM.

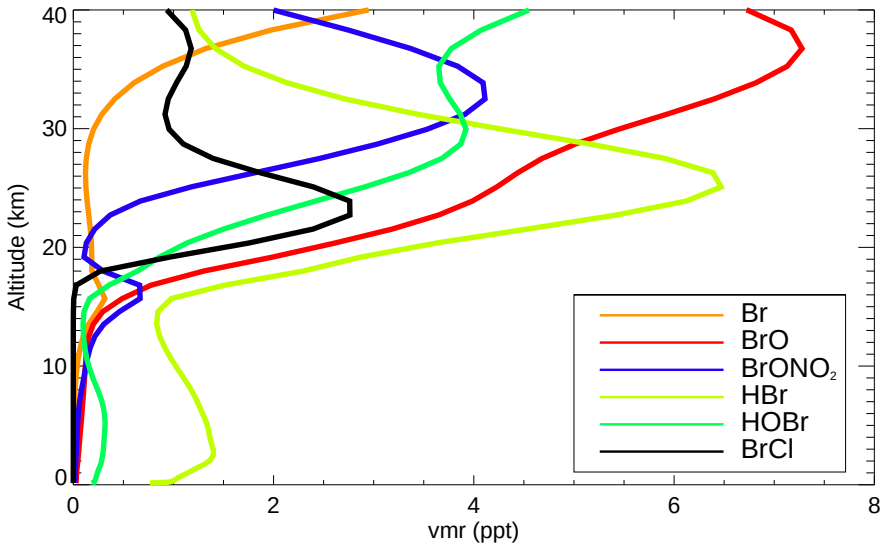

FIGURE 6.10: Modelled monthly mean profiles of the mixing ratio of Br_y species in the tropics (±20°) from run $\mathbf{S}_{2000Ord}$ (Ordóñez2012 VSLS).

6.5 Impact of VSLS on O_3

Reactive bromine species (Br_x = [BrO] + [Br]) are known to impact O_3 in both the troposphere (e.g., Yang et al., 2005) and also the stratosphere (e.g., Salawitch et al., 2005). However, at present the contribution of Br_y^{VSLS} to polar and also global O_3 loss is poorly quantified. Figure 6.11 shows the modelled impact of Br_y^{VSLS} on the mixing ratio of stratospheric O_3, i.e. the difference between UKCA run with VSLS and run without. The impact is largest over the South Pole, where Br_y^{VSLS} enhance polar O_3 loss through the BrO-ClO coupled cycle in the lower stratosphere. The decrease in O_3 is largest in SH winter (JJA) and Spring (SON), when the Antarctic Ozone Hole is formed.

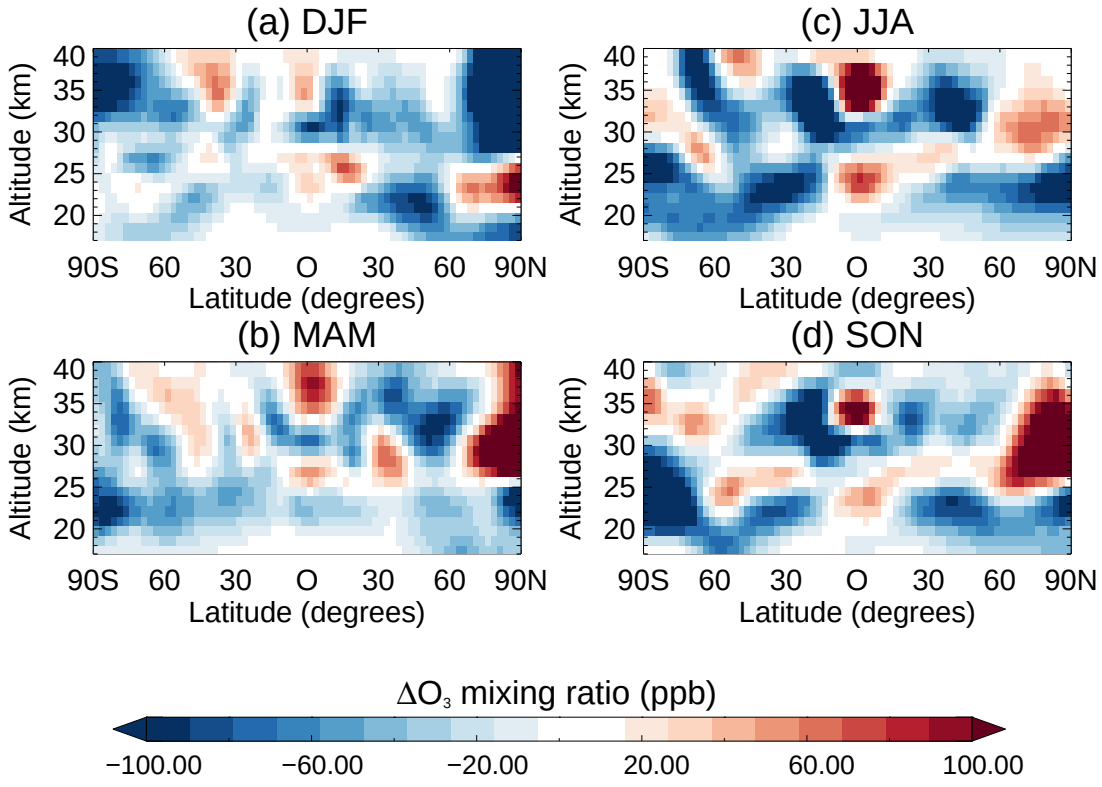

FIGURE 6.11: Zonal mean reduction in the modelled O_3 mixing ratio (ppb) due to inclusion of Br-containing VSLS (run $\mathbf{S}_{2000Ord}$ minus $\mathbf{S}_{2000N}$) for (a) DJF, (b) MAM, (c) JJA and (d) SON under 2000 conditions.

Interestingly, the addition of Br-containing VSLS also leads to some regions of the stratosphere where the modelled O_3 change is positive. These increases are likely due to dynamical changes resulting from bromine-induced O_3 loss. Recent independent simulations

using the whole-atmosphere chemistry (CheST) version of UKCA, as opposed to the stratospheric version used here, have also shown regions of enhanced stratospheric O_3 with the inclusion of VSLS (X. Yang, personal communication, 2012). Further work would be required to investigate these dynamical changes. However, overall Br_y^{VSLS} is found to reduce the total O_3 column (Figure 6.12).

The impact of VSLS on column O_3 is largest in polar regions where a peak reduction of up to ∼15 DU occurs over Antarctica. This modest reduction, representing a decrease of ∼7%, occurs in late winter (JJA) and early spring (SON). The model also shows a significant impact of VSLS on Arctic O_3 with the largest decreases occurring during winter (DJF) and spring (MAM). At mid-latitudes, the modelled impact on O_3 (<∼2 DU) is lower than the ∼10 DU reported by Feng et al. (2007) using the SLIMCAT CTM. However, the authors report a Br_y^{VSLS} contribution of 6 ppt in the lower stratosphere - significatly larger than the ∼3 ppt modelled here. Due to a likely underestimation of PGI, as discussed in Section 6.4, the modelled impact of VSLS on O_3 reported here, may represent a lower limit.

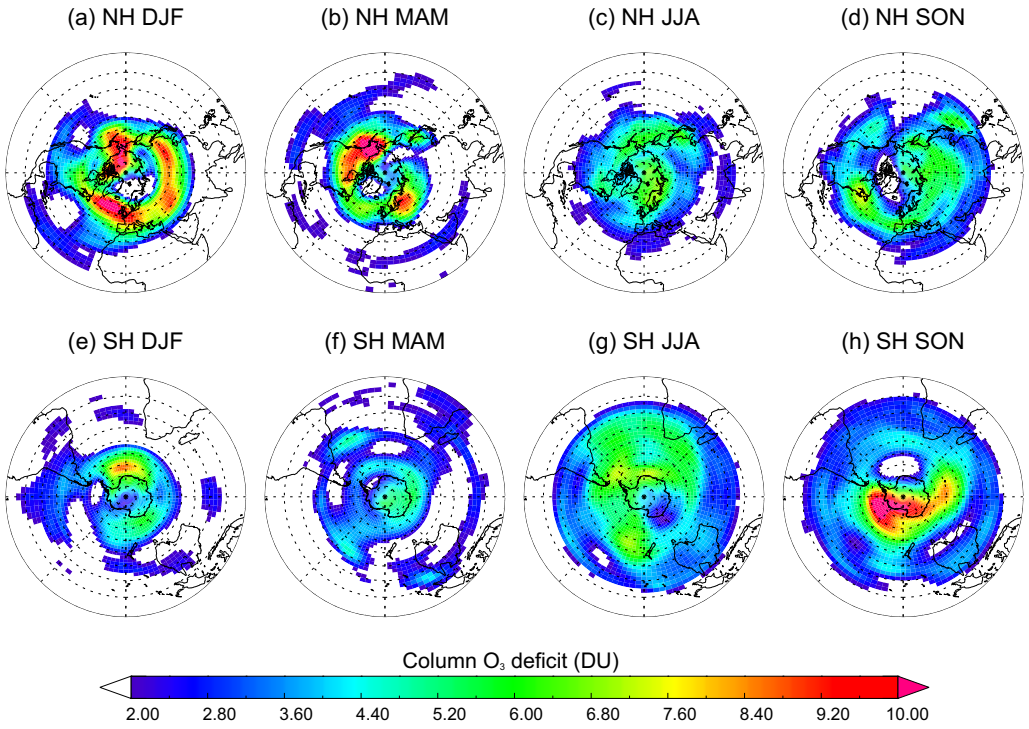

FIGURE 6.12: Mean reduction of the modelled total O_3 column (DU) due to inclusion of Br-containing VSLS (run $\mathbf{S}_{2000Ord}$ minus $\mathbf{S}_{2000N}$) for (a,e) DJF, (b,f) MAM, (c,g) JJA and (d,h) SON under 2000 conditions.

6.6 Summary

This chapter has described the treatment of biogenic bromine-containing VSLS in the UKCA CCM. Five VSLS were added to the model: $CHBr_3$, CH_2Br_2, $CHBr_2Cl$, CH_2BrCl and $CHBrCl_2$. In previous CTM experiments (Chapters 4 and 5), emissions of VSLS were not specified. Instead, a uniform volume mixing ratio was used to constrain their surface abundance. Here, for $CHBr_3$ and CH_2Br_2, the most abundant VSLS, both *top down* and *bottom up* global emission estimates were used. The performance of UKCA with these spatially-varying emission fluxes has been assessed. The model is able to reproduce the observed mixing ratio of these gases at global NOAA/ESRL ground-based stations fairly well. UKCA with the *top down* emission fluxes proposed by Ordóñez et al. (2012) performs particularly well. With this set up, the CCM captures the seasonal $CHBr_3$ and CH_2Br_2 cycle along with monthly mean mixing ratios observed at numerous stations.

The CCM has also been validated with high-altitude aircraft observations. In the TTL, UCKA reproduces the vertical distribution of $CHBr_3$ and CH_2Br_2 resonably well. Therefore, some confidence can be given to the modelled estimate of SGI, which is found to deliver 1.7 ppt of bromine to the stratosphere. This total, which is for all five VSLS considered, is significantly lower than the ∼3.25 ppt reported in Chapter 5 from the TOMCAT CTM. However, both model estimates are within the range of 1.5 (0.7-3.4) ppt reported by Montzka and Reimann (2011) based on compiled aircraft observations.

UCKA has also been used to quantify the total (SGI + PGI) stratospheric bromine loading from VSLS (Br_y^{VSLS}) and its impact on O_3. Based on a run using the Ordóñez et al. (2012) emissions for $CHBr_3$ and CH_2Br_2, Br_y^{VSLS} is found to be ∼3 ppt and so on the lower end of the 6 (3-8) ppt range reported by Montzka and Reimann (2011). This estimate is also ∼1 ppt lower than the CTM estimate of Chapter 5. However, the contribution from PGI is expected to be underestimated in UKCA by ∼0.5-1.0 ppt due to a possible wet bias in the upper troposphere. The impact of Br_y^{VSLS} on total O_3 is found to be modest. The largest impact occurs in polar regions, where the reduction in column O_3 peaks at ∼15 DU in late winter/early spring over Antarctica. At mid-latitudes, UKCA with a background aerosol loading, shows a small (<∼2 DU) impact of Br-containing VSLS on total column O_3. These modelled impacts likely represent a lower limit given the underestimation of PGI discussed above.

Chapter 7

Future Changes to the Stratospheric Source Gas Injection of VSLS

7.1 Introduction

In Chapters 5 and 6 global models were used to estimate the contemporary contribution of biogenic very short-lived substances (VSLS) to stratospheric inorganic bromine (Br_y^{VSLS}). In Chapter 6, the impact of Br_y^{VSLS} on stratospheric ozone (O_3) was found to be significant. In recent years, there has been suggestions that Br_y^{VSLS} may increase in a future climate (e.g., Pyle et al., 2007). Dynamical changes as a result of global warming will likely impact the troposphere-stratosphere transport of VSLS (Dessens et al., 2009). In addition, changes to the tropospheric oxidising capacity (Zeng et al., 2008) will likely impact VSLS loss rates. These processes are poorly studied and a better understanding of them is required in order to assess the role of bromine chemistry on the future evolution of stratospheric O_3.

In this chapter, the chemistry-climate model (CCM) work of Chapter 6 is extended to examine how chemical/dynamical changes, under projected 2100 climates, may impact the abundance of very short-lived (VSL) source gases (SGs) in the lower stratosphere. Specifically, the aims of this chapter are to:

1. Investigate how the stratospheric source gas injection (SGI) of VSLS may respond to chemical/dynamical changes under projected Intergovernmental Panel on Climate Change (IPCC) future scenarios.

2. Quantify the future change in the amount of bromine reaching the stratosphere via the SGI of VSLS. Determine its sensitivity to moderate-high climate change projections.

The chapter is structured as follows. Section 7.2 contains a brief description of the model set up and experiments performed (Chapter 6 should also be consulted for a description of the UKCA CCM). Section 7.3 contains this chapter's results and also the discussion. A summary and some concluding remarks may be found in Section 7.4. The work contained in this chapter has been submitted to the journal Geophysical Research Letters (GRL) (Hossaini et al., 2012a).

7.2 Model and Experiments

Three 20-year time-slice experiments were performed using the UKCA CCM, introduced in Chapter 6, under 2000 and 2100 conditions. All experiments were performed at a resolution of 3.75° longitude × 2.5° latitude and with 60 hybrid-height levels (surface to ∼80 km). For 2000 (run $\mathbf{S}_{2000}$), UKCA was forced with prescribed monthly mean fields of sea surface temperature (SST) and sea ice (Rayner et al., 2003). The greenhouse gas (GHG) loading and long-lived halocarbons, were prescribed according to the WMO A1 scenario (WMO, 2011). As in Chapter 6, a background stratospheric aerosol climatology was used.

For 2100 experiments (runs $\mathbf{S}_{RCP4.5}$ and $\mathbf{S}_{RCP8.5}$), SSTs and sea ice fields were taken from (2100) output of the HadGEM2-CCS (coupled ocean) climate model (Martin et al., 2011). The loading of GHGs was constrained by two IPCC representative concentration pathway (RCP) projections (e.g., van Vuuren et al., 2011). For run $\mathbf{S}_{RCP4.5}$, the model was forced with RCP 4.5 (Thomson et al., 2011) - a scenario where peak radiative forcing (RF) stabilises and does not exceed 4.5 W/m^2 at 2100. Similarly, run $\mathbf{S}_{RCP8.5}$ was forced with RCP 8.5 (Riahi et al., 2011) - a scenario in which large GHG emissions are sustained in the 21st century, leading to a RF of 8.5 W/m^2 in 2100. These RCPs span

moderate to extreme climate change and are used here to examine the sensitivity of VSLS troposphere-stratosphere transport under potential 2100 conditions. A prescribed surface volume mixing ratio (vmr) of the long-lived bromine (and chlorine) SGs for 2100 were also taken from these RCPs. See Table 7.1 for summary.

TABLE 7.1: Prescribed surface volume mixing ratio of key greenhouse gases and long-lived bromocarbons for runs $\mathbf{S}_{2000}$, $\mathbf{S}_{RCP4.5}$ and $\mathbf{S}_{RCP8.5}$.

Species	Run $\mathbf{S}_{2000}$	Run $\mathbf{S}_{RCP4.5}$	Run $\mathbf{S}_{RCP8.5}$
CO_2 (ppm)	370	538	935
CH_4 (ppb)	1765	1577	3750
N_2O (ppb)	316	372	435
H-1211 (ppt)	4.04	0.05	0.04
H-1202 (ppt)	0.05	<0.01	<0.01
H-1301 (ppt)	2.73	0.98	0.78
H-2402 (ppt)	0.41	<0.01	<0.01
CH_3Br (ppt)	8.66	6.40	5.70

As discussed in Chapter 6, five biogenic VSLS tracers were added to UKCA. For major VSLS $CHBr_3$ and CH_2Br_2, the monthly-varying emission estimates of Ordóñez et al. (2012) were used for both 2000 and 2100 experiments. Their global source strengths are 533 Gg yr^{-1} and 67.3 Gg yr^{-1}, respectively. For minor (and relatively long-lived) VSLS $CHBr_2Cl$, $CHBrCl_2$ CH_2BrCl, a prescribed mixing ratio (0.3, 0.3 and 0.5 ppt), based on observations in the MBL (WMO, 2011), was used to constrain their surface abundance. This model set up was evaluated with ground-based and aircraft observations in Chapter 6.

7.3 Results and Discussion

Aircraft observations suggest 0.09 (0.0-0.31) ppt of $CHBr_3$ at the tropical ($\pm 20^\circ$ latitude) tropopause (TT, $\sim$17 km) (WMO, 2011). In this region, UKCA is able to reproduce the observed mixing ratios of major VSLS well (see Chapter 6). The modelled 2000 zonally averaged TT abundance of $CHBr_3$ is $\sim$0.1 ppt. For 2100, this estimate increases slightly to 0.15 ppt under RCP 4.5, and significantly to 0.35 ppt, under RCP 8.5. The local increase is largest over the Western Pacific during northern hemisphere winter (DJF, Figure 7.1), peaking at $\sim$0.8 ppt (i.e. 2.4 ppt bromine).

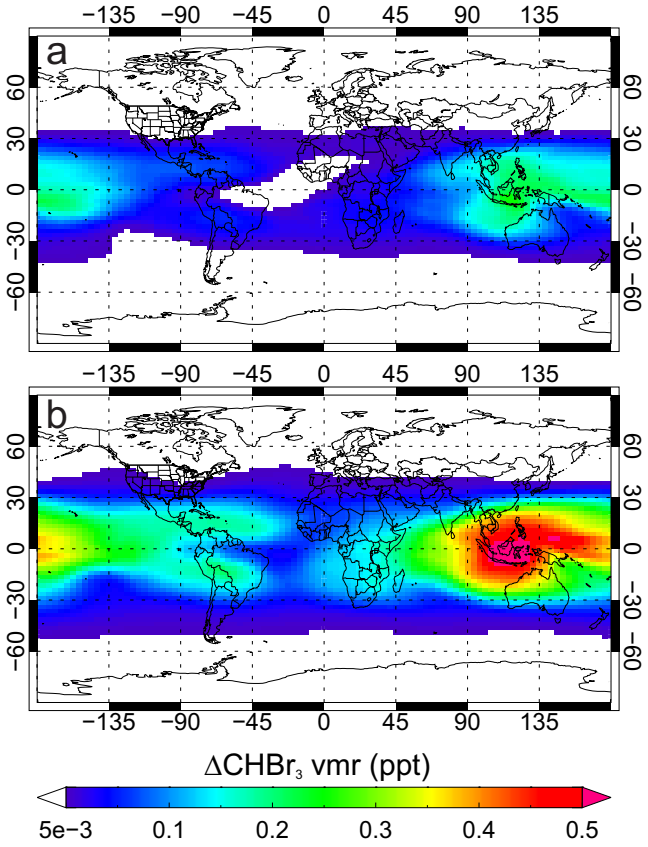

FIGURE 7.1: DJF mean increase in $CHBr_3$ volume mixing ratio (ppt) at ∼17 km for (a) RCP 4.5 and (b) RCP 8.5.

SGI refers to the transport of organic VSLS to the stratosphere where, on degradation, they release in-situ Br_y^{VSLS}. Efficient SGI requires troposphere-to-stratosphere transport to be on timescales comparable to, or shorter than, tropospheric loss rates. $CHBr_3$, which may account up to ∼35% of the total SGI from VSLS (see Chapter 5), has a surface lifetime of ∼24 days and its primary tropospheric sink is photolysis. As the shortest lived gas considered here, its abundance in the lower stratosphere is most sensitive to changes to the tropospheric circulation, particularly in the tropics where emissions are relatively large.

The modelled 2100 convective updraft mass flux mostly decreases in the tropical lower and mid-troposphere (Figure 7.2). A reduction in the tropical tropospheric circulation has been shown by previous model studies to be a consequence of climate change (e.g., Vecchi et al., 2006). However, in the upper troposphere (UT, ∼12-17 km), the change is positive with large increases over the Western Pacific (Figure 7.3a), where strong convection is sustained to higher altitudes. The prevalence of deep convection, important for the transport of

VSLS to the UT, may increase in response to global warming (e.g., Chou and Chen, 2010). The results here are consistent with Stevenson et al. (2005) and Dessens et al. (2009) who also show an increase in the updraft strength in the UT.

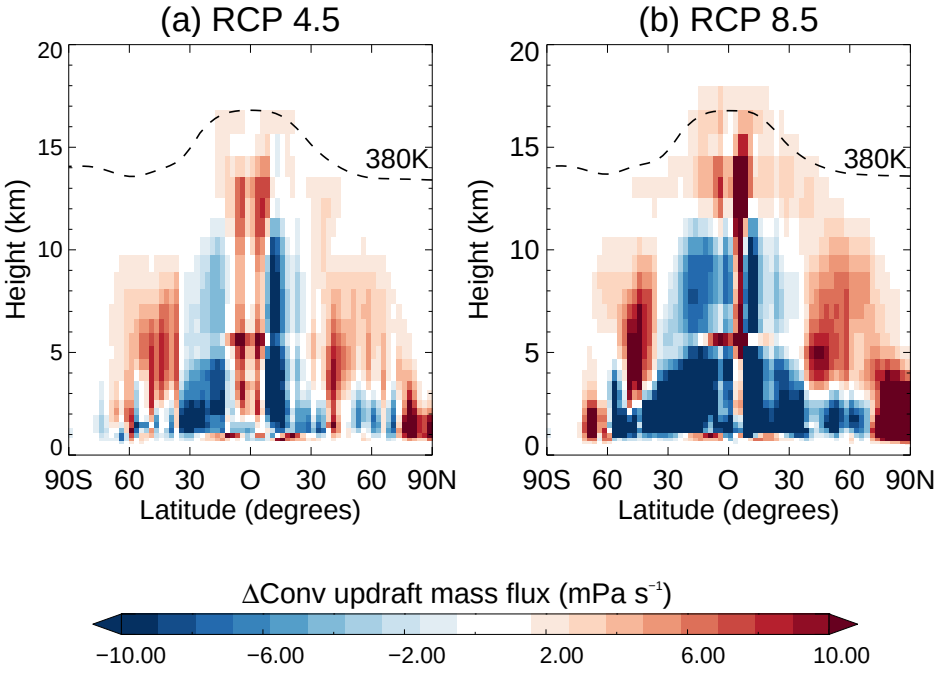

FIGURE 7.2: 2100 annual zonal mean change with respect to 2000 in the convective updraft mass flux (mPa s^{-1}) for (a) RCP 4.5 and (b) RCP 8.5.

Age-of-air, here defined as the mean time since a parcel was in contact with the surface, is reduced (Figure 7.3b). This reduction reflects change to both large-scale and convective-scale motions and correlates with enhanced $CHBr_3$ at 17 km also (Figure 7.3c). For CH_2BrCl, CH_2Br_2 (Figure 7.3d), $CHBrCl_2$ and $CHBr_2Cl$, whose surface lifetimes (137, 123, 78 and 59 days) are considerably longer (WMO, 2011), perturbations to tropospheric transport time-scales have a significant, yet smaller impact on their abundance in the lower stratosphere. Rather, these less photolabile gases are more sensitive to changes to primary oxidant OH.

Figure 7.4a shows the modelled 2100 change in [OH] with respect to (w.r.t) 2000. Warmer lower atmospheric temperature leads to enhanced water vapour and thus enhanced OH production through the $H_2O + O(^1D)$ channel. Under RCP 4.5, [OH] increases throughout the troposphere, with a mean increase of $\sim 0.2 \times 10^6$ molecule cm^{-3} (15% increase w.r.t 2000) occuring at $\sim$15 km. Zeng et al. (2008) show a similar response for a 2100 CCM experiment in which $[CO_2]$ was doubled. Due to difference in experimental set up, a direct

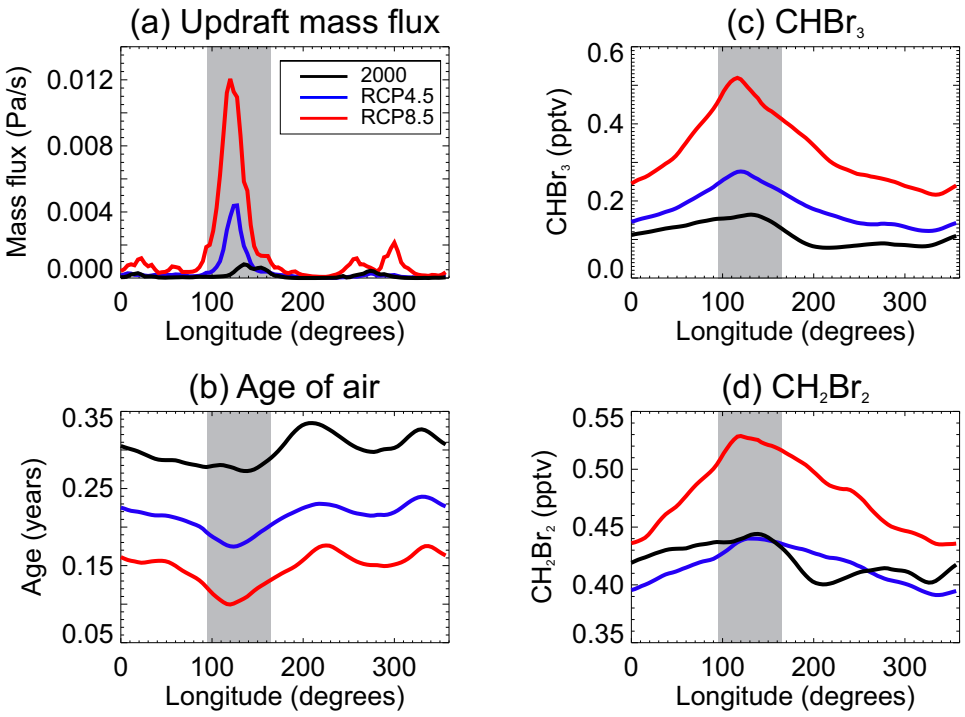

FIGURE 7.3: Longitudinal dependence of (a) convective updraft mass flux (pa/s), (b) age-of-air (years), (c) $CHBr_3$ (ppt) and (d) CH_2Br_2 (ppt) averaged over the tropics (±20°) at ∼17 km for 2000 and 2100 experiments. The Western Pacific region (95-165° longitude) is shaded.

comparison of results is not appropriate. However, qualitatively, increased tropospheric [OH] is consistent between models and is of a similar magnitude.

However, for RCP 8.5, despite enhanced water vapour, below ∼10 km the [OH] response is negative. Between RCPs there is large variation in [CH_4] (Table 7.1). Under RCP 4.5, a scenario where GHG emissions are mitigated, 2100 CH_4 is ∼10% lower w.r.t 2000. Conversely, under RCP 8.5, a non-mitigation scenario, it increases by ∼112%. Enhanced CH_4 tends to reduce [OH] (e.g., Wuebbles et al., 1989) and has a positive feedback on its own lifetime. The rate of the CH_4 + OH reaction has a strong temperature-dependence and increases with the large increase in tropospheric temperature under RCP 8.5 (>4.5 K at the surface).

Changes to the tropospheric oxidising capacity have a small impact on $CHBr_3$. Although minor, enhanced [OH] under RCP 4.5 reduces the $CHBr_3$ lifetime, particularly near the surface, where oxidation by OH can compete with the faster photolysis sink (see Chapter 4). However, overall the $CHBr_3$ change w.r.t 2000 (Figure 7.4b) is small. Under RCP 8.5, the dominant process is the significant increase in the strength of deep tropical convection

which enables more $CHBr_3$ to reach the upper troposphere-lower stratosphere (UTLS) (see Figure 7.3 also).

For CH_2Br_2, under RCP 4.5 the change w.r.t 2000 (Figure 7.4c) closely follows Δ[OH]. Its tropospheric lifetime is reduced due to enhanced [OH] and the positive temperature-dependence of the oxidation. For RCP 8.5, the situation is more complex. The CH_2Br_2 lifetime is extended near the surface (due to decreased [OH]). However, the significantly warmer surface temperature compensates by speeding up the OH sink reaction and overall resulting in little change below 10 km. In the upper troposphere, where this sink is significantly slower, the enhanced convective mass flux dominates by transporting more tracer to the UTLS region.

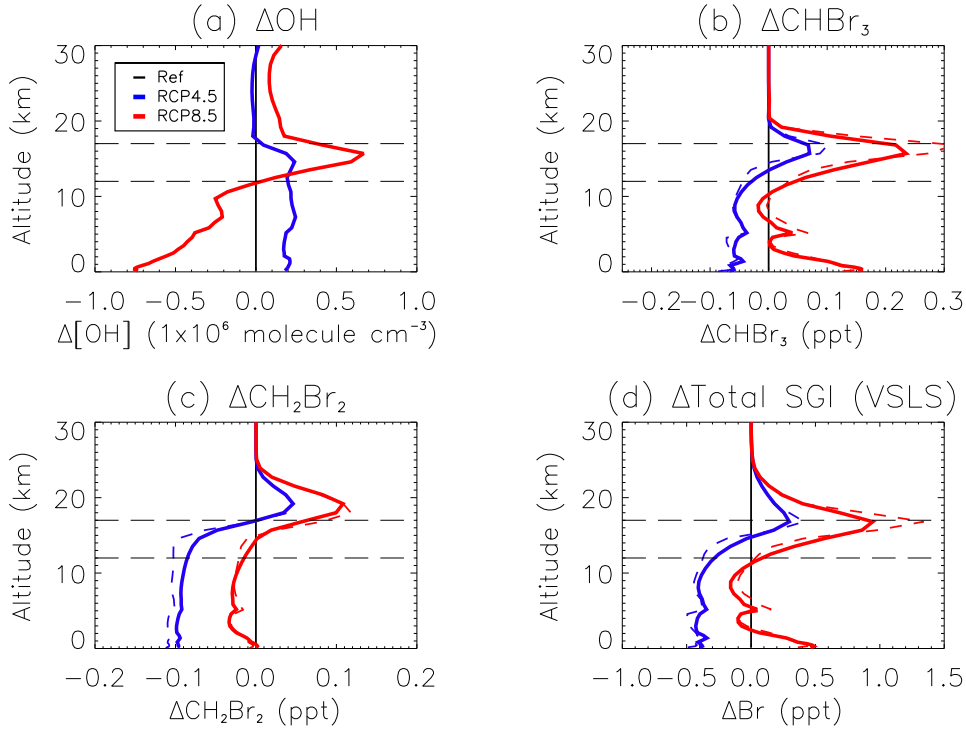

FIGURE 7.4: 2100 annual zonal mean change with respect to 2000 of (a) OH, (b) $CHBr_3$, (c) CH_2Br_2 and (d) total SGI in the tropics ($\pm 20°$). Upper and lower dashed lines denotes the cold point tropopause and the approximate base of the tropical tropopause layer, respectively. Dashed profiles represent mean over the tropical Western Pacific region (90-165° longitude).

Overall, the total SGI from brominated-VSLS increases from a zonally averaged 1.7 ppt (2000) to 1.9 ppt (2100, RCP 4.5) and 2.7 ppt (2100, RCP 8.5). The CCM experiments have assumed 2100 VSLS emissions are the same as present day. It is currently unknown if and how emissions may change in response to climate or other forcings. However, an

increase in the tropical MBL abundance of VSLS due to changes to primary production, sea-air fluxes, land-use practice or indeed any other factors, would likely increase the SGI estimates reported here.

7.4 Summary

The stratospheric source gas injection of VSLS will likely increase in response to climate change. The magnitude of this increase will be determined by competing chemical and dynamical factors. The increase is largely due to stronger tropical deep convection which transports more VSLS to the lower stratosphere. For relatively short-lived gases such as bromoform, whose primary tropospheric sink is photolysis, and therefore subject to relatively minor change, enhanced convection in 2100 leads to an increase in their lower stratospheric abundance. For dibromomethane, and other VSLS whose primary tropospheric sink is through oxidation, their abundance is highly sensitive to changes to the hydroxyl radical. For IPCC RCP 4.5 and RCP 8.5, the tropospheric oxidising capacity may significantly differ and more work is required to best constrain such changes.

For 2000, the modelled source gas injection of bromine from VSLS is ∼1.7 ppt and largest over the tropical West Pacific. For 2100, this estimate increases to ∼1.9 and ∼2.7 ppt when the model is forced with IPCC RCP 4.5 and 8.5. Emissions of major VSLS bromoform and dibromomethane have been held fixed between 2000 and 2100 simulations. Potential increases to primary VSLS emissions in the future (not considered here) would likely increase these estimates of SGI. The so-called product gas injection pathway (PGI) (e.g., WMO, 2011), which is significantly more uncertain at present, has not been considered here but will be the subject of future work.

Chapter 8

Conclusions

In this thesis, the emissions, transport and tropospheric chemistry of biogenic very short-lived species (VSLS) have been investigated using state-of-the-art global models. The results here will contribute to the present understanding of the processes controlling the atmospheric abundance of VSLS and ultimately their impact on ozone (O_3).

Idealised experiments with the TOMCAT/SLIMCAT chemical transport model (CTM) were performed in order to determine the stratospheric bromine (Br) loading due to VSLS (Br_y^{VSLS}) and the relative importance of source gases (SGs) versus product gases (PGs). Novel comparisons of CTM output with high-altitude aircraft observations in the tropical tropopause layer (TTL) were performed. The emphasis has been on major SGs bromoform ($CHBr_3$) and dibromomethane (CH_2Br_2), for which detailed degradation schemes were implemented in the model Although, a range of both biogenic and anthropogenic Br-containing species were considered.

In addition, the UKCA chemistry-climate model (CCM) has also been used to quantify Br_y^{VSLS} in the lower stratosphere. The CCM, which contains a detailed stratospheric chemistry scheme, has been used to determine the impact of Br_y^{VSLS} on global O_3. Furthermore, the CCM has been used to assess how the stratospheric source gas injection of VSLS may respond to climate change. These novel calculations using the recent Intergovernmental Panel on Climate Change (IPCC) representative concentration pathways (RCPs), allow for a preliminary assessment on the role of VSLS and bromine chemistry on future stratospheric O_3.

8.1 Major Findings

The major findings of this work are now summarised below with reference to the thesis aims outlined in Section 1.3.

1. **Biogenic VSLS emissions provide a significant source of stratospheric Br_y.** CTM simulations show $CHBr_3$, CH_2Br_2, $CHBr_2Cl$, CH_2BrCl and $CHBrCl_2$ contribute ∼5 ppt of Br_y^{VSLS} to the stratosphere (∼25% of total stratospheric Br_y in 2009). The SGI pathway accounts for between ∼69-75% of this supply, with the remainder from PGI. The longest lived organic product gas (PG) from $CHBr_3$ and CH_2Br_2 degradation is CBr_2O. Its tropospheric lifetime with respect to photolysis is ∼7 days. It is unlikely that organic PGs make a significant contribution to the total PGI from VSLS. Therefore, the assumption of instantaneous Br_y production, following SG degradation, seems reasonable for stratospheric modelling.

2. **The impact of Br-containing VSLS on stratospheric O_3 is modest**.
CCM simulations, with various emission estimates for major VSLS $CHBr_3$ and CH_2Br_2, show the impact of Br_y^{VSLS} on stratospheric O_3 is modest. The largest impact occurs over Antarctica, where Br_y^{VSLS} reduces the total column O_3 by up to ∼15 DU (a ∼7% decrease) during Spring by enhancing the coupled BrO-ClO loss cycle. At mid-latitudes, the impact of Br_y^{VSLS} is small (<∼2 DU) during periods of background aerosol loading. However, these estimates may represent a lower limit as the modelled magnitude of Br_y^{VSLS} from the CCM (∼3 ppt) is at the lower end of previous estimates and also lower than the CTM estimate reported here (see above).

3. **The stratospheric source gas injection of VSLS will likely increase in response to climate change**.
CCM simulations, representative of IPCC projected 2100 climates, show an increase in the stratospheric SGI of bromine from VSLS. For 2000, SGI supplies ∼1.7 ppt of Br_y to the lower stratosphere. For 2100, this increases to ∼1.9 and ∼2.7 ppt under the RCP 4.5 (moderate climate change) and RCP 8.5 (high climate change) scenarios. The increase is largely due to enhanced tropical deep convection, reducing transport time-scales in the upper troposphere, particularly over the tropical Western Pacific region. If regional emissions were to increase, these estimates of SGI would likely increase further.

8.2 Synthesis

Biogenic VSLS, naturally emitted from the ocean, are important trace gases in both the troposphere and the stratosphere as they are a source of inorganic bromine (and chlorine). Due to their relatively short atmospheric lifetime, combined with highly non-uniform surface emissions in space and time, modelling their tropospheric distribution is challenging. For the most abundant VSLS $CHBr_3$ and CH_2Br_2, comparison of their modelled and observed tropospheric abundance provides a good test of both a model's transport (e.g. convection) and also chemistry (e.g. [OH], photolysis rates).

For global models to reproduce surface observations of VSLS, a reasonable treatment of their emission is required. In this thesis, the UKCA CCM with various available emission estimates for $CHBr_3$ and CH_2Br_2, has been compared with observations from 15 ground-based stations of the National Oceanic and Atmospheric Administration (NOAA) Earth System Research Laboratory (ESRL). UKCA with the *top down* emissions proposed by Ordóñez et al. (2012), which are weighted to observed chlorophyll-a in the ocean, performs very well. Clearly, in recent years significant progress has been made to constrain global VSLS emissions. However, it seems further work is required for a comprehensive *bottom up* emission estimate for use in global models. Ship campaigns, such as the 2011 Stratospheric Halogen Impacts in a Varying Atmosphere (SHIVA), should provide useful data on sea-air fluxes of VSLS for this purpose.

High-altitude observations of VSLS are currently sparse. Observations in the TTL are required in order to constrain estimates of their stratospheric SGI and to evaluate the performance of global models in this important region. The results of this thesis indicate significant variation in the modelled vertical distribution of $CHBr_3$ and CH_2Br_2 in the TTL between the UKCA CCM and the TOMCAT/SLIMCAT CTM. The CCM, which calculates its own large scale circulation, shows relatively slow transport through the TTL which provides a good fit to observations of these SGs. However, the CTM with its vertical transport calculated from the analyses winds, tends to overestimate their abundance. It is therefore expected that estimates of the stratospheric SGI from "TOMCAT" calculations represent an upper limit. More observations in the upper TTL will be required in order to support this conclusion.

From the CTM runs performed in this thesis, the total (SGI + PGI) Br-loading from VSLS (Br_y^{VSLS}) is estimated to be ∼5 ppt. This likely represents an upper limit given the possible overestimation of SGI discussed above. This modelled Br_y^{VSLS} is in good agreement with estimates based on balloon-borne differential optical absorption spectroscopy (DOAS) (Dorf et al., 2008) and ground-based zenith sky UV-visible (Sinnhuber et al., 2002) observations of stratospheric BrO (also ∼5 ppt). However, it is generally lower than estimates based on satellite measured BrO, which can be significantly larger (>6 ppt) (e.g., Sioris et al., 2006; Kovalenko et al., 2007). UKCA CCM simulations show a smaller stratospheric Br_y^{VSLS} contribution of ∼3 ppt. Due to a large wet bias in the model's upper troposphere and lower stratosphere, PGI is likely underestimated in these runs. Between both models, the ∼3-5 ppt range of Br_y^{VSLS} is in agreement with the recent WMO estimate and range of 6 (3-8) ppt (Montzka and Reimann, 2011).

The impact of Br_y^{VSLS} on stratospheric O_3 is significant. Previous modelling work has shown a larger impact post volcanic events (e.g. Mount Pinatubo), when aerosol loading is relatively high and significant heterogeneous halogen activation occurs (e.g., Feng et al., 2007). This thesis shows that with a background aerosol loading, the impact of VSLS on total column O_3 is small at mid-latitudes - consistent with the modelling work of Salawitch et al. (2005) and Feng et al. (2007). In polar regions, the impact is larger where the depletion due to Br_y^{VSLS} peaks at 15 DU over the South Pole during late Winter/early Spring. The impact of VSLS is largest in the lower stratosphere where Br_y^{VSLS} is readily released from source gases. Overall, given the importance of bromine chemistry for O_3 loss in the troposphere (e.g., von Glasow et al., 2004) and also the mid-latitude and polar stratosphere (e.g., Sinnhuber et al., 2009; Salawitch et al., 2005), Br-containing VSLS should be explicitly treated in global models for studies of atmospheric composition.

The Western Pacific is a strong convective source region (e.g., Fueglistaler et al., 2009) and has been previously identified as important for the troposphere-stratosphere transport of VSLS (Aschmann et al., 2009). The results of this thesis are in agreement and have shown that even tracers with lifetimes as short as 6 hours can reach the lower stratosphere in this region. If convection, or indeed the larger scale circulation, can transport VSLS away from the surface, their lifetimes may be considerably longer. The results here have shown that in the cold TTL, the OH oxidation sink of a number of VSLS is particularly slow due to the temperature-dependence of the reaction. For major VSLS CH_2Br_2, whose primary

sink is via OH, its lifetime in the TTL can exceed ∼500 days. This is considerably longer than the World Meteorological Organization (WMO) working definition of a VSLS; i.e. a gas whose lifetime is less than or equal to ∼6 months (WMO, 2007).

As the phase out of long-lived anthropogenic bromine (and chlorine) compounds continues under the Montreal Protocol (and amendments), the relative importance of VSLS for stratospheric halogen loading will increase. The results of this thesis show that their absolute contribution may also increase in response to climate change. For 2100 the modelled stratospheric SGI of bromine from VSLS may increase by between 12-60%, relative to 2000. It seems likely also that the Western Pacific region will remain an important source route for the troposphere-stratosphere transport of VSLS. Changes to regional land use and practice, such as seaweed farming, which is currently a growing sector, or enhanced ocean productivity, could potentially increase the surface loading of VSLS. This, combined with the modelled dynamical changes under an extreme climate scenario such as RCP 8.5, could lead to a significant increase in stratospheric VSLS loading.

8.3 Future Work

At present, quantifying Br_y^{VSLS} in the stratosphere is an area of active research in both the measurement and modelling communities (e.g., WMO, 2007, 2011). To constrain this contribution, more observations of major bromine-containing source gases, $CHBr_3$ and CH_2Br_2, in the TTL are needed. Future projects involving high-altitude, long endurance, unmanned aircraft, such as the NASA Global Hawk, should significantly enhance the global coverage of VSLS (and other trace gas) observations. In addition, an attempt to observe the expected organic products of $CHBr_3$ and CH_2Br_2 degradation, namely CBr_2O and CHBrO, would be useful. This could potentially validate the conclusion drawn in this thesis, that these gases are short-lived and make a negligible contribution to stratospheric Br_y. For global models, it is likely that estimates of Br_y^{VSLS} vary significantly. The upcoming TRANSCOM-VSLS project will perform a multi-model intercomparison to assess variability between models. The models used in this thesis (TOMCAT/SLIMCAT and UKCA) will participate in this activity.

A sound treatment of brominated VSLS emissions are required in order for global models to simulate a realistic Br_y budget in both the troposphere and stratosphere. Given the

wide-ranging impact and importance of halogen chemistry, from the boundary layer to the stratosphere, future work should aim to constrain VSLS emissions from various key geographical source regions (e.g. Western Pacific). More observations of the sea-air flux of VSLS are required in order to improve bottom-up derived emission estimates and ultimately global-scale emission inventories for use in both chemical-transport and chemistry-climate models. Recent projects, such as the 2011 SHIVA campaign, will provide useful ship-borne data in the poorly sampled West Pacific for this purpose.

To assess the significance of VSLS on future global stratospheric O_3, further work is required to 1) determine potential changes to VSLS emission rates and 2) determine the efficiency of reactive bromine O_3 loss cycles under evolving stratospheric composition (e.g. decreasing chlorine, and potentially increasing hydrogen oxides). The focus of this thesis has been on Br-containing VSLS and their impact on stratospheric O_3. However, this work will be extended to include biogenic chlorine and iodine-containing VSLS and to examine their impact in the troposphere also. This will include modelling work to examine the impact of VSLS and halogen chemistry on the lifetime of key greenhouse gases (e.g. methane) and other climate-relevant gases, such as dimethyl sulphide (DMS).

References

Aschmann, J., B. M. Sinnhuber, E. L. Atlas, and S. M. Schauffler, 2009: Modeling the transport of very short-lived substances into the tropical upper troposphere and lower stratosphere. *ATMOSPHERIC CHEMISTRY AND PHYSICS*, **9**, 9237–9247.

Aschmann, J., B.-M. Sinnhuber, M. P. Chipperfield, and R. Hossaini, 2011: Impact of deep convection and dehydration on bromine loading in the upper troposphere and lower stratosphere. *ATMOSPHERIC CHEMISTRY AND PHYSICS*, **11**, 2671–2687, doi:10.5194/acp-11-2671-2011.

Ashfold, M. J., N. R. P. Harris, E. L. Atlas, A. J. Manning, and J. A. Pyle, 2012: Transport of short-lived species into the tropical tropopause layer. *ATMOSPHERIC CHEMISTRY AND PHYSICS*, **12**, 6309–6322, doi:10.5194/acp-12-6309-2012.

Bates, D. and M. Nicolet, 1950: The photochemistry of atmospheric water vapor. *JOURNAL OF GEOPHYSICAL RESEARCH*, **55**, 301–327, doi:10.1029/JZ055i003p00301.

Beyersdorf, A. J., D. R. Blake, A. Swanson, S. Meinardi, F. S. Rowland, and D. Davis, 2010: Abundances and variability of tropospheric volatile organic compounds at the South Pole and other Antarctic locations. *ATMOSPHERIC ENVIRONMENT*, **44**, 4565–4574, doi:10.1016/j.atmosenv.2010.08.025.

Braesicke, P., O. J. Smith, P. Telford, and J. A. Pyle, 2011: Ozone concentration changes in the Asian summer monsoon anticyclone and lower stratospheric water vapour: An idealised model study. *GEOPHYSICAL RESEARCH LETTERS*, **38**, doi:10.1029/2010GL046228.

Breider, T. J., M. P. Chipperfield, N. A. D. Richards, K. S. Carslaw, G. W. Mann, and D. V. Spracklen, 2010: Impact of BrO on dimethylsulfide in the remote marine boundary layer. *GEOPHYSICAL RESEARCH LETTERS*, **37**, doi:10.1029/2009GL040868.

Brewer, A., 1949: Evidence for a world circulation provided by the measurements of helium and water vapour distribution in the stratosphere. *QUARTERLY JOURNAL OF THE ROYAL METEOROLOGICAL SOCIETY*, **75**, 351–363, doi:10.1002/qj.49707532603.

Butler, J. H., D. B. King, J. M. Lobert, S. A. Montzka, S. A. Yvon-Lewis, B. D. Hall, N. J. Warwick, D. J. Mondeel, M. Aydin, and J. W. Elkins, 2007: Oceanic distributions and emissions of short-lived halocarbons. *GLOBAL BIOGEOCHEMICAL CYCLES*, **21**, doi:10.1029/2006GB002732.

Butz, A., H. Boesch, C. Camy-Peyret, M. P. Chipperfield, M. Dorf, S. Kreycy, L. Kritten, C. Prados-Roman, J. Schwaerzle, and K. Pfeilsticker, 2009: Constraints on inorganic gaseous iodine in the tropical upper troposphere and stratosphere inferred from balloon-borne solar occultation observations. *ATMOSPHERIC CHEMISTRY AND PHYSICS*, **9**, 7229–7242.

Carpenter, L. and P. Liss, 2000: On temperate sources of bromoform and other reactive organic bromine gases. *JOURNAL OF GEOPHYSICAL RESEARCH-ATMOSPHERES*, **105**, 20539–20547, doi:10.1029/2000JD900242.

Carpenter, L., W. Sturges, S. Penkett, P. Liss, B. Alicke, K. Hebestreit, and U. Platt, 1999: Short-lived alkyl iodides and bromides at Mace Head, Ireland: Links to biogenic sources and halogen oxide production. *JOURNAL OF GEOPHYSICAL RESEARCH-ATMOSPHERES*, **104**, 1679–1689, doi:10.1029/98JD02746.

Carpenter, L., D. Wevill, S. O'Doherty, G. Spain, and P. Simmonds, 2005: Atmospheric bromoform at Mace Head, Ireland: seasonality and evidence for a peatland source. *ATMOSPHERIC CHEMISTRY AND PHYSICS*, **5**, 2927–2934.

CCMVal, 2010: SPARC Report on the Evaluation of Chemistry-Climate Models. *SPARC Report No. 5, WCRP-132, WMO/TD-NO. 1526.* .

Chapman, S., 1930: A theory of upper-atmosphere ozone. *Mem. Roy. Meteorol. Soc.*, **3**.

Chipperfield, M., 2009: Nitrous oxide delays ozone recovery. *NATURE GEOSCIENCE*, **2**, 742–743, doi:10.1038/ngeo678.

Chipperfield, M. and V. Fioletov, 2007: Halogenated very short-lived substances, in: Scientific Assessment of Ozone Depletion: 2006. *Global Ozone Research and Monitoring Project, Report No. 50, Chapt. 3, World Meteorological Organization, Geneva.* .

Chipperfield, M. and J. Pyle, 1998: Model sensitivity studies of Arctic ozone depletion. *JOURNAL OF GEOPHYSICAL RESEARCH-ATMOSPHERES*, **103**, 28389–28403, doi:10.1029/98JD01960.

Chipperfield, M. P., 2006: New version of the TOMCAT/SLIMCAT off-line chemical transport model: Intercomparison of stratospheric tracer experiments. *QUARTERLY JOURNAL OF THE ROYAL METEOROLOGICAL SOCIETY*, **132**, 1179–1203, doi:10.1256/qj.05.51.

Chou, C. and C.-A. Chen, 2010: Depth of convection and the weakening of tropical circulation in global warming. *JOURNAL OF CLIMATE*, **23**, 3019–3030, doi:10.1175/2010JCLI3383.1.

Clerbaux, C. and D. Cunnold, 2007: Long-lived compounds, in: Scientific Assessment of Ozone Depletion: 2006. *Global Ozone Research and Monitoring Project, Report No. 50, Chapt. 2, World Meteorological Organization, Geneva.* .

Colman, J., A. Swanson, S. Meinardi, B. Sive, D. Blake, and F. Rowland, 2001: Description of the analysis of a wide range of volatile organic compounds in whole air samples collected during PEM-Tropics A and B. *ANALYTICAL CHEMISTRY*, **73**, 3723–3731, doi:10.1021/ac010027g.

Crutzen, P., 1970: Influence of nitrogen oxides on atmospheric ozone content. *QUARTERLY JOURNAL OF THE ROYAL METEOROLOGICAL SOCIETY*, **96**, 320–&, doi:10.1002/qj.49709640815.

Crutzen, P. and M. Lawrence, 2000: The impact of precipitation scavenging on the transport of trace gases: A 3-dimensional model sensitivity study. *JOURNAL OF ATMOSPHERIC CHEMISTRY*, **37**, 81–112, doi:10.1023/A:1006322926426.

Davies, T., M. Cullen, A. Malcolm, M. Mawson, A. Staniforth, A. White, and N. Wood, 2005: A new dynamical core for the Met Office's global and regional modelling of the atmosphere. *QUARTERLY JOURNAL OF THE ROYAL METEOROLOGICAL SOCIETY*, **131**, 1759–1782, doi:10.1256/qj.04.101.

Deiber, G., C. George, S. Le Calve, F. Schweitzer, and P. Mirabel, 2004: Uptake study of $ClONO_2$ and $BrONO_2$ by halide containing droplets. *ATMOSPHERIC CHEMISTRY AND PHYSICS*, **4**, 1291–1299.

Dessens, O., G. Zeng, N. Warwick, and J. Pyle, 2009: Short-lived bromine compounds in the lower stratosphere; impact of climate change on ozone. *ATMOSPHERIC SCIENCE LETTERS*, **10**, 201–206, doi:10.1002/asl.236.

Deushi, M. and K. Shibata, 2011: Impacts of increases in greenhouse gases and ozone recovery on lower stratospheric circulation and the age of air: Chemistry-climate model simulations up to 2100. *JOURNAL OF GEOPHYSICAL RESEARCH-ATMOSPHERES*, **116**, doi:10.1029/2010JD015024.

Dorf, M., H. Boesch, A. Butz, C. Camy-Peyret, M. P. Chipperfield, A. Engel, F. Goutail, K. Grunow, F. Hendrick, S. Hrechanyy, B. Naujokat, J. P. Pommereau, M. Van Roozendael, C. Sioris, F. Stroh, F. Weidner, and K. Pfeilsticker, 2006: Balloon-borne stratospheric BrO measurements: comparison with Envisat/SCIAMACHY BrO limb profiles. *ATMOSPHERIC CHEMISTRY AND PHYSICS*, **6**, 2483–2501.

Dorf, M., A. Butz, C. Camy-Peyret, M. P. Chipperfield, L. Kritten, and K. Pfeilsticker, 2008: Bromine in the tropical troposphere and stratosphere as derived from balloon-borne BrO observations. *ATMOSPHERIC CHEMISTRY AND PHYSICS*, **8**, 7265–7271.

Dvortsov, V., M. Geller, S. Solomon, S. Schauffler, E. Atlas, and D. Blake, 1999: Rethinking reactive halogen budgets in the midlatitude lower stratosphere. *GEOPHYSICAL RESEARCH LETTERS*, **26**, 1699–1702, doi:10.1029/1999GL900309.

Edwards, J. and A. Slingo, 1996: Studies with a flexible new radiation code .1. Choosing a configuration for a large-scale model. *QUARTERLY JOURNAL OF THE ROYAL METEOROLOGICAL SOCIETY*, **122**, 689–719, doi:10.1256/smsqj.53106.

Erle, F., A. Grendel, D. Perner, U. Platt, and K. Pfeilsticker, 1998: Evidence of heterogeneous bromine chemistry on cold stratospheric sulphate aerosols. *GEOPHYSICAL RESEARCH LETTERS*, **25**, 4329–4332, doi:10.1029/1998GL900087.

Farman, J., B. Gardiner, and J. Shanklin, 1985: Large losses of total ozone in Antarctica reaveal seasonal ClOx/NOx interaction. *NATURE*, **315**, 207–210, doi:10.1038/315207a0.

Feng, W., M. P. Chipperfield, S. Dhomse, B. M. Monge-Sanz, X. Yang, K. Zhang, and M. Ramonet, 2011: Evaluation of cloud convection and tracer transport in

a three-dimensional chemical transport model. *ATMOSPHERIC CHEMISTRY AND PHYSICS*, **11**, 5783–5803, doi:10.5194/acp-11-5783-2011.

Feng, W., M. P. Chipperfield, M. Dorf, K. Pfeilsticker, and P. Ricaud, 2007: Mid-latitude ozone changes: studies with a 3-D CTM forced by ERA-40 analyses. *ATMOSPHERIC CHEMISTRY AND PHYSICS*, **7**, 2357–2369.

Forster, P., V. Ramaswamy, P. Artaxo, T. Berntsen, R. Betts, D. Fahey, J. Haywood, J. Lean, D. Lowe, G. Myhre, J. Nganga, R. Prinn, G. Raga, M. Schulz, and R. V. Dorland, 2007: Changes in Atmospheric Constituents and in Radiative Forcing. in: Climate Change 2007: The Physical Science Basis. Contribution of Working Group I to the Fourth Assessment Report of the Intergovernmental Panel on Climate Change [Solomon, S. et al. (eds.)]. *Cambridge University Press, Cambridge, United Kingdom.*

Fueglistaler, S., A. E. Dessler, T. J. Dunkerton, I. Folkins, Q. Fu, and P. W. Mote, 2009: Tropical tropopause layer. *REVIEWS OF GEOPHYSICS*, **47**, doi:10.1029/2008RG000267.

Gettelman, A., P. H. Lauritzen, M. Park, and J. E. Kay, 2009: Processes regulating short-lived species in the tropical tropopause layer. *JOURNAL OF GEOPHYSICAL RESEARCH-ATMOSPHERES*, **114**, doi:10.1029/2009JD011785.

Giannakopoulos, C., M. Chipperfield, K. Law, and J. Pyle, 1999: Validation and intercomparison of wet and dry deposition schemes using Pb-210 in a global three-dimensional off-line chemical transport model. *JOURNAL OF GEOPHYSICAL RESEARCH-ATMOSPHERES*, **104**, 23761–23784, doi:10.1029/1999JD900392.

Harris, N. R. P., E. Kyro, J. Staehelin, D. Brunner, S. B. Andersen, S. Godin-Beekmann, S. Dhomse, P. Hadjinicolaou, G. Hansen, I. Isaksen, A. Jrrar, A. Karpetchko, R. Kivi, B. Knudsen, P. Krizan, J. Lastovicka, J. Maeder, Y. Orsolini, J. A. Pyle, M. Rex, K. Vanicek, M. Weber, I. Wohltmann, P. Zanis, and C. Zerefos, 2008: Ozone trends at northern mid- and high latitudes - a European perspective. *ANNALES GEOPHYSICAE*, **26**, 1207–1220.

Hendrick, F., P. V. Johnston, M. De Maziere, C. Fayt, C. Hermans, K. Kreher, N. Theys, A. Thomas, and M. Van Roozendael, 2008: One-decade trend analysis of stratospheric BrO over Harestua (60 degrees N) and Lauder (45 degrees S) reveals a decline. *GEOPHYSICAL RESEARCH LETTERS*, **35**, doi:10.1029/2008GL034154.

Hofmann, D. and S. Solomon, 1989: Ozone destruction through heterogeneous chemistry following the eruption of El Chichon. *JOURNAL OF GEOPHYSICAL RESEARCH-ATMOSPHERES*, **94**, 5029–5041, doi:10.1029/JD094iD04p05029.

Holtslag, A. and B. Boville, 1993: Local versus nonlocal boundary-layer diffusion in a global climate model. *JOURNAL OF CLIMATE*, **6**, 1825–1842.

Hossaini, R., M. P. Chipperfield, S. Dhomse, C. Ordonez, A. Saiz-Lopez, N. L. Abraham, A. Archibald, P. Braesicke, P. Telford, N. Warwick, X. Yang, and J. Pyle, 2012a: A future increase in the stratospheric source gas injection of biogenic bromocarbons. *in press, GEOPHYSICAL RESEARCH LETTERS*.

Hossaini, R., M. P. Chipperfield, W. Feng, T. J. Breider, E. Atlas, S. A. Montzka, B. R. Miller, F. Moore, and J. Elkins, 2012b: The contribution of natural and anthropogenic very short-lived species to stratospheric bromine. *ATMOSPHERIC CHEMISTRY AND PHYSICS*, **12**, 371–380, doi:10.5194/acp-12-371-2012.

Hossaini, R., M. P. Chipperfield, B. M. Monge-Sanz, N. A. D. Richards, E. Atlas, and D. R. Blake, 2010: Bromoform and dibromomethane in the tropics: a 3-D model study of chemistry and transport. *ATMOSPHERIC CHEMISTRY AND PHYSICS*, **10**, 719–735, doi:10.5194/acp-10-719-2010.

Hoyle, C. R., V. Marecal, M. R. Russo, G. Allen, J. Arteta, C. Chemel, M. P. Chipperfield, F. D'Amato, O. Dessens, W. Feng, J. F. Hamilton, N. R. P. Harris, J. S. Hosking, A. C. Lewis, O. Morgenstern, T. Peter, J. A. Pyle, T. Reddmann, N. A. D. Richards, P. J. Telford, W. Tian, S. Viciani, A. Volz-Thomas, O. Wild, X. Yang, and G. Zeng, 2011: Representation of tropical deep convection in atmospheric models - Part 2: Tracer transport. *ATMOSPHERIC CHEMISTRY AND PHYSICS*, **11**, 8103–8131, doi:10.5194/acp-11-8103-2011.

Johnston, H., 1971: Reduction of stratospheric ozone by nitrogen oxide catalysts from supersonic transport exhaust. *SCIENCE*, **173**, 517–&, doi:10.1126/science.173.3996.517.

Kanavy, H. E. and M. R. Gerstenblith, 2011: Ultraviolet Radiation and Melanoma. *SEMINARS IN CUTANEOUS MEDICINE AND SURGERY*, **30**, 222–228, doi:10.1016/j.sder.2011.08.003.

Kerkweg, A., P. Joeckel, N. Warwick, S. Gebhardt, C. A. M. Brenninkmeijer, and J. Lelieveld, 2008: Consistent simulation of bromine chemistry from the marine boundary layer to the stratosphere - Part 2: Bromocarbons. *ATMOSPHERIC CHEMISTRY AND PHYSICS*, **8**, 5919–5939.

Ko, K. and W. Poulet, 2003: Halogenated very short-lived substances, in: Scientific Assessment of Ozone Depletion: 2006. *Global Ozone Research and Monitoring Project, Report No. 50, Chapt. 2, World Meteorological Organization, Geneva.* .

Kovalenko, L. J., N. L. Livesey, R. J. Salawitch, C. Camy-Peyret, M. P. Chipperfield, R. E. Cofield, M. Dorf, B. J. Drouin, L. Froidevaux, R. A. Fuller, F. Goutail, R. F. Jarnot, K. Jucks, B. W. Knosp, A. Lambert, I. A. MacKenzie, K. Pfeilsticker, J. P. Pommereau, W. G. Read, M. L. Santee, M. J. Schwartz, W. V. Snyder, R. Stachnik, P. C. Stek, P. A. Wagner, and J. W. Waters, 2007: Validation of Aura Microwave Limb Sounder BrO observations in the stratosphere. *JOURNAL OF GEOPHYSICAL RESEARCH-ATMOSPHERES*, **112**, doi:10.1029/2007JD008817.

Krueger, K., S. Tegtmeier, and M. Rex, 2008: Long-term climatology of air mass transport through the Tropical Tropopause Layer (TTL) during NH winter. *ATMOSPHERIC CHEMISTRY AND PHYSICS*, **8**, 813–823.

— 2009: Variability of residence time in the tropical tropopause layer during northern hemisphere winter. *ATMOSPHERIC CHEMISTRY AND PHYSICS*, **9**, 6717–6725, doi:10.5194/acp-9-6717-2009.

Lary, D., M. Chipperfield, R. Toumi, and T. Lenton, 1996: Heterogeneous atmospheric bromine chemistry. *JOURNAL OF GEOPHYSICAL RESEARCH-ATMOSPHERES*, **101**, 1489–1504, doi:10.1029/95JD02839.

Lary, D. and R. Toumi, 1997: Halogen-catalyzed methane oxidation. *JOURNAL OF GEOPHYSICAL RESEARCH-ATMOSPHERES*, **102**, 23421–23428, doi:10.1029/97JD00914.

Laube, J. C., A. Engel, H. Boenisch, T. Moebius, D. R. Worton, W. T. Sturges, K. Grunow, and U. Schmidt, 2008: Contribution of very short-lived organic substances to stratospheric chlorine and bromine in the tropics - a case study. *ATMOSPHERIC CHEMISTRY AND PHYSICS*, **8**, 7325–7334.

Law, K. and W. Sturges, 2007: Halogenated very short-lived substances, in: Scientific Assessment of Ozone Depletion: 2006. *Global Ozone Research and Monitoring Project, Report No. 50, Chapt. 2, World Meteorological Organization, Geneva.* .

Liang, Q., R. S. Stolarski, S. R. Kawa, J. E. Nielsen, A. R. Douglass, J. M. Rodriguez, D. R. Blake, E. L. Atlas, and L. E. Ott, 2010: Finding the missing stratospheric Br_y: a global modeling study of $CHBr_3$ and CH_2Br_2. *ATMOSPHERIC CHEMISTRY AND PHYSICS*, **10**, 2269–2286.

Lock, A., A. Brown, M. Bush, G. Martin, and R. Smith, 2000: A new boundary layer mixing scheme. Part I: Scheme description and single-column model tests. *MONTHLY WEATHER REVIEW*, **128**, 3187–3199, doi:10.1175/1520-0493(2000)128¡3187:ANBLMS¿2.0.CO;2.

Lovelock, J. and R. Maggs, 1973: Halogenated hydrocarbons in and over Atlantic. *NATURE*, **241**, 194–196, doi:10.1038/241194a0.

Low, J., N. Wang, J. Williams, and R. Cicerone, 2003: Measurements of ambient atmospheric C_2H_5Cl and other ethyl and methyl halides at coastal California sites and over the Pacific Ocean. *JOURNAL OF GEOPHYSICAL RESEARCH-ATMOSPHERES*, **108**, doi:10.1029/2003JD003620.

Martin, G. M., N. Bellouin, W. J. Collins, I. D. Culverwell, P. R. Halloran, S. C. Hardiman, T. J. Hinton, C. D. Jones, R. E. McDonald, A. J. McLaren, F. M. O'Connor, M. J. Roberts, J. M. Rodriguez, S. Woodward, M. J. Best, M. E. Brooks, A. R. Brown, N. Butchart, C. Dearden, S. H. Derbyshire, I. Dharssi, M. Doutriaux-Boucher, J. M. Edwards, P. D. Falloon, N. Gedney, L. J. Gray, H. T. Hewitt, M. Hobson, M. R. Huddleston, J. Hughes, S. Ineson, W. J. Ingram, P. M. James, T. C. Johns, C. E. Johnson, A. Jones, C. P. Jones, M. M. Joshi, A. B. Keen, S. Liddicoat, A. P. Lock, A. V. Maidens, J. C. Manners, S. F. Milton, J. G. L. Rae, J. K. Ridley, A. Sellar, C. A. Senior, I. J. Totterdell, A. Verhoef, P. L. Vidale, A. Wiltshire, and H. D. Team, 2011: The HadGEM2 family of Met Office Unified Model climate configurations. *GEOSCIENTIFIC MODEL DEVELOPMENT*, **4**, 723–757, doi:10.5194/gmd-4-723-2011.

McCormick, M., H. Steele, P. Hamill, W. Chu, and T. Swissler, 1982: Polar Stratospheric Cloud Sightings BY SAM-II. *JOURNAL OF THE ATMOSPHERIC SCIENCES*, **39**, 1387–1397, doi:10.1175/1520-0469(1982)039¡1387:PSCSBS¿2.0.CO;2.

McElroy, M., R. Salawitch, S. Wofsy, and J. Logan, 1986: Reduction of Antarctic ozone due to synergistic interactions of chlorine and bromine. *NATURE*, **321**, 759–762, doi:10.1038/321759a0.

McGivern, W., J. Francisco, and S. North, 2002: Investigation of the atmospheric oxidation pathways of bromoform: Initiation via OH/Cl reactions. *JOURNAL OF PHYSICAL CHEMISTRY A*, **106**, 6395–6400, doi:10.1021/jp0255886.

McGivern, W., H. Kim, J. Francisco, and S. North, 2004: Investigation of the atmospheric oxidation pathways of bromoform and dibromomethane: Initiation via UV photolysis and hydrogen abstraction. *JOURNAL OF PHYSICAL CHEMISTRY A*, **108**, 7247–7252, doi:10.1021/jp0311613.

McLinden, C. A., C. S. Haley, N. D. Lloyd, F. Hendrick, A. Rozanov, B. M. Sinnhuber, F. Goutail, D. A. Degenstein, E. J. Llewellyn, C. E. Sioris, M. Van Roozendael, J. P. Pommereau, W. Lotz, and J. P. Burrows, 2010: Odin/OSIRIS observations of stratospheric BrO: Retrieval methodology, climatology, and inferred Br-y. *JOURNAL OF GEOPHYSICAL RESEARCH-ATMOSPHERES*, **115**, doi:10.1029/2009JD012488.

Millán, L., N. Livesey, W. Read, L. Froidevaux, D. Kinnison, R. Harwood, I. A. MacKenzie, and M. P. Chipperfield, 2012: New aura microwave limb sounder observations of Bro and implications for Br_y. *Atmospheric Measurement Techniques*, **5**, 1741–1751, doi:10.5194/amt-5-1741-2012.

Molina, L. and M. Molina, 1987: Production of Cl_2O_2 from the self-reaction of the ClO radical. *JOURNAL OF PHYSICAL CHEMISTRY*, **91**, 433–436, doi:10.1021/j100286a035.

Molina, M. and F. Rowland, 1974: Stratospheric sink for chlorofluoromethane - chlorine atomic-catalysed destruction of ozone. *NATURE*, **249**, 810–812, doi:10.1038/249810a0.

Molina, M., T. Tso, L. Molina, and F. Wang, 1987: Antarctic stratospheric chemistry of chlorine nitrate, hydrogen-chloride and ice - release of active chlorine. *SCIENCE*, **238**, 1253–1257, doi:10.1126/science.238.4831.1253.

Monge-Sanz, B. M., M. P. Chipperfield, A. J. Simmons, and S. M. Uppala, 2007: Mean age of air and transport in a CTM: Comparison of different ECMWF analyses. *GEOPHYSICAL RESEARCH LETTERS*, **34**, doi:10.1029/2006GL028515.

Montzka, S., J. Butler, B. Hall, D. Mondeel, and J. Elkins, 2003: A decline in tropospheric organic bromine. *GEOPHYSICAL RESEARCH LETTERS*, **30**, doi:10.1029/2003GL017745.

Montzka, S. and S. Reimann, 2011: Ozone-depleting substances (ODSs) and related chemicals, in: Scientific Assessment of Ozone Depletion: 2010. *Global Ozone Research and Monitoring Project, Report No. 52, Chapt. 1, World Meteorological Organization, Geneva* .

Moortgat, G., R. Meller, and W. Schneider, 1993: Temperature dependence (256-296 K) of the absorption cross-sections of bromoform in the wavelength range 285-360nmm, in The Tropospheric Chemistry of Ozone in the Polar Regions. *NATO ASI Series, Vol. I7, edited by: Niki, H. and Becker, K. H, Springer Verlag, Berlin.* .

Morgenstern, O., P. Braesicke, M. M. Hurwitz, F. M. O'Connor, A. C. Bushell, C. E. Johnson, and J. A. Pyle, 2008: The world avoided by the Montreal Protocol. *GEOPHYSICAL RESEARCH LETTERS*, **35**, doi:10.1029/2008GL034590.

Morgenstern, O., P. Braesicke, F. M. O'Connor, A. C. Bushell, C. E. Johnson, S. M. Osprey, and J. A. Pyle, 2009: Evaluation of the new UKCA climate-composition model - Part 1: The stratosphere. *GEOSCIENTIFIC MODEL DEVELOPMENT*, **2**, 43–57, doi:10.5194/gmd-2-43-2009.

Nielsen, J. and A. Douglass, 2001: Simulation of bromoform's contribution to stratospheric bromine. *JOURNAL OF GEOPHYSICAL RESEARCH-ATMOSPHERES*, **106**, 8089–8100, doi:10.1029/2000JD900767.

O'Brien, L. M., N. R. P. Harris, A. D. Robinson, B. Gostlow, N. Warwick, X. Yang, and J. A. Pyle, 2009: Bromocarbons in the tropical marine boundary layer at the Cape Verde Observatory - measurements and modelling. *ATMOSPHERIC CHEMISTRY AND PHYSICS*, **9**, 9083–9099, doi:10.5194/acp-9-9083-2009.

Ordóñez, C., J.-F. Lamarque, S. Tilmes, D. E. Kinnison, E. L. Atlas, D. R. Blake, G. S. Santos, G. Brasseur, and A. Saiz-Lopez, 2012: Bromine and iodine chemistry in a global chemistry-climate model: description and evaluation of very short-lived oceanic sources. *ATMOSPHERIC CHEMISTRY AND PHYSICS*, **12**, 1423–1447, doi:10.5194/acp-12-1423-2012.

Palmer, C. J. and C. J. Reason, 2009: Relationships of surface bromoform concentrations with mixed layer depth and salinity in the tropical oceans. *GLOBAL BIOGEOCHEMICAL CYCLES*, **23**, doi:10.1029/2008GB003338.

Park, S., E. L. Atlas, R. Jimenez, B. C. Daube, E. W. Gottlieb, J. Nan, D. B. A. Jones, L. Pfister, T. J. Conway, T. P. Bui, R. S. Gao, and S. C. Wofsy, 2010: Vertical transport rates and concentrations of OH and Cl radicals in the Tropical Tropopause Layer from observations of CO(2) and halocarbons: implications for distributions of long- and short-lived chemical species. *ATMOSPHERIC CHEMISTRY AND PHYSICS*, **10**, 6669–6684, doi:10.5194/acp-10-6669-2010.

Pfeilsticker, K., W. Sturges, H. Bosch, C. Camy-Peyret, M. Chipperfield, A. Engel, R. Fitzenberger, M. Muller, S. Payan, and B. Sinnhuber, 2000: Lower stratospheric organic and inorganic bromine budget for the Arctic winter 1998/99. *GEOPHYSICAL RESEARCH LETTERS*, **27**, 3305–3308, doi:10.1029/2000GL011650.

Prather, M., 1986: Numerical advection by conservation of 2nd-order moments. *JOURNAL OF GEOPHYSICAL RESEARCH-ATMOSPHERES*, **91**, 6671–6681, doi:10.1029/JD091iD06p06671.

Pratt, G., K. Palmer, C. Wu, F. Oliaei, C. Hollerbach, and M. Fenske, 2000: An assessment of air toxics in Minnesota. *ENVIRONMENTAL HEALTH PERSPECTIVES*, **108**, 815–825, doi:10.1289/ehp.00108815.

Priestley, A., 1993: A quasi-conservative version of the semi-lagrangian advection scheme. *MONTHLY WEATHER REVIEW*, **121**, 621–629, doi:10.1175/1520-0493.

Pyle, J. A., N. Warwick, X. Yang, P. J. Young, and G. Zeng, 2007: Climate/chemistry feedbacks and biogenic emissions. *PHILOSOPHICAL TRANSACTIONS OF THE ROYAL SOCIETY A-MATHEMATICAL PHYSICAL AND ENGINEERING SCIENCES*, **365**, 1727–1740, doi:10.1098/rsta.2007.2041.

Pyle, J. A., N. J. Warwick, N. R. P. Harris, M. R. Abas, A. T. Archibald, M. J. Ashfold, K. Ashworth, M. P. Barkley, G. D. Carver, K. Chance, J. R. Dorsey, D. Fowler, S. Gonzi, B. Gostlow, C. N. Hewitt, T. P. Kurosu, J. D. Lee, S. B. Langford, G. Mills, S. Moller, A. R. MacKenzie, A. J. Manning, P. Misztal, M. S. M. Nadzir, E. Nemitz, H. M. Newton, L. M. O'Brien, S. Ong, D. Oram, P. I. Palmer, L. K. Peng, S. M. Phang, R. Pike,

T. A. M. Pugh, N. A. Rahman, A. D. Robinson, J. Sentian, A. Abu Samah, U. Skiba, H. E. Ung, S. E. Yong, and P. J. Young, 2011: The impact of local surface changes in Borneo on atmospheric composition at wider spatial scales: coastal processes, land-use change and air quality. *PHILOSOPHICAL TRANSACTIONS OF THE ROYAL SOCIETY B-BIOLOGICAL SCIENCES*, **366**, 3210–3224, doi:10.1098/rstb.2011.0060.

Quack, B., E. Atlas, G. Petrick, V. Stroud, S. Schauffler, and D. Wallace, 2004: Oceanic bromoform sources for the tropical atmosphere. *GEOPHYSICAL RESEARCH LETTERS*, **31**, doi:10.1029/2004GL020597.

Quack, B., E. Atlas, G. Petrick, and D. W. R. Wallace, 2007: Bromoform and dibromomethane above the Mauritanian upwelling: Atmospheric distributions and oceanic emissions. *JOURNAL OF GEOPHYSICAL RESEARCH-ATMOSPHERES*, **112**, doi:10.1029/2006JD007614.

Quack, B. and D. Wallace, 2003: Air-sea flux of bromoform: Controls, rates, and implications. *GLOBAL BIOGEOCHEMICAL CYCLES*, **17**, doi:10.1029/2002GB001890.

Ravishankara, A. R., J. S. Daniel, and R. W. Portmann, 2009: Nitrous Oxide (N_2O): The Dominant Ozone-Depleting Substance Emitted in the 21st Century. *SCIENCE*, **326**, 123–125, doi:10.1126/science.1176985.

Rayner, N., D. Parker, E. Horton, C. Folland, L. Alexander, D. Rowell, E. Kent, and A. Kaplan, 2003: Global analyses of sea surface temperature, sea ice, and night marine air temperature since the late nineteenth century. *JOURNAL OF GEOPHYSICAL RESEARCH-ATMOSPHERES*, **108**, doi:10.1029/2002JD002670.

Reeves, C., 2003: Atmospheric budget implications of the temporal and spatial trends in methyl bromide concentration. *JOURNAL OF GEOPHYSICAL RESEARCH-ATMOSPHERES*, **108**, doi:10.1029/2002JD002943.

Reeves, C. E., W. T. Sturges, G. A. Sturrock, K. Preston, D. E. Oram, J. Schwander, R. Mulvaney, J.-M. Barnola, and J. Chappellaz, 2005: Trends of halon gases in polar firn air: implications for their emission distributions. *ATMOSPHERIC CHEMISTRY AND PHYSICS*, **5**, 2055–2064, doi:10.5194/acp-5-2055-2005.

Riahi, K., S. Rao, V. Krey, C. Cho, V. Chirkov, G. Fischer, G. Kindermann, N. Nakicenovic, and P. Rafaj, 2011: RCP 8.5-A scenario of comparatively high greenhouse gas emissions. *CLIMATIC CHANGE*, **109**, 33–57, doi:10.1007/s10584-011-0149-y.

Salawitch, R., 2006: Atmospheric chemistry - Biogenic bromine. *NATURE*, **439**, 275–277, doi:10.1038/439275a.

Salawitch, R., D. Weisenstein, L. Kovalenko, C. Sioris, P. Wennberg, K. Chance, M. Ko, and C. McLinden, 2005: Sensitivity of ozone to bromine in the lower stratosphere. *GEOPHYSICAL RESEARCH LETTERS*, **32**, doi:10.1029/2004GL021504.

Sander, S., R. Friedl, D. Golden, M. Kurylo, G. Moortgat, H. Keller-Rudek, P. Wine, A. Ravishankara, C. Kolb, M. Molina, B. Finlayson-Pitts, R. Huie, and V. Orkin, 2006: Chemical kinetics and photochemical data for use in atmospheric studies,, Evaluation Number 15, JPL Publication 06-2. *Jet Propulsion Laboratory*.

Schauffler, S., E. Atlas, D. Blake, F. Flocke, R. Lueb, J. Lee-Taylor, V. Stroud, and W. Travnicek, 1999: Distributions of brominated organic compounds in the troposphere and lower stratosphere. *JOURNAL OF GEOPHYSICAL RESEARCH-ATMOSPHERES*, **104**, 21513–21535, doi:10.1029/1999JD900197.

Scheele, M., P. Siegmund, and P. van Velthoven, 2005: Stratospheric age of air computed with trajectories based on various 3D-Var and 4D-Var data sets. *ATMOSPHERIC CHEMISTRY AND PHYSICS*, **5**, 1–7.

Schofield, R., P. V. Johnston, A. Thomas, K. Kreher, B. J. Connor, S. Wood, D. Shooter, M. P. Chipperfield, A. Richter, R. von Glasow, and C. D. Rodgers, 2006: Tropospheric and stratospheric BrO columns over Arrival Heights, Antarctica, 2002. *JOURNAL OF GEOPHYSICAL RESEARCH-ATMOSPHERES*, **111**, doi:10.1029/2005JD007022.

Sinnhuber, B., D. Arlander, H. Bovensmann, J. Burrows, M. Chipperfield, C. Enell, U. Friess, F. Hendrick, P. Johnston, R. Jones, K. Kreher, N. Mohamed-Tahrin, R. Muller, K. Pfeilsticker, U. Platt, J. Pommereau, I. Pundt, A. Richter, A. South, K. Tornkvist, M. Van Roozendael, T. Wagner, and F. Wittrock, 2002: Comparison of measurements and model calculations of stratospheric bromine monoxide. *JOURNAL OF GEOPHYSICAL RESEARCH-ATMOSPHERES*, **107**, doi:10.1029/2001JD000940.

Sinnhuber, B., A. Rozanov, N. Sheode, O. Afe, A. Richter, M. Sinnhuber, F. Wittrock, J. Burrows, G. Stiller, T. von Clarmann, and A. Linden, 2005: Global observations of stratospheric bromine monoxide from SCIAMACHY. *GEOPHYSICAL RESEARCH LETTERS*, **32**, doi:10.1029/2005GL023839.

Sinnhuber, B. M. and I. Folkins, 2006: Estimating the contribution of bromoform to stratospheric bromine and its relation to dehydration in the tropical tropopause layer. *ATMOSPHERIC CHEMISTRY AND PHYSICS*, **6**, 4755–4761.

Sinnhuber, B. M., N. Sheode, M. Sinnhuber, M. P. Chipperfield, and W. Feng, 2009: The contribution of anthropogenic bromine emissions to past stratospheric ozone trends: a modelling study. *ATMOSPHERIC CHEMISTRY AND PHYSICS*, **9**, 2863–2871.

Sioris, C. E., L. J. Kovalenko, C. A. McLinden, R. J. Salawitch, M. Van Roozendael, F. Goutail, M. Dorf, K. Pfeilsticker, K. Chance, C. von Savigny, X. Liu, T. P. Kurosu, J. P. Pommereau, H. Boesch, and J. Frerick, 2006: Latitudinal and vertical distribution of bromine monoxide in the lower stratosphere from Scanning Imaging Absorption Spectrometer for Atmospheric Chartography limb scattering measurements. *JOURNAL OF GEOPHYSICAL RESEARCH-ATMOSPHERES*, **111**, doi:10.1029/2005JD006479.

Solomon, S., 1999: Stratospheric ozone depletion: a review of concepts and history. *REVIEWS OF GEOPHYSICS*, **37**, 275–316.

Solomon, S., R. Garcia, F. Rowland, and D. Wuebbles, 1986: On The Depletion Of Antarctic Ozone. *NATURE*, **321**, 755–758, doi:10.1038/321755a0.

Stevenson, D., R. Doherty, M. Sanderson, C. Johnson, B. Collins, and D. Derwent, 2005: Impacts of climate change and variability on tropospheric ozone and its precursors. *FARADAY DISCUSSIONS*, **130**, 41–57, doi:10.1039/b417412g.

Stockwell, D. and M. Chipperfield, 1999: A tropospheric chemical-transport model: Development and validation of the model transport schemes. *QUARTERLY JOURNAL OF THE ROYAL METEOROLOGICAL SOCIETY*, **125**, 1747–1783, doi:10.1256/smsqj.55713.

Stolarski, R. and R. Cicerone, 1974: Stratospheric chlorine - possible sink for ozone. *CANADIAN JOURNAL OF CHEMISTRY-REVUE CANADIENNE DE CHIMIE*, **52**, 1610–1615, doi:10.1139/v74-233.

Swanson, A., D. Davis, R. Arimoto, P. Robert, E. Atlas, F. Flocke, S. Meinardi, F. Rowland, and D. Blake, 2004: Organic trace gases of oceanic origin observed at South Pole during ISCAT 2000. *ATMOSPHERIC ENVIRONMENT*, **38**, 5463–5472, doi:10.1016/j.atmosenv.2004.03.072.

Tegtmeier, S., K. Krüger, B. Quack, I. Pisso, A. Stohl, and X. Yang, 2012: Bridging the gap between bromocarbon oceanic emissions and upper air concentrations. *ATMOSPHERIC CHEMISTRY AND PHYSICS DISCUSSIONS*, **12**, 4477–4505, doi:10.5194/acpd-12-4477-2012.

Theys, N., M. Van Roozendael, F. Hendrick, C. Fayt, C. Hermans, J.-L. Baray, F. Goutail, J.-P. Pommereau, and M. De Maziere, 2007: Retrieval of stratospheric and tropospheric BrO columns from multi-axis DOAS measurements at Reunion Island (21 degrees S, 56 degrees E). *ATMOSPHERIC CHEMISTRY AND PHYSICS*, **7**, 4733–4749.

Thomson, A. M., K. V. Calvin, S. J. Smith, G. P. Kyle, A. Volke, P. Patel, S. Delgado-Arias, B. Bond-Lamberty, M. A. Wise, L. E. Clarke, and J. A. Edmonds, 2011: RCP4.5: a pathway for stabilization of radiative forcing by 2100. *CLIMATIC CHANGE*, **109**, 77–94, doi:10.1007/s10584-011-0151-4.

Tiedtke, M., 1989: A comprehensive mass flux scheme for cumulus parameterization in large-scale models. *MONTHLY WEATHER REVIEW*, **117**, 1779–1800, doi:10.1175/1520-0493.

Toon, O., P. Hamill, R. Turco, and J. Pinto, 1986: Condensation of HNO3 and HCL in the winter polar stratospheres. *GEOPHYSICAL RESEARCH LETTERS*, **13**, 1284–1287, doi:10.1029/GL013i012p01284.

Toon, O. and M. Tolbert, 1995: Spectroscopic evidence against nitric-acid trihydrate in polar stratospheric clouds . *NATURE*, **375**, 218–221, doi:10.1038/375218a0.

van der Leun, J., J. F. Bornman, and X. Tang, 2007: Environmental effects of ozone depletion and its interactions with climate change: 2006 assessment. *PHOTOCHEMICAL & PHOTOBIOLOGICAL SCIENCES*, **6**, 209–211, doi:10.1039/b700016b.

van Vuuren, D. P., J. Edmonds, M. Kainuma, K. Riahi, A. Thomson, K. Hibbard, G. C. Hurtt, T. Kram, V. Krey, J.-F. Lamarque, T. Masui, M. Meinshausen, N. Nakicenovic,

S. J. Smith, and S. K. Rose, 2011: The representative concentration pathways: an overview. *CLIMATIC CHANGE*, **109**, 5–31, doi:10.1007/s10584-011-0148-z.

Vecchi, G., B. Soden, A. Wittenberg, I. Held, A. Leetmaa, and M. Harrison, 2006: Weakening of tropical Pacific atmospheric circulation due to anthropogenic forcing. *NATURE*, **441**, 73–76, doi:10.1038/nature04744.

von Glasow, R., R. von Kuhlmann, M. Lawrence, U. Platt, and P. Crutzen, 2004: Impact of reactive bromine chemistry in the troposphere. *ATMOSPHERIC CHEMISTRY AND PHYSICS*, **4**, 2481–2497.

Wamsley, P., J. Elkins, D. Fahey, G. Dutton, C. Volk, R. Myers, S. Montzka, J. Butler, A. Clarke, P. Fraser, L. Steele, M. Lucarelli, E. Atlas, S. Schauffler, D. Blake, F. Rowland, W. Sturges, J. Lee, S. Penkett, A. Engel, R. Stimpfle, K. Chan, D. Weisenstein, M. Ko, and R. Salawitch, 1998: Distribution of halon-1211 in the upper troposphere and lower stratosphere and the 1994 total bromine budget. *JOURNAL OF GEOPHYSICAL RESEARCH-ATMOSPHERES*, **103**, 1513–1526, doi:10.1029/97JD02466.

Warwick, N. J., J. A. Pyle, G. D. Carver, X. Yang, N. H. Savage, F. M. O'Connor, and R. A. Cox, 2006: Global modeling of biogenic bromocarbons. *JOURNAL OF GEOPHYSICAL RESEARCH-ATMOSPHERES*, **111**, doi:10.1029/2006JD007264.

Wayne, R. P., 1991: *Chemistry of atmospheres. An introduction to the chemistry of the atmosphere of Earth, the planets and their satellites (Second Ed)*. Oxford University Press, Oxford, United Kingdom.

WMO, 2003: Scientific Assessment of Ozone Depletion: 2002. *Global Ozone Research and Monitoring Project, Report No. 47, World Meteorological Organization, Geneva, Switzerland.* .

— 2007: Scientific Assessment of Ozone Depletion: 2006. *Global Ozone Research and Monitoring Project, Report No. 50, World Meteorological Organization, Geneva, Switzerland.* .

— 2011: Scientific Assessment of Ozone Depletion: 2010. *Global Ozone Research and Monitoring Project, Report No. 52, World Meteorological Organization, Geneva, Switzerland.* .

Wofsy, S., M. McElroy, and Y. Yung, 1975: Chemistry of atmospheric bromine. *GEOPHYSICAL RESEARCH LETTERS*, **2**, 215–218, doi:10.1029/GL002i006p00215.

Wofsy, S. C., H. S. Team, C. M. Team, and S. Team, 2011: HIAPER Pole-to-Pole Observations (HIPPO): fine-grained, global-scale measurements of climatically important atmospheric gases and aerosols. *PHILOSOPHICAL TRANSACTIONS OF THE ROYAL SOCIETY A-MATHEMATICAL PHYSICAL AND ENGINEERING SCIENCES*, **369**, 2073–2086, doi:10.1098/rsta.2010.0313.

Wohltmann, I. and M. Rex, 2008: Improvement of vertical and residual velocities in pressure or hybrid sigma-pressure coordinates in analysis data in the stratosphere. *ATMOSPHERIC CHEMISTRY AND PHYSICS*, **8**, 265–272.

Wuebbles, D., K. Grant, P. Connell, and J. Penner, 1989: The Role Of Atmospheric Chemistry In Climate Change. *JAPCA-THE JOURNAL OF THE AIR & WASTE MANAGEMENT ASSOCIATION*, **39**, 22–28.

Yang, X., R. Cox, N. Warwick, J. Pyle, G. Carver, F. O'Connor, and N. Savage, 2005: Tropospheric bromine chemistry and its impacts on ozone: A model study. *JOURNAL OF GEOPHYSICAL RESEARCH-ATMOSPHERES*, **110**, doi:10.1029/2005JD006244.

Yokouchi, Y., L. Barrie, D. Toom, and H. Akimoto, 1996: The seasonal variation of selected natural and anthropogenic halocarbons in the Arctic troposphere. *ATMOSPHERIC ENVIRONMENT*, **30**, 1723–1727, doi:10.1016/1352-2310(95)00393-2.

Yokouchi, Y., F. Hasebe, M. Fujiwara, H. Takashima, M. Shiotani, N. Nishi, Y. Kanaya, S. Hashimoto, P. Fraser, D. Toom-Sauntry, H. Mukai, and Y. Nojiri, 2005: Correlations and emission ratios among bromoform, dibromochloromethane, and dibromomethane in the atmosphere. *JOURNAL OF GEOPHYSICAL RESEARCH-ATMOSPHERES*, **110**, doi:10.1029/2005JD006303.

Young, P. J., K. H. Rosenlof, S. Solomon, S. C. Sherwood, Q. Fu, and J.-F. Lamarque, 2012: Changes in stratospheric temperatures and their implications for changes in the Brewer Dobson circulation, 1979-2005. *JOURNAL OF CLIMATE*, **25**, 1759–1772, doi:10.1175/2011JCLI4048.1.

Yvon-Lewis, S. A., E. S. Saltzman, and S. A. Montzka, 2009: Recent trends in atmospheric methyl bromide: analysis of post-montreal protocol variability. *ATMOSPHERIC CHEMISTRY AND PHYSICS*, **9**, 5963–5974, doi:10.5194/acp-9-5963-2009.

Zeng, G., J. A. Pyle, and P. J. Young, 2008: Impact of climate change on tropospheric ozone and its global budgets. *ATMOSPHERIC CHEMISTRY AND PHYSICS*, **8**, 369–387.